NAVAL POSTGRADUATE SCHOOL
Monterey, California

THESIS

FISHERIES ASPECTS OF SEAMOUNTS AND TAYLOR COLUMNS

by

Russell E. Brainard

September 1986

Thesis Co-advisor: R.W. Garwood, Jr.
Thesis Co-advisor: Andrew Bakun

Approved for public release; distribution unlimited

SECURITY CLASSIFICATION OF THIS PAGE

AD-A171 369

REPORT DOCUMENTATION PAGE

1a. REPORT SECURITY CLASSIFICATION	1b. RESTRICTIVE MARKINGS
2a. SECURITY CLASSIFICATION AUTHORITY	3. DISTRIBUTION / AVAILABILITY OF REPORT: Approved for public release; distribution is unlimited.
2b. DECLASSIFICATION / DOWNGRADING SCHEDULE	
4. PERFORMING ORGANIZATION REPORT NUMBER(S)	5. MONITORING ORGANIZATION REPORT NUMBER(S)
6a. NAME OF PERFORMING ORGANIZATION: Naval Postgraduate School; 6b. OFFICE SYMBOL (If applicable): 68	7a. NAME OF MONITORING ORGANIZATION: Naval Postgraduate School
6c. ADDRESS (City, State, and ZIP Code): Monterey, California 93943-5100	7b. ADDRESS (City, State, and ZIP Code): Monterey, California 93943-5100
8a. NAME OF FUNDING / SPONSORING ORGANIZATION; 8b. OFFICE SYMBOL (If applicable)	9. PROCUREMENT INSTRUMENT IDENTIFICATION NUMBER
8c. ADDRESS (City, State, and ZIP Code)	10. SOURCE OF FUNDING NUMBERS: PROGRAM ELEMENT NO. / PROJECT NO. / TASK NO. / WORK UNIT ACCESSION NO

11. TITLE (Include Security Classification)

FISHERIES ASPECTS OF SEAMOUNTS AND TAYLOR COLUMNS

12. PERSONAL AUTHOR(S)

Brainard, Russell E.

13a. TYPE OF REPORT	13b. TIME COVERED	14. DATE OF REPORT (Year, Month, Day)	15. PAGE COUNT
Master's Thesis	FROM _____ TO _____	1986 September	89

16. SUPPLEMENTARY NOTATION

17. COSATI CODES		
FIELD	GROUP	SUB-GROUP

18. SUBJECT TERMS (Continue on reverse if necessary and identify by block number)

Seamount; Upwelling; Larval retention; Seamount oceanography; Taylor column; Fisheries; Nutrient enrichment

19. ABSTRACT (Continue on reverse if necessary and identify by block number)

Three hypotheses to explain the high biological productivity observed over the southern Emperor-northern Hawaiian Ridge seamounts are suggested: larval retention by hydrodynamic trapping in a Taylor column, nutrient enrichment by topographically-induced upwelling, and attraction of organisms to stationary physical substrates. Quasi-geostrophic wave-topography interactions are considered, with particular regard to Taylor column dynamics. Data from three hydrographic surveys over Southeast Hancock Seamount conducted during summer 1984 and winter 1985 are examined for evidence supporting these hypotheses. The two summer surveys show features consistent with a two-layer system having bottom-intensified anticyclonic flow around the seamount, in agreement with stratified Taylor column theory. The winter survey indicates more homogeneous anticyclonic flow around the seamount, suggesting the existence of a barotropic Taylor column. Possibly intense internal wave motion and upwelling are suggested by strong, localized vertical isotherm deflections in across-seamount sections taken during the summer surveys. These deflections are reminiscent of wave-topography interactions in atmospheric flow over terrestrial mountains. The second summer survey showed possible upwelling in the lee of topographically-forced divergence.

20. DISTRIBUTION / AVAILABILITY OF ABSTRACT	21. ABSTRACT SECURITY CLASSIFICATION
☒ UNCLASSIFIED/UNLIMITED ☐ SAME AS RPT ☐ DTIC USERS	Unclassified

22a. NAME OF RESPONSIBLE INDIVIDUAL	22b. TELEPHONE (Include Area Code)	22c. OFFICE SYMBOL
Prof. R.W. Garwood, Jr.	408-646-3260	68Gd

DD FORM 1473, 84 MAR — 83 APR edition may be used until exhausted. All other editions are obsolete

SECURITY CLASSIFICATION OF THIS PAGE

Approved for public release; distribution is unlimited.

Fisheries Aspects of Seamounts
and Taylor Columns

by

Russell E. Brainard
LTJG, NOAA Corps
B.S., Texas A&M University, 1981

Submitted in partial fulfillment of the
requirements for the degree of

MASTER OF SCIENCE IN OCEANOGRAPHY

from the

NAVAL POSTGRADUATE SCHOOL
September 1986

Author: Russell E. Brainard
Russell E. Brainard

Approved by: Roland W. Garwood Jr.
R.W. Garwood, Jr., Co-Advisor

Andrew Bakun
Andrew Bakun, Co-Advisor

C.N.K. Mooers
C.N.K. Mooers, Chairman,
Department of Oceanography

John N. Dyer
John N. Dyer,
Dean of Science and Engineering

ABSTRACT

Three hypotheses to explain the high biological productivity observed over the southern Emperor-northern Hawaiian Ridge seamounts are suggested: larval retention by hydrodynamic trapping in a Taylor column, nutrient enrichment by topographically-induced upwelling, and attraction of organisms to stationary physical substrates. Quasi-geostrophic wave-topography interactions are considered, with particular regard to Taylor column dynamics. Data from three hydrographic surveys over Southeast Hancock Seamount conducted during summer 1984 and winter 1985 are examined for evidence supporting these hypotheses. The two summer surveys show features consistent with a two-layer system having bottom-intensified anticyclonic flow around the seamount, in agreement with stratified Taylor column theory. The winter survey indicates more homogeneous anticyclonic flow around the seamount, suggesting the existence of a barotropic Taylor column. Possibly intense internal wave motion and upwelling are suggested by strong, localized vertical isotherm deflections in across-seamount sections taken during the summer surveys. These deflections are reminiscent of wave-topography interactions in atmospheric flow over terrestrial mountains. The second summer survey showed possible upwelling in the lee of topographically-forced divergence.

TABLE OF CONTENTS

LIST OF FIGURES

ACKNOWLEDGEMENTS

I extend special thanks to Andrew Bakun for stimulating my interest in this research and for his valuable advice and to RADM Kelly Taggart for allowing me the opportunity to continue my education at the Naval Postgraduate School. I also thank Professor Bill Garwood for his comments and suggestions, particularly in preparing the manuscript. Thanks also go to Dr. George Boehlert of the Honolulu Laboratory for providing the data and to Dr. Michele Rienecker for kindly providing most of the software used in the analysis. The continual help and support of the staff at Pacific Fisheries Environmental Group, especially Rosemary Troian, was invaluable. Particular appreciation is extended to Paul Wittmann for the many nights and weekends spent processing the data. Finally, I would like to thank LTJG Mark Sampson and Bonnie Larson for their support and encouragement.

I. INTRODUCTION

Submarine mountains, called seamounts, are prominent, widely distributed features of the ocean bottom. Early biological studies over seamounts typically concentrated on describing benthic biota, often with reports of unique flora and fauna. Only recently have studies investigated the fishery resources associated with seamounts and their interaction with ocean currents. These recent biological studies have suggested that seamounts may support highly productive ecosystems (Borets, 1975; Takahashi and Sasaki, 1977; Genin and Boehlert, 1985). In fact, many seamounts are now known to be excellent fishing grounds for both pelagic nekton, such as tuna, and several epibenthic species (Uda and Ishino, 1958; Hubbs, 1959; Herlinveaux, 1971; Hughes, 1981; Uchida and Tagami, 1984; Genin and Boehlert, 1985). The reasons for the high productivity associated with seamounts are not known, however, it is known that the interaction between seamounts and impinging ocean currents creates a complex physical and biological structure in the overlying and adjacent waters (Meincke, 1971; Vastano and Warren, 1976; Fukasawa and Nagata, 1978; Owens and Hogg, 1980; Gould *et al.*, 1981; Sundby, 1984; Roden and Taft, 1985; Genin and Boehlert, 1985). The details of this complex structure are unclear and poorly understood. Physical oceanographers have generally concentrated their research on the much larger basin scale circulation. Those physical oceanographic studies which have investigated the interaction between ocean currents and seamounts have generally examined the effect of the topography on the large-scale flow, neglecting the small-scale flow necessary to resolve fishery related problems. This study will examine the topographic-scale flow associated with seamount-current interactions in an attempt to gain insights about productivity and resilience of fishery resources often observed in the vicinity of seamounts.

Seamounts were long ignored as sites of potentially important demersal fisheries due to their limited areal extent. This changed in 1967, however, when a Soviet trawler discovered significant amounts of pelagic armorhead, *Pentaceros richardsoni* and alfonsin, *Baryx splendeus* on the southern Emperor-northern Hawaiian Ridge seamounts. Both of these rare fish are eagerly sought and highly prized by Japanese and Soviet fishermen. Soon after this discovery, a relatively large fishery was

established over these central North Pacific seamounts. In the first eight years of the fishery, the combined Soviet and Japanese catch of armorhead alone was nearly 900,000 metric tons (MT). In the early 1970's, Soviet estimates of standing stocks on all seamounts were as high as 400,000 MT (Takahashi and Sasaki,1977; Borets,1979). Considering the limited areal extent of the seamounts, these fish catch statistics revealed a unique, highly productive ecosystem capable of, if managed properly, maintaining a renewable, commercially feasible resource. Of the seamounts with demonstrated fishable populations, the Hancock Seamounts, which are within the 200 mile U.S. Exclusive Economic Zone (EEZ), contained approximately 10% of the armorhead population.

Due to a probable combination of overfishing and poor recruitment, the large fishery of the early 1970's began a rapid decline in the late 1970's and early 1980's. The severe stock depletion is reflected in Japanese catch-per-unit-effort records which show a decrease from a high of over 80 MT per trawling hour in 1972 to approximately 0.29 MT per trawling hour in 1984. This devastating demise led the Honolulu Laboratory (HL) of the National Marine Fisheries Service (NMFS) to recommend closure to foreign fishing of all seamounts within the EEZ for a period of at least six years. This closure to foreign fishing was established to allow recovery of the stock and to provide time to conduct research on the fishery potential for the region and to gain a better scientific understanding of the physical and biological mechanisms responsible for the once abundant fishery. Further, enhanced stock on a single seamount may serve as a reproductive refuge, enhancing recruitment to all seamounts. This possibility needs to be investigated since it would be an important factor in determining if management efforts should extend to international agreements covering all seamounts.

The purpose of the present study is to investigate some hypothesized physical mechanisms, which may be at least partially responsible for maintaining the once thriving southern Emperor - northern Hawaiian Ridge seamount fishery, and to determine whether biological and hydrographic observations over Southeast Hancock Seamount can be plausibly explained, at least qualitatively, by any one or a combination of these hypotheses.

Numerous hypotheses have been suggested to explain the initiation and maintenance of the abundant fisheries sometimes observed over topographic features of the ocean floor. Three specific hypotheses and their relation to the southern Emperor-northern Hawaiian Ridge seamounts will be considered here. The first

hypothesis involves a larval retention mechanism which might act to increase the survival rate of various species of marine organisms over the seamounts by allowing them to remain trapped over or near the seamount peak, rather than being advected downstream into the surrounding open ocean. It has been suggested that Taylor column-like structures may exist over seamounts, and that these might provide the necessary trapping feature required to lengthen their residence time over the seamount and perhaps prevent them from being advected away (Shomura and Barkley, 1980; Boehlert, 1985; Genin and Boehlert, 1985). This mechanism could also act to retain or accumulate nutrients or background oceanic plankton and micronekton. For our purposes here, a Taylor column (Proudman, 1916; Taylor, 1917, 1923) will simply imply a relatively stationary column of water trapped over a seamount. (A more thorough theoretical discussion on Taylor column dynamics and its geophysical applications follows in the next chapter.) If a Taylor column-like structure were to exist, even for relatively short transient events, more larvae might tend to remain over the seamount during their critical free-drifting planktonic stage, thus tending to increase and/or concentrate the total population over the seamount. Further, this mechanism would not necessarily have to trap the larvae of the important commercial species, such as the armorhead which remains pelagic for almost two years prior to recruitment to the seamounts. By simply increasing the biomass of organisms lower in the food web, higher populations of the larger species would tend to be attracted and maintained. This mechanism will be given considerable attention throughout this investigation.

The second hypothesis considers various nutrient enrichment mechanisms. Nutrients, particularly phosphates, nitrates, and silicates, frequently act as the limiting resource controlling productivity. These three essential nutrients are generally in short supply in surface waters, where they are utilized by the phytoplankton. An abrupt nutrient increase is usually observed below the euphotic zone as a result of their release from decomposing organic particles sinking from above and a lack of functional photosynthetic organisms in the deeper water (McConnaughey,1978). Since these nutrients are required by the phytoplankton, which form the base of the marine food web, nutrients are likewise required in the euphotic zone to establish and maintain a productive fishery. The previously mentioned fish catch statistics indicate productivity higher than would be expected without nutrient enrichment. Horizontal advection of nutrients seems unlikely. Therefore, the only plausible nutrient source appears to be upwelling of nutrient-rich water from below.

Several possible explanations for this upwelling process have been suggested. Unfortunately, these mechanisms are rather speculative at this point and cannot be adequately resolved with the data available here. The first process, which is related to the aforementioned Taylor column concept, is discussed more thoroughly in the section on Taylor column theory. Another, equally speculative, possible mechanism for transporting nutrients upward involves internal wave-topography interactions. In this case, analogy is made to mountain waves in the atmosphere which have been observed to have dramatic effects on the air flow, frequently in the form of intense vertical motions (Alaka, 1960; Nicholls,1973; Queney,1977; and Smith,1979). McCartney (1972, 1975) examined topographically generated Rossby waves and found a closed streamline region and possible Rossby wave wakes or meanders downstream of topographic features. Meincke (1971) reports that the most likely mechanism for the generation of an anticyclonic vortex observed over the Great Meteor Seamount was enhanced vertical mixing on the plateau of the seamount due to vertical shear in tidal currents. He explains that the shear is caused by bottom friction and baroclinic modes. The role of wave-topography interactions, including tidal phenomena, and the associated upwelling is discussed in greater detail in the following chapter on the theoretical aspects of flow over topography.

The final hypothesis to be considered involves provision by the seamount of a physical substrate to which organisms can attach or orient themselves. For the case of filter-feeders which affix themselves to the seamount and allow the current to advect food to them in the form of plankton, a minimum expenditure of energy is required to survive, thereby significantly reducing the amount of food required per individual. This would tend to allow a higher concentration of organisms to inhabit the seamount. This, in turn, would attract and help maintain organisms which feed on the filter-feeders, and so on up the food web. Furthermore, behavioral studies indicate that the nekton frequently remain somewhat stationary relative to physical substrates, even when the substrate itself is moving (Blackburn, 1965; Sund, Blackburn, and Williams, 1981). This orientation or attraction has been observed for substrates varying from rockpiles, banks, and artificial reefs to free-drifting objects such as wooden crates.

II. THEORETICAL ASPECTS OF FLOW OVER TOPOGRAPHY

A. FUNDAMENTAL THEORY

1. *Geostrophic Flow Over Topography*

In steady, low Rossby number, frictionless conditions the strength of ocean currents is determined by the geostrophic balance between the pressure gradient force and the Coriolis force. Using the geostrophic equations on an f-plane and the continuity equation with variable bottom topography, the following relationship can be derived for a barotropic (homogeneous) fluid (Defant, 1961):

$$(\partial h/\partial y)(\partial \eta/\partial x) - (\partial h/\partial x)(\partial \eta/\partial y) = 0 ,$$

where η and h are sea surface elevation and depth, respectively, and $\eta << h$. This relation indicates that if depth varies, then steady, frictionless barotropic currents are only possible if the topography of the sea surface conforms, on a relative scale, with that of the sea bottom. This implies that the current must follow the isobaths, but the strength of the current is indeterminate and depends only on the sea surface slope. In other words, the above relationship indicates that in steady, low Rossby number, frictionless, barotropic currents flowing over raised topography, the sea surface will be higher, as will be the pressure over the topographic feature. Relative high pressure over the topographic feature implies anticyclonic flow. In the presence of horizontal density gradients, a baroclinic component will also exist, and the total geostrophic current magnitude will decrease with depth when the baroclinic and barotropic components are opposite in sign, and increase with depth for like signs. For the case where signs are opposite and the baroclinic component is dominant, the flow will be cyclonic, except near the surface, where there is only the anticyclonic barotropic flow. Furthermore, it is possible to have cyclonic, baroclinically-dominated flow in the upper layer overlying anticyclonic barotropically-dominated flow. The thicknesses of the respective layers are dependent upon the strength of the barotropic component, which is invariant with depth, and the strength of the baroclinic component, which is depth-dependent.

2. *Quasi-Geostrophic Flow*

For the typical geophysical situation where the Brunt-Vaisala frequency, N, is large compared with the Coriolis parameter, f, Gill (1982) finds five regimes of wave-topography interactions. Gill's rotating wave regime ($L = U/|f|$) and quasi-geostrophic flow regime ($L >> U/|f|$) are possible for oceanic flow around seamounts. Here, L is the horizontal length scale of the topographic feature and U is the horizontal velocity scale. Thus, relatively small horizontal length scales or high horizontal velocity scales are required for the rotating wave regime, e.g., for $L = 1.3$ km, $U = 0.1$ ms^{-1}, and for $L = 13.8$ km, $U = 1.0$ ms^{-1}. In a similar manner, the quasi-geostrophic flow regime requires a relatively large horizontal length scale, or an extremely low horizontal velocity scale. A scale analysis of the data presented here indicates that the quasi-geostrophic flow regime is particularly important for the flow over Southest Hancock Seamount. Therefore, the following development is primarily concerned with quasi-geostrophic flow, which implies a force balance which is predominantly geostrophic in the horizontal and hydrostatic in the vertical.

Following the development of Hogg (1980), appropriate scales for pressure and density can be derived from the geostrophic-hydrostatic balance according to:

$$(u,v,w) = U(u^*,v^*,w^*H/L)$$

$$(x,y,z) = (Lx^*,Ly^*,Hz^*)$$

$$p = \rho_0 UfLp^*$$

$$\rho = (\rho_0 UfL/gH)\rho^*$$

$$f = f_0 + \beta y = f_0(1+\beta^* y),\ \beta^* = \beta L/f_0 .$$

Using the Boussinesq approximation and cross differentiating the resulting momentum equations, pressure can be removed from the horizontal momentum equations to determine the dimensionless quasi-geostrophic vorticity equation (dropping *'s):

$$d/dt(\zeta + f(y)) = -(\partial u/\partial x + \partial v/\partial y) + E_H \nabla_h^2 \zeta + E_V \partial^2 \zeta/\partial z^2$$

where ζ is the relative vorticity, $f(y)$ is the planetary vorticity, and E_H and E_V are the horizontal and vertical Ekman numbers, respectively. Assuming incompressibility results in:

$$d/dt(\zeta + f) = w_z + E_H \nabla_h^2 \zeta + E_V \partial^2 \zeta/\partial z^2 ,$$

which relates changes in the absolute vorticity to mass divergence and eddy diffusion. Scaling this equation, Hogg showed that only small vertical velocities are required to create changes of first order in the relative vorticity.

For the case of a stratified ocean, expressions for the conservation of water properties must also be taken into account. Assuming ρ can be approximated by a linear function of T and S, which are in turn assumed to be linearly related, with salinity partially compensating temperature,

$$\rho = \rho_0(1-\alpha^*(T^*-T_0)),$$

where α^* is an effective expansion coefficient. Then, T^* can be separated into a basic state that would exist in the absence of motion and a perturbation field according to

$$T(x,t) = T_0 + \overline{T}(z^*) + \delta T(T^*(z^*) + T'(x^*,t^*)),$$

where δT is the total temperature change from top to bottom and $\overline{T}(z^*)$ is a non-dimensional monotonic function of depth. In this manner, Hogg derived the following dimensionless form of the heat equation

$$d/dt(T') + S^2\overline{T}_z w = (K_H/f_0L^2)\nabla_h^2 T' + (K_V/fH^2)\partial^2T'/\partial z^2,$$

where $K_{H,V}$ are the appropriate diffusivities. This equation contains a stratification parameter

$$S^2 = (NH/fL)^2,$$

which is also called the Burger or Eady number. For topographic scale flows, such as expected over Southeast Hancock Seamount, the ratio of the buoyancy frequency to the inertial frequency, N/f, ranges from about 25 for the main pycnocline in winter to approximately 200 for the seasonal pycnocline in summer. Using these extreme values of N/f to determine the stratification parameter over Southeast Hancock results in a range from 2.3 to 18.0. The horizontal and vertical Ekman numbers are $O(10^{-3})$ and $O(10^{-8})$, respectively. The advective Rossby number, Ro = U/fL, over the seamount was about 0.07, assuming a horizontal velocity of 0.1 ms^{-1}. Finally, the fractional change in water depth due to the topography, $\delta = h_0/H$, where h_0 is the height scale for the topography, is approximately 0.95.

Making the assumption that the fluid is inviscid, except near rigid boundaries, Ekman layers will be present on boundaries. The effect of these Ekman layers on the

interior, inviscid motions can be represented by a small vertical velocity at the top of the thin boundary layer, a process known as Ekman pumping. Hogg then shows that when the Rossby number is much greater than $E_V^{1/2}$ (as is the case for the Hancock situation), it is safe to ignore all diffusive effects, which leads to

$$d/dt(\zeta + \beta y + (1/S^2)(\partial/\partial z(T/\bar{T}_z)) = 0 ,$$

where the argument of the derivative is the potential vorticity, consisting of the relative vorticity, the planetary vorticity, and a term proportional to the vertical separation between isotherms. This equation expresses the conservation of potential vorticity following the motion of an individual fluid element, i.e., potential vorticity is conserved along streamlines.

Assuming the upstream flow is broad and uniform in the horizontal, Merkine and Rivas (1976) showed that topographically induced relative vorticity is independent of the incident flow. Physically, a bottom boundary condition of zero flow imposes a uniform temperature distribution over the bottom, including the topographic feature. With this temperature surface draped over the topography, geostrophic currents are established through the thermal wind relation and these are related only to the stratification and isotherm distortions (Hogg, 1980).

B. TAYLOR COLUMN THEORY

1. *Fundamental Concepts*

As mentioned in the introduction, it is hypothesized that Taylor column processes can explain nutrient enrichment and larval retention over seamounts. These processes will now be more thoroughly reviewed. Taylor columns have received much attention, both theoretical and experimental, since Hide (1961) speculated that the Great Red Spot of Jupiter is a result of topographic blocking of a flow in a rapidly rotating fluid. Hide argued that dynamical constraints on the flow, as first deduced theoretically by Proudman (1916) and Taylor (1917), and demonstrated in the laboratory by Taylor (1923), will lead to the formation of a stagnant body of fluid above an assumed Jovian obstacle with two dimensional flow around the obstacle. Hide named this phenomenon a Taylor column (Bannon, 1979).

The Taylor-Proudman theorem states that steady, inviscid, homogeneous flow is independent of position along the axis of rotation. Since the flow cannot vary vertically, it must move around topographic features, i.e. barotropic flow must follow

isobaths (Greenspan, 1968). This creates an isolated vertical column of fluid over the topographic feature. This theorem does not predict that the fluid inside the column is necessarily stagnant. In fact, any flow satisfying continuity and having the streamlines follow the bathymetric contours is possible (Davies, 1972).

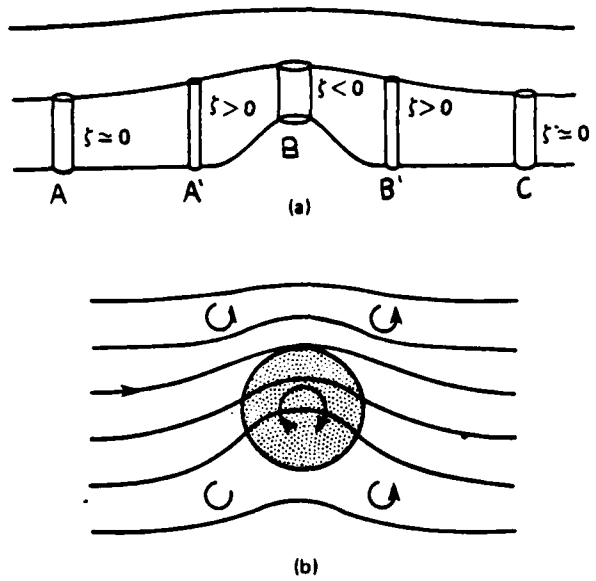

Fig. 2.1. Quasi-geostrophic flow over a circular hill. (a) Vertical section through the center of the hill, showing displacement of isopycnals and the behavior of vortex tubes. On the flanks of the hill they are stretched slightly, producing cyclonic relative vorticity, whereas the vortex tube is significantly shortened over the hill, producing strong anticyclonic relative vorticity. (From R.B. Smith (1979, Fig. 17), after Buzzi and Tibaldi (1977)) (b) The streamline pattern over the hill, showing the associated relative vorticity. (From R.B. Smith (1979, Fig. 18))

On the basis of the arguments presented in the previous section, it is reasonable to expect anticyclonic flow around a barotropic Taylor column. Simplifying the potential vorticity equation to

$$(\zeta + f)/D = \text{constant} \ ,$$

similar deductions for the motion of a column of water of depth D are possible, provided there is no frictional input of vorticity, and vertical shear is negligible (Pond and Pickard, 1983). This implies that negative relative vorticity (anticyclonic) is generated as depth decreases, and positive relative vorticity (cyclonic) is generated as

depth increases along streamlines. Figure 2.1 is a kinematic representation of quasi-geostrophic flow over a circular hill. As fluid at A, which has zero relative vorticity, is advected to A′, where the isopycnals have been displaced in response to the upcoming topographic feature, vortex tubes are stretched and cyclonic vorticity is induced. Next, as the fluid progresses from A′ to B, at the top of the topographic feature, vortex tubes are compressed and anticyclonic vorticity is induced. Huppert and Bryan (1976) showed that this anticyclonic vorticity remains over the topographic feature to make up part of the steady-state solution, i.e., a barotropic Taylor column. As the fluid originally at B is advected downstream to B′, vortex lines are stretched and cyclonic vorticity is again induced. Finally, as the fluid is advected to C, vortex lines are compressed to their original height, and zero relative vorticity is again achieved. Although streamlines must be followed, it can be argued that if water from the far field were ultimately trapped over the seamount, it would have the circulation indicated.

Dynamically, the response in a homogeneous fluid to flow upward over a topographic feature is an incremental rise in sea level over the feature, resulting in locally high fluid pressure, with an anticyclonic geostrophic circulation around it. If the fluid is stratified in density, relatively heavy water originally upstream of the topographic feature is initially (before steady-state is achieved) advected to the top of the feature. Relatively lighter fluid initially at the top is advected off the feature. In a steady-state condition, the heavy water at the top of the feature implies higher pressure and the associated anticyclonic baroclinic flow, whereas the lighter fluid implies cyclonic flow associated with the vertical shear. According to Huppert and Bryan (1976), the cyclonic feature is either displaced well downstream, or it interacts with the anticyclonic flow above the topographic feature, thereby remaining trapped close to the seamount peak (Figure 2.2).

2. *Theoretical Studies*

Various theoretical model studies, each retaining different terms in the equations of motion, have been advanced to investigate the potential implications of Taylor's laboratory observations for geophysical situations. Jacobs (1964) extended the mathematical development of the problem for a large obstacle when the friction terms dominate the inertial terms. For this case, vertical velocities associated with flow over the topography are counteracted by Ekman pumping in the boundary layer to produce a stagnant region when the slope of the topographic feature is of order unity. Hide (1961), Hide and Ibbetson (1966), and Ingersoll (1969) alternatively explained the

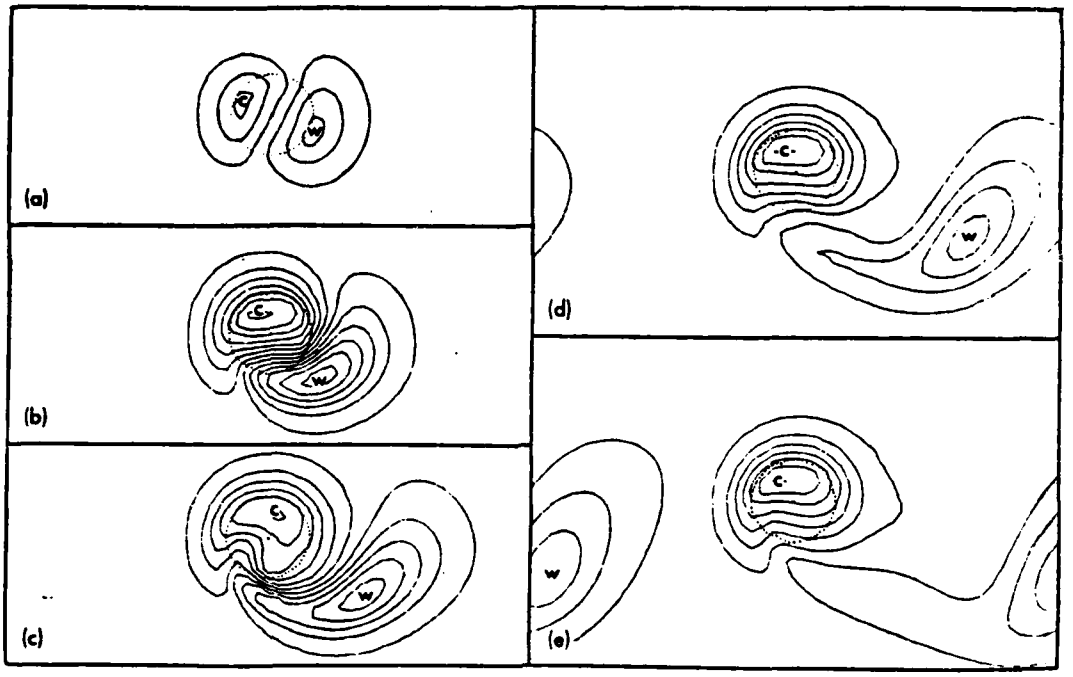

Fig. 2.2. The flow of an inviscid, stratified fluid is initiated from relative rest in a uniformly rotating system. The evolution of flow redistibutes vorticity and temperature in a way such that relatively cold water with anticyclonic vorticity exists over the topographic feature, while water shed from above the feature sinks, thereby inducing a warm anomaly with cyclonic vorticity. For sufficiently strong oncoming flows, the shed fluid continually drifts downstream, as shown here. The isopycnals are shown at a depth of 3720 m, for $U_o = 5.1$ cms^{-1}, and the height of the topography is 200 m. (a) 2.3 days, (b) 6.9 days, (c) 13.9 days, (d) 23.1 days and (e) 34.7 days. From Huppert and Bryan (1976).

inertial Taylor column, where the inertial terms, although small, dominate friction. These studies recognized that the height of the topographic feature need not be large in order to produce a significant effect. The key parameter is

$$\mathbf{B}_T = \delta/Ro = (h_o/H) * (fL/U) .$$

For $\mathbf{B}_T$ smaller than a critical number of order unity, no closed streamlines develop. For $\mathbf{B}_T$ larger that this critical value, closed streamlines do occur. Huppert (1975), investigating the effects of obstacle shape and orientation, found that the extent and shape of the resulting Taylor column differs significantly for different obstacles. For the homogeneous case with a circularly symmetric obstacle, $\mathbf{B}_T$ must satisfy the inequality

$$B_T > \min(r/_0 \int^r xh(x)dx) \ ,$$

where r is the radius of the obstacle, for closed streamlines to occur. Furthermore, flow incident on any obstacle with a vertical face, no matter how small the obstacle height, will result in closed streamlines.

Using steady, inviscid, quasi-geostrophic theory, an approach well-posed provided the flow possesses no closed streamlines, Ingersoll (1969) gave a heuristic argument based on vanishingly small viscosity to obtain the boundary condition of zero tangential velocity on closed streamlines. Although theory predicts Taylor column formation to the right of the topographic feature, in agreement with laboratory experiments, the specification of both the stream function and its normal derivative about the column is an overspecification of the appropriate elliptic equation (Bannon,1980).

In the case of the stratified Taylor column, stratification generally reduces the critical topographic height necessary for closed streamlines by concentrating the vorticity generation in the lower layers, Hogg (1973) and Huppert (1975). If the stratification is sufficiently strong, the effects will be trapped in the lower layer, thereby isolating the stagnation region from the surface layers. For the stratified case, the aforementioned critical parameter B_T must be multiplied by the stratification parameter, S. When this new parameter, SB_T, is smaller than a critical number of order unity, the cyclonic eddy is swept downstream, and the streamline pattern over the topographic feature will not have closed streamlines. When SB_T is greater than this critical value, but less than another critical number of order ten, the cyclonic eddy is still carried downstream, but closed streamlines (a stratified Taylor column) develop over the feature. Finally, for an even larger SB_T, flow speeds are sufficiently small that the cyclonic eddy interacting with the trapped anticyclonic eddy cannot be advected away and remains attached to the right side of the topography looking downstream (Huppert and Bryan, 1976). This is shown in Figure 2.2.

Buzzi and Tibaldi (1977) and Vaziri and Boyer (1971) examined frictional effects for the stratified and homogeneous cases, respectively. In both cases, friction is provided through Ekman suction of $O(E_v^{1/2})$ on the lower boundary, where E_v is the vertical Ekman number. The effect of this suction is to reduce vortex compression on the upstream side of the topographic feature and increase it downstream. This inclusion of frictional effects, therefore, introduces an upstream-downstream asymmetry (Hogg, 1980).

C. OCEANIC OBSERVATIONS OF TAYLOR COLUMNS

Although Hide's original hypothesis is controversial (Stone and Baker, 1968; Hide, 1971), evidence for the existence of Taylor columns has been presented for other geophysical fluid flows, including oceanic cases.

From the studies presented above, two characteristic features of well-developed "classical" Taylor columns in the ocean were identified. These are doming of isotherms, brought about by the fluid being forced to initially rise over the seamount, and the associated geostrophically induced anticyclonic tendency of the flow field. A third feature common to theoretical studies of slow, steady flow over topography was an asymmetric velocity field having accelerated flow to the left and decelerated flow, perhaps to the point of stagnation or reversal (a Taylor column), to the right of the flow when looking downstream. Although these characteristic features would seem relatively easy to observe in the ocean, surprisingly few observational reports of Taylor columns have been described in the literature. Those studies which do discuss observed Taylor column-like features in the ocean provide only indirect, inconclusive evidence for their existence, at least in the "classical" sense (Meincke, 1971; Hogg, 1973; Roberts et al., 1974; Vastano and Warren, 1976; Huppert and Bryan, 1976; Owens and Hogg, 1980; Roden and Taft, 1985; Genin and Boehlert, 1985). This deficiency is at least partially due to a general lack of observations over seamounts on a scale sufficiently small to resolve the characteristic features. As mentioned in the introduction, most physical oceanographic studies conducted over the past several decades have concentrated primarily on flow scales which are too large to resolve the small scale topographic effects important for fisheries. Furthermore, most of the theoretical studies are dependent upon simplifying assumptions, many of which are not strictly valid for the actual ocean. Certainly, the assumption of steady state, used in most of the theoretical studies, is not truly representative of the ocean, which has been shown to have significant temporal variability, even in its more quiescent locations (Schmitz, 1975, 1980).

D. UPWELLING AND NUTRIENT ENRICHMENT

Although the details are very complex and not understood, the concept of the proposed larvae and nutrient retention mechanism by Taylor column dynamics is rather simple. The basic premise involves the trapping of larvae and nutrients over a seamount by a hydrodynamical mechanism, such as a Taylor column. If such a

phenomenon occurs, it would likely result in higher larval survivability and an increased biomass. The details of the association between Taylor column dynamics and nutrient enrichment are not so trivial, and await further investigation. The following mechanisms to explain this association remain speculative.

As described above, "classical" Taylor columns are initiated, under suitable conditions, when steady, slow flow is forced to rise upon encountering the seamount. The initial rise might therefore upwell nutrients from the lower layer to the euphotic zone. In addition to injecting nutrients, this initial doming of isotherms would create a relative high pressure region over the seamount, thus inducing anticyclonic flow. If the system were frictionless, then this fully-developed Taylor column would remain trapped over the seamount indefinitely. However, the system cannot be frictionless, and the geostrophically balanced anticyclonic flow must be affected by bottom friction, which induces radial outflow at the bottom around the seamount due to bottom-layer Ekman transport. Figure 2.3 shows two suggested sources to replace this radially outflowing water (Bakun, In press). The first possible source of water is the high pressure region above the seamount. In this case, as water from the high pressure region over the seamount supplies the radial outflow, the pressure over the seamount is reduced and the Taylor column would weaken. When this happens, the incident flow would again tend to upwell more *nutrient-rich* water over the seamount. By continuity there will be a balance between the volume of water from the oncoming flow being forced to rise over the seamount and the volume of water exiting the system by radial outflow forced by bottom friction. Thus, this mechanism continually provides nutrients to the stagnant, closed-streamlined region over the seamount. In addition to providing nutrients to the region over the seamount, this mechanism might also explain convergence of oceanic plankton and micronekton, which could attract and be utilized by higher trophic level organisms over the seamount. The second suggested source for radially outflowed water is water upwelled along the flanks of the seamount. For enrichment to occur, this mechanism would require diffusion of the upwelled nutrients into the trapped Taylor column over the seamount.

Another possible mechanism for transporting nutrients upward is Meincke's (1971) explanation for an anticyclonic vortex observed over Great Meteor Seamount. He argues that kinetic energy is lost from the baroclinic tidal waves due to near-bottom and interior vertical shear. Subsequently, intensified vertical mixing contributes to an increase of potential energy of the stratification above the seamount. If vertical mixing

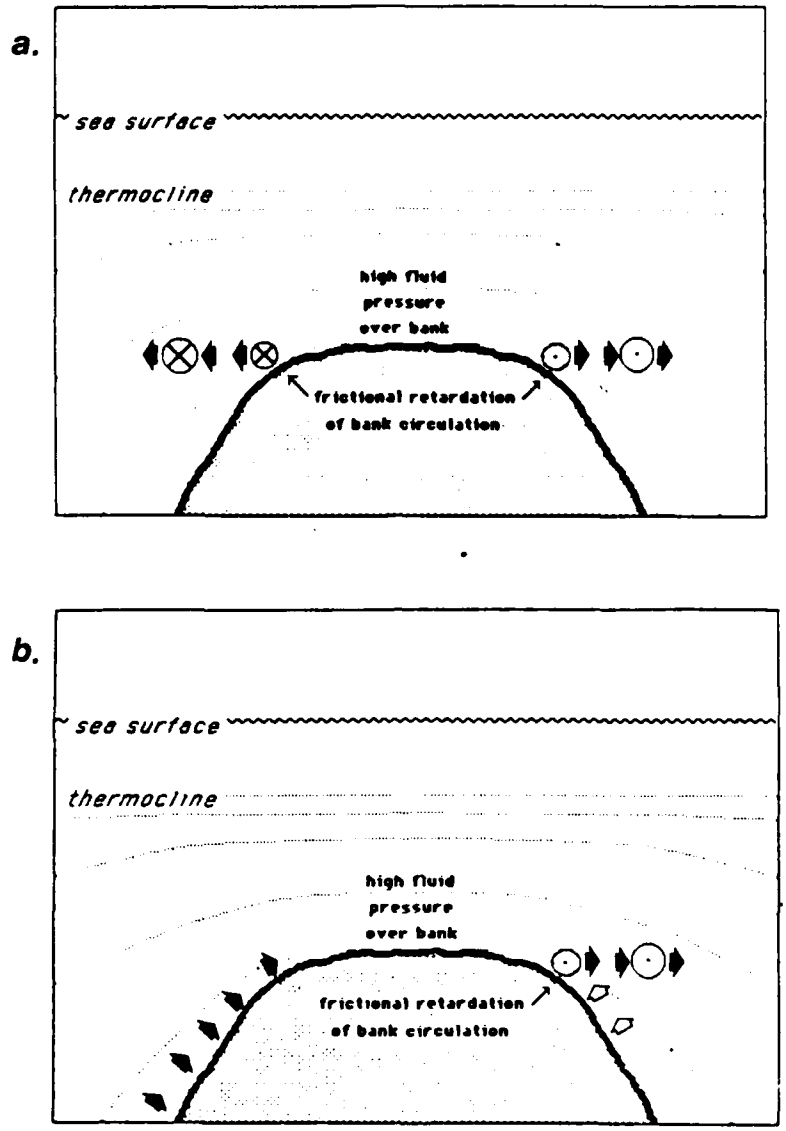

Fig. 2.3. Schematic representation of two proposed nutrient enrichment mechanisms for a stratified Taylor column over a submerged bank: (a) frictional retardation of flow adjacent to the bank surface may result in sub-geostrophic flow and associated unbalanced pressure gradient leading to a secondary radial outflow (short black arrows) from the bank area (circles containing 'x' indicate flow of the primary bank circulation into the plane of the figure; circles containing dots indicate flow out of the figure); (b) representation of upwelling circulation which may balance radial outflow. From Bakun (In press).

is indeed enhanced as reported, then this is another mechanism for upwelling nutrients to the euphotic zone.

III. REGIONAL GEOGRAPHIC, BATHYMETRIC, AND OCEANOGRAPHIC SETTING

A. GEOGRAPHY

The Hawaiian Ridge is an important geomorphological feature of the central North Pacific Ocean. The ridge is comprised of hundreds of islands and seamounts which extend almost 3700 km in a relatively straight ESE-WNW line from a point about 270 km ESE of the island of Hawaii to the southern end of the Emperor Seamounts, which appear to be an extension of the ridge to the north. The vertical extent and steepness of many of the islands and seamounts comprising the Hawaiian Ridge are unsurpassed by any other features of the earth's surface. The horizontal separation between islands and/or seamounts varies from about 10 km to several hundred kilometers. In many cases, the water depth in the gaps approaches that of the surrounding deep ocean bottom. Frequently, clusters or groups of individual peaks are observed in association with a single larger-scale seamount.

As mentioned in the introduction, this study examines the oceanographic conditions over Southeast Hancock Seamount, the highest of several peaks which collectively comprise what is called Hancock Seamount. Hancock Seamount is located approximately 2500 km WNW of Honolulu, or 270 km WNW of Kure Atoll, the nearest terrestrial feature. These peaks form part of the northwestern extreme of the Hawaiian Ridge, almost at the junction of the Hawaiian Ridge and the Emperor Seamounts.

B. BATHYMETRY

A fine scale, high precision bathymetric survey of Hancock Seamount has not yet been performed. However, the *Bathymetric Atlas of the North Pacific Ocean* (*N.O. Pub.No. 1301-2-3*) shows the predominant bathymetric features of Hancock Seamount and the surrounding ocean bottom (Figure 3.1). The topography is complex with at least eight individual peaks associated with Hancock Seamount. There is a sharp rise in elevation as the seamount is approached from the surrounding ocean, which has a typical bottom depth of 5200 m. On Figure 3.1, the summit of Southeast Hancock Seamount is labeled 217 fathoms (397 m). Since the time of the surveys used for the chart, the summit depth of Southeast Hancock has been redetermined to be 260 m. In

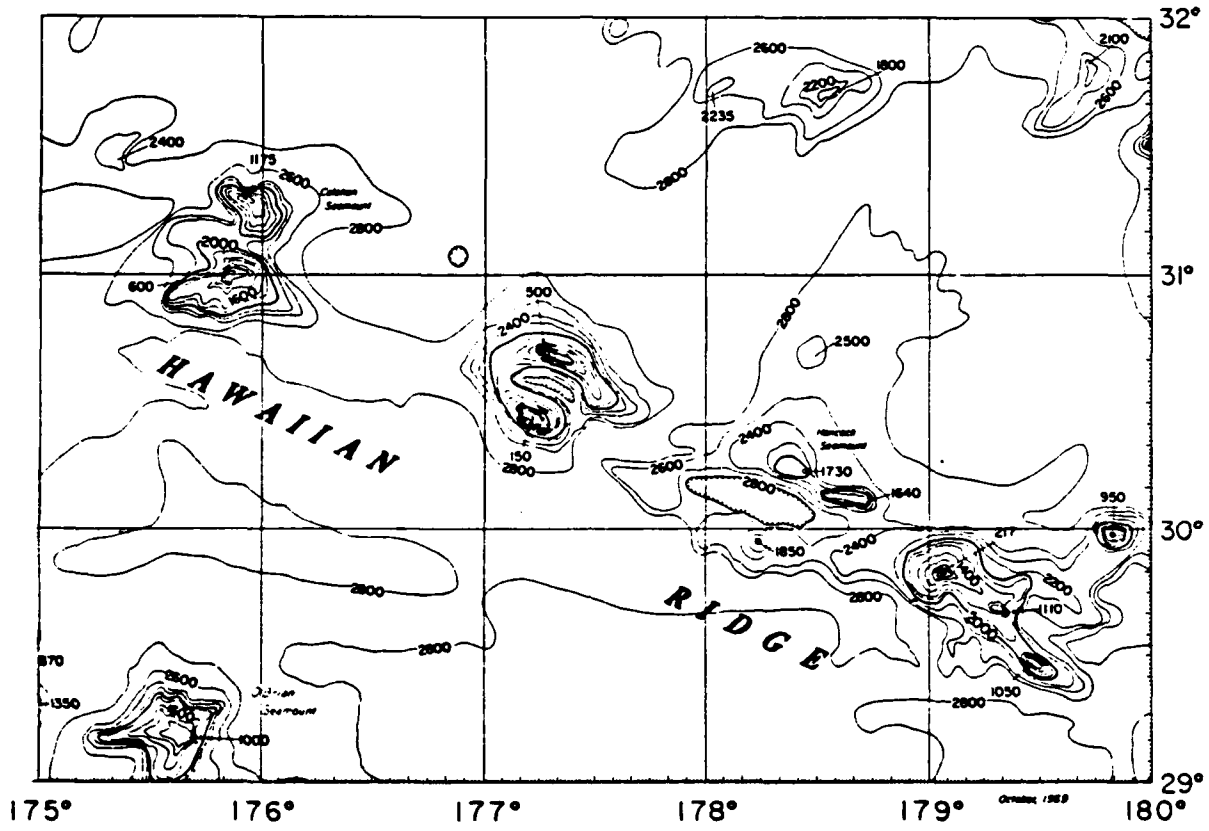

Fig. 3.1. Bathymetry of the northwestern Hawaiian Ridge, including Hancock Seamount. Southeast Hancock Seamount is the peak at 29°48′N, 179°04′E labeled 217. Soundings are in fathoms. (From *N.O. Pub. No. 1301-2-3*).

either case, Southeast Hancock rises well above each of the remaining peaks of Hancock Seamount (about 1500 m higher than the next highest peak). The rise from 5200 m to 260 m occurs in a distance as short as 22 km, corresponding to an average slope of 0.22.

Although the other peaks of Hancock Seamount are much lower than Southeast Hancock, they might nevertheless have a significant effect on the flow field. They certainly have the potential for producing complexity in the flow field, which would influence the incident flow over the principal peak. The effect of these other peaks, and the complex topography in general, is considered during the analysis of hydrographic data over Southeast Hancock.

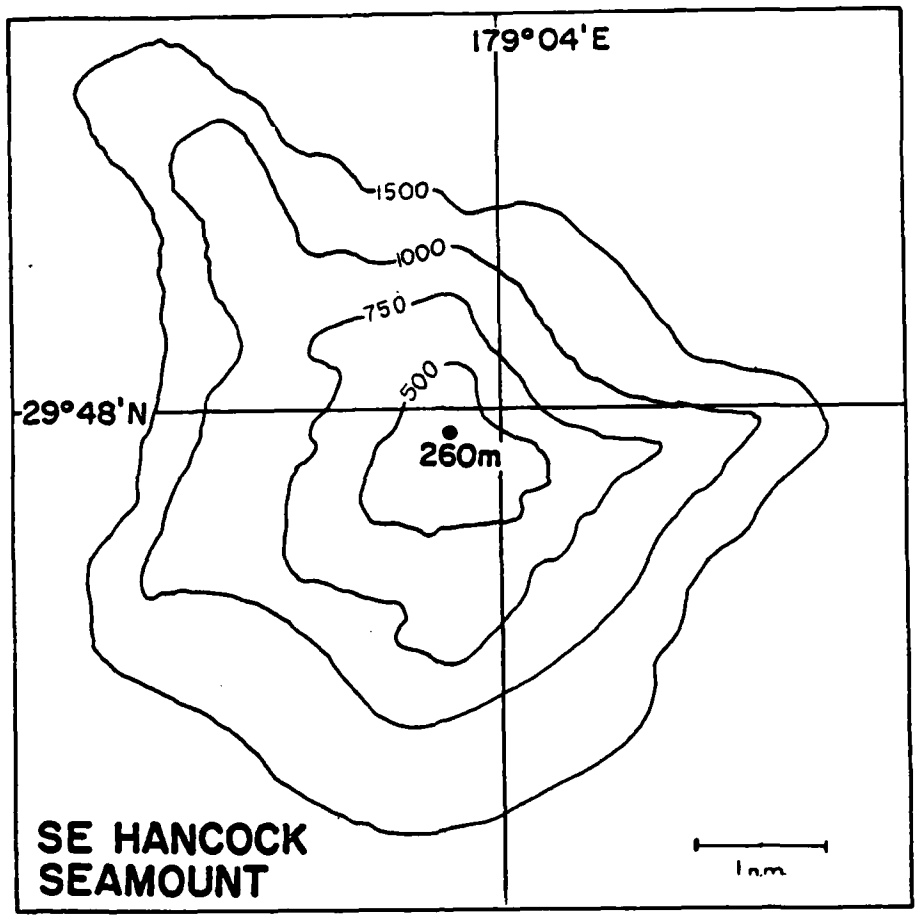

Fig. 3.2. Large-scale bathymetric chart of the summit of Southeast Hancock Seamount, produced from a survey in 1984 aboard the NOAA Ship TOWNSEND CROMWELL. Soundings are in meters.

In addition to the relatively low resolution bathymetric chart presented, a rather rough, higher resolution bathymetric survey of Southeast Hancock was conducted during one of the early seamount resources cruises of the Honolulu Laboratory in 1984 aboard the NOAA Ship TOWNSEND CROMWELL. Although this survey produced a much higher resolution chart of Southeast Hancock Seamount (Figure 3.2), the geodetic control used in the survey was marginal. Therefore, the absolute positions on the resulting chart (unpublished) are probably in error. For the purposes of this analysis, however, absolute positioning is not crucial to the results.

C. CLIMATOLOGY

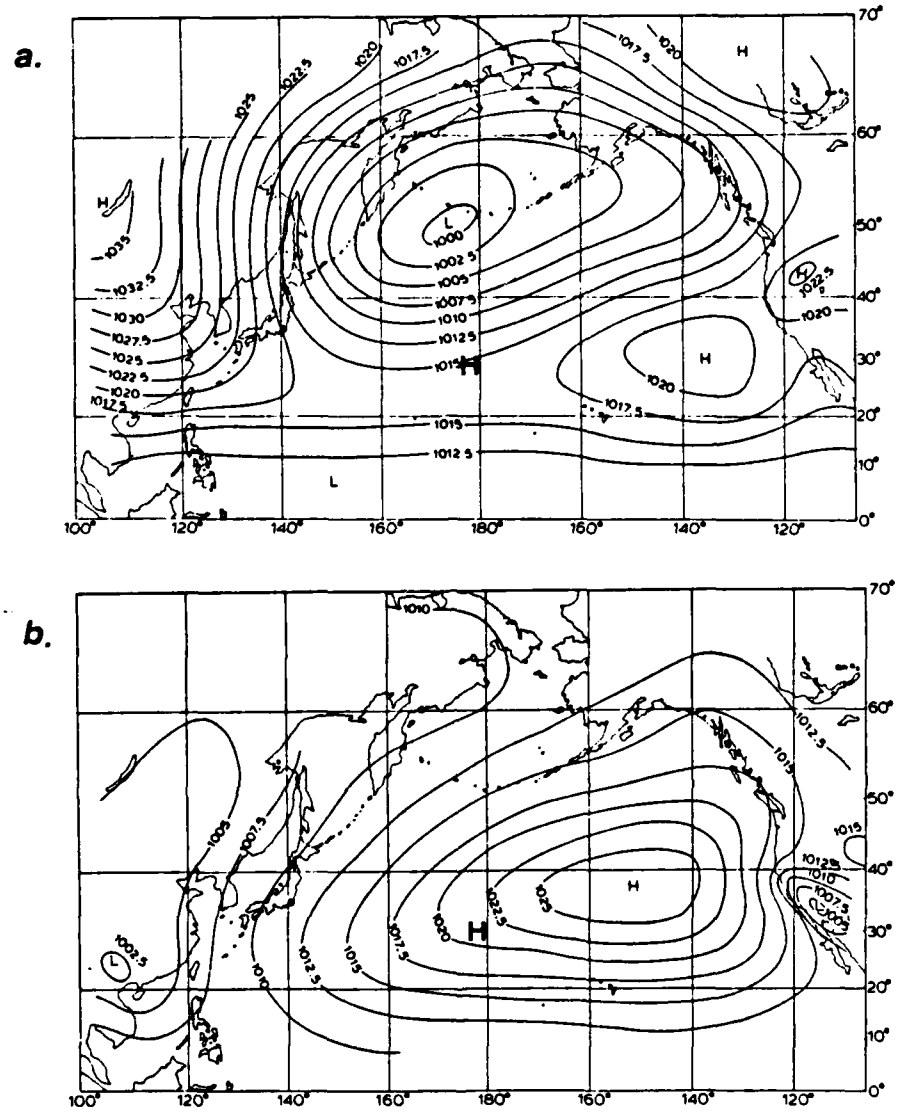

Fig. 3.3. Mean sea level pressure (mbar) over the North Pacific in (a) January and (b) July. The approximate locations of Hancock Seamount are indicated by the large H's. From Terada and Hanzawa (1984).

The ocean circulation, which can be divided into thermohaline and wind-driven components, is ultimately driven by solar energy. The thermohaline circulation, which is characterized by an initial vertical flow due to sinking, followed by a resultant horizontal flow, is generally due to surface density changes caused by heating/cooling,

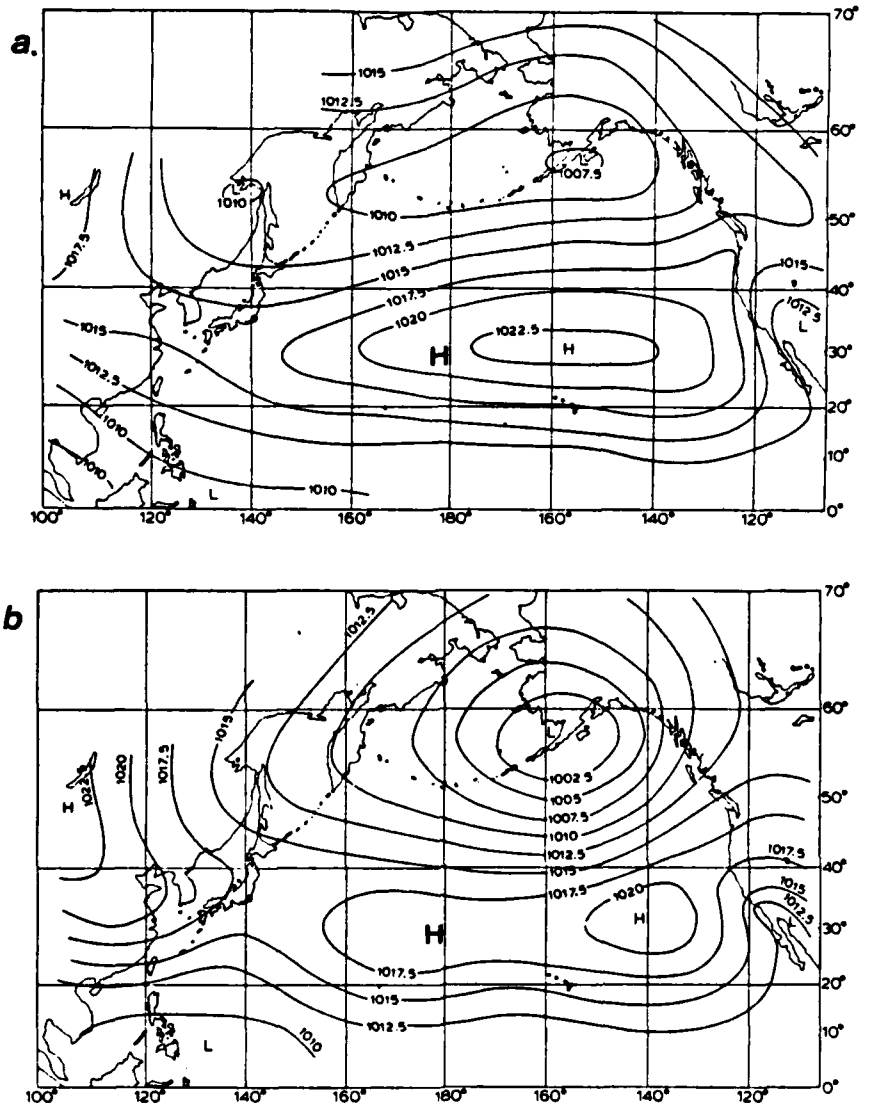

Fig. 3.4. Mean sea level pressure (mbar) over the North Pacific in (a) April and (b) October. The approximate locations of Hancock Seamount are indicated by the large H's. From Terada and Hanzawa (1984).

freezing or melting of ice, and evaporation. The wind-driven component, which is primarily a horizontal motion in the upper few hundred meters, is due to wind stress. Since both components of the oceanic circulation are atmospherically forced, knowledge of the atmospheric processes in the vicinity of Hancock Seamount are required for this analysis. With this in mind, a brief description of the dominant atmospheric processes is presented.

The regional atmospheric climatology in the vicinity of Hancock Seamount varies with the seasonal extremes of the mean pressure distribution over the North Pacific Ocean. During the boreal winter, the atmospheric circulation over the North Pacific is dominated by a deep, extensive low, whereas in summer it is completely covered by an anticyclone (Figure 3.3). The April map shows the expanding high and contracting low, and the October map shows the rapidly developing mean low and shrinking high (Figure 3.4).

The center of the subtropical ridge of high mean pressure is found in all months in the southeastern North Pacific. In summer, the high extends over most of the ocean, and in winter a greatly reduced high lies over the southeastern part and is connected with the Siberian High by a ridge running along 25° N. The tropics, therefore, are under the influence of the south side of the high and its northeasterly trade winds throughout the year.

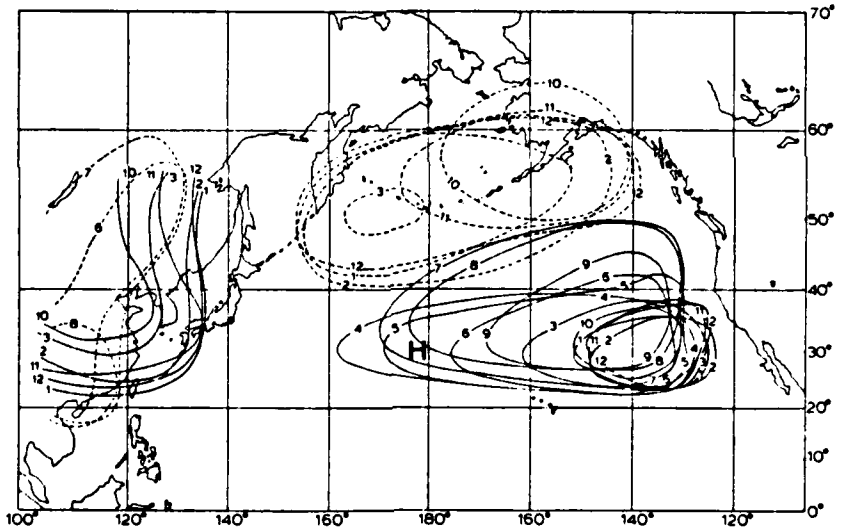

Fig. 3.5. Positions of monthly mean 1020-mbar isobars (solid lines) and 1005-mbar isobars (broken lines) over the North Pacific. The approximate location of Hancock Seamount is indicated by the large H. From Terada and Hanzawa (1984).

To illustrate the seasonal change of the mean subtropical high, the 1020 mb isobar for every month is depicted in Figure 3.5. Note that the area within the 1020 mb isobar is similar from October to February and is confined to a region

bounded by 22°-38° N and 123°-150° W. The size and location of the high in these months are closely related to the development of the Aleutian Low and Siberian High.

As summer approaches, the high expands and becomes more intense, first slowly but then rapidly between June and July. In summer, the 1020 mb isobar extends north to 50° N and west to 170° E. From August to October, the high shrinks rapidly as the Aleutian Low deepens. The winter climate of the North Pacific is also closely related to the high pressure over Asia whose average central value exceeds 1040 mb in winter.

The long-term monthly mean position of the center of the Aleutian Low slowly shifts WSW over the Aleutian Islands from its October position over the northern end of the Alaskan Peninsula (near Kodiak Island) to its position just south of the Rat Islands (near the southwestern end of the Aleutians) from December through March. The mean monthly pressure typically remains well below 1000 mbs over a large region at the southwestern end of the Aleutian Islands from December through February. The 1020 mb isobar of the high and the 1005 mb isobar of the low are closest from December through February.

The climatological mean winds vary substantially from the winter to summer cases (Figure 3.6). More detailed monthly mean winds for the North Pacific can be found in the monthly issued *Pilot Charts of the North Pacific Ocean* (N.O. 55), and in the *U.S. Navy Marine Climatic Atlas of the World, Vol. II: the North Pacific Ocean.* Additionally, tabular meteorological data at Midway Island, the closest meteorological station to Hancock Seamount, is given in *Summary of Synoptic Meteorological Observations: Hawaiian and Selected North Pacific Island Coastal Marine Areas, Vol 2.* Considering each of these sources, and interpolating to Hancock Seamount, the following local climatological winds can be deduced. Winds are strongest during the winter months, with a mean speed of 15.5 knots (8.4 ms^{-1}) from December through February, and weakest in summer, with a mean speed of 10.5 knots (5.7 ms^{-1}) from May through September. Likewise, wind direction changes markedly from season-to-season. During the winter months, November through February, wind direction is variable, with winds coming from each quadrant about equally. January and February have a slightly dominant (> 60% of the time) westerly flow, however. Easterly winds predominate in the summer, particularly from July through October (> 80% of the time).

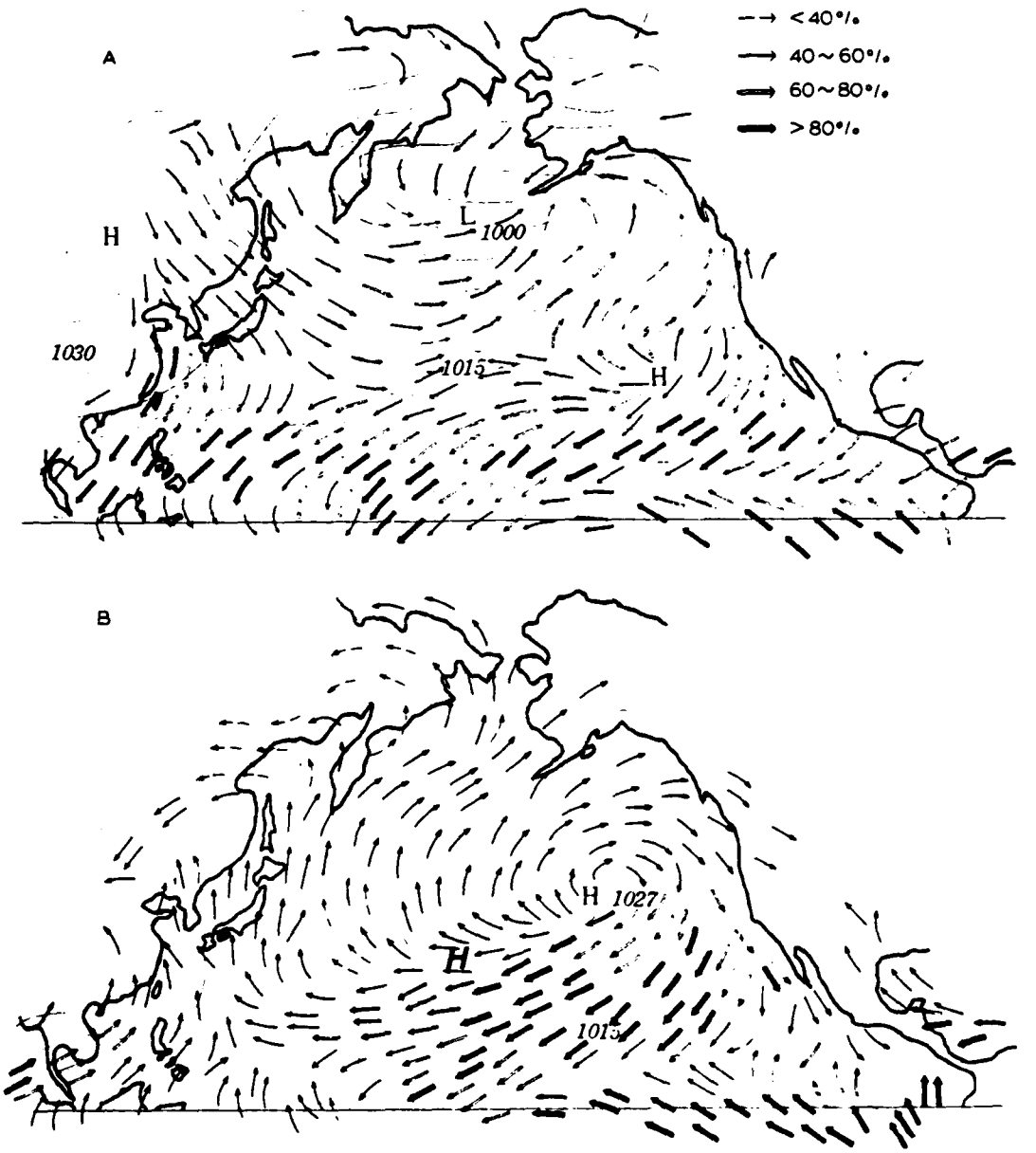

Fig. 3.6. Frequency of wind directions over the North Pacific in A) winter and B) summer. The approximate location of Hancock Seamount is indicated by the italicized H in B (it is under the 1015 mbs label in A). From Terada and Hanzawa (1984).

D. OCEANOGRAPHY

1. *Thermohaline Structure*

Hancock Seamount is situated along the North Pacific (oceanic) subtropical front, which migrates meridionally from winter to summer. In response to the seasonal atmospheric changes, the sea surface temperature (SST) distribution across the North Pacific changes significantly from winter to summer (Figure 3.7). At Hancock Seamount, the seasonal SST change is as much as $9^{o}C$. Vertical profiles of temperature also reveal the large seasonal change in the heat content of the surface layer (Figure 5.1). The surface layer salinity changes only slightly from winter to summer. It is much more variable in summer than in winter, probably due to the increased variability of the wind speed and hence mixed layer depth in summer.

2. *Surface Currents*

Since the purpose of this study is to examine hydrodynamic mechanisms associated with the observed high productivity over seamounts, any information regarding the flow impinging upon Hancock Seamount will improve the analysis. The surface currents in the vicinity of Hancock Seamount, which is situated in the center of the North Pacific gyre, are variable and not well described. The *Pilot Charts of the North Pacific Ocean* were used to estimate the long-term monthly mean surface currents at Hancock Seamount (Figure 3.8). This estimate is by no means an accurate representation of the true current at any particular time, but represents the time-averaged current as constructed from ship drift observations. Further, it was necessary to interpolate the currents of four nearby locations to estimate the currents at Hancock Seamount. Given these limitations, there is a relatively stronger (19-26 cms^{-1}) southward current from October through March. In the summer months, April through September, the currents are generally weaker and much more variable in direction, shifting from a northeastward flow in April and May to a southwestward flow in June, to northwestward flow in July, to southwestward in August, and eastnortheastward flow in September. Thus, in winter months, the surface flow is generally strongly southward, and, in summer months, it is too variable to generalize.

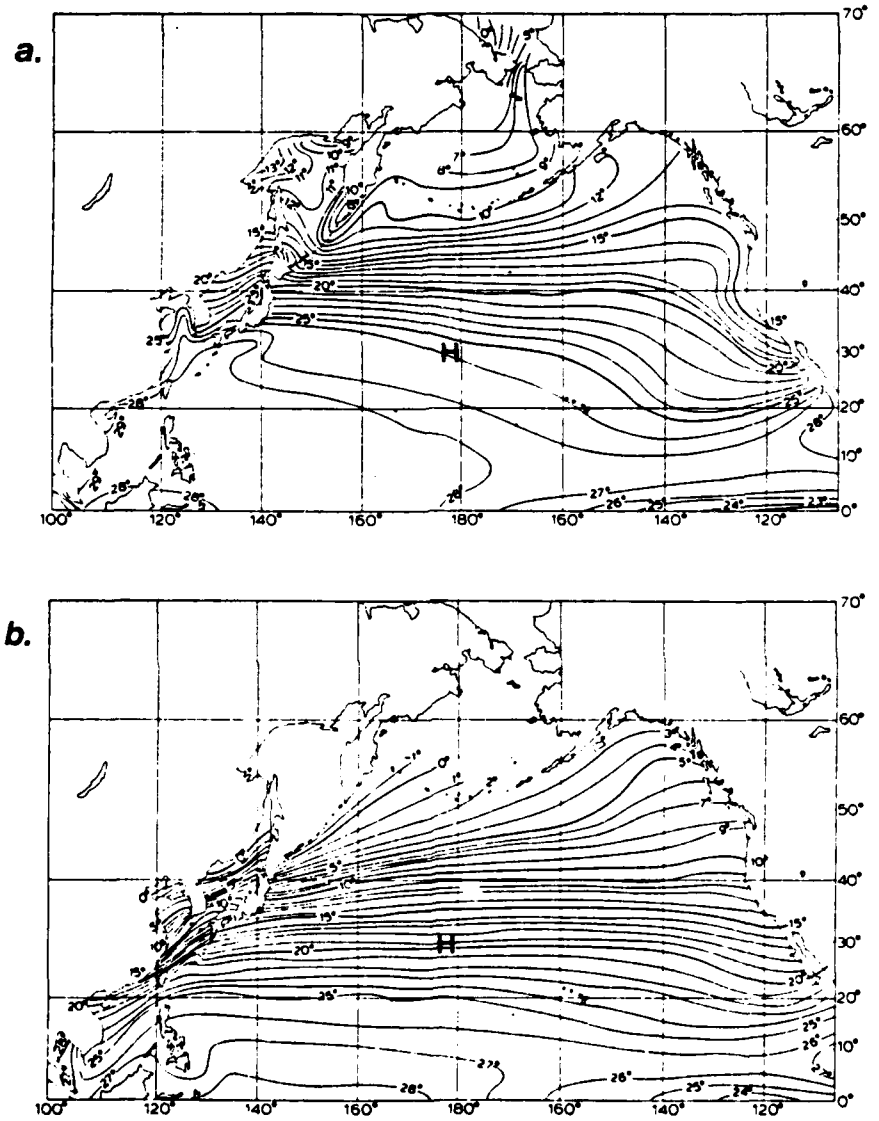

Fig. 3.7. Sea surface temperature (^{o}C) of the North Pacific in (a) August and (b) February. The approximate locations of Hancock Seamount are indicated by the large H's. From Terada and Hanzawa (1984).

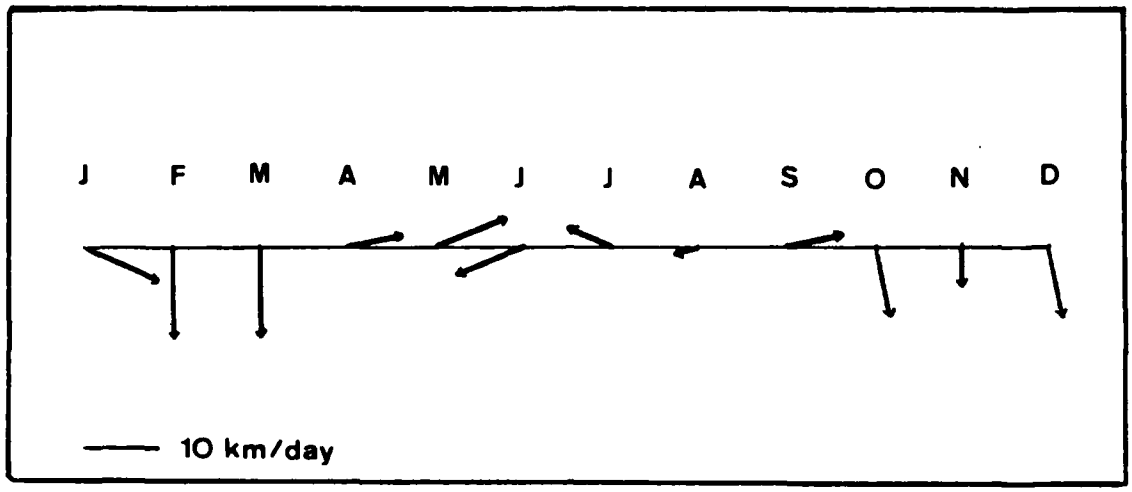

Fig. 3.8. Long-term monthly mean surface currents at Hancock Seamount, as constructed from the *Pilots Charts of the North Pacific Ocean*, which are based primarily on historical ship drift observations.

IV. SAMPLING SCHEME AND DATA DESCRIPTION

The data to be analyzed here were acquired during two cruises of the NOAA Ship TOWNSEND CROMWELL under the planning and direction of Dr. George Boehlert, Chief of Insular Resources Investigations of the Honolulu Laboratory. The objectives of these two cruises were to study the plankton and nekton communities of Hancock Seamount and their relationship to the physical environment. More specifically, it was intended to describe the hydrographic and current structure in a 40 km x 40 km square encompassing Southeast Hancock Seamount and to sample the plankton and micronekton in the context of the hydrodynamics. Secondarily, data on pelagic armorhead, alfonsin, and other fishes over the seamount were acquired. The field plan consisted of four components: hydrography and surface currents, plankton sampling, micronekton sampling, and hydroacoustics.

As described, the ocean conditions at Hancock Seamount differ distinctly from summer to winter. To understand the hydrodynamics over the seamount, and its relation to fisheries, it was necessary to investigate the physical and biological

environment of the seamount in both summer and winter. Thus, the cruises were planned such that the first, TC8405, was undertaken in summer from June 18 to August 13, 1984, and the second, TC8501, was undertaken in winter from January 16 to March 8, 1985. The TC8405 cruise consisted of two sets of hydrographic data, one taken at the beginning of the cruise, which will herein be referred to as TC8405A, and one at the latter end of the cruise, herein to be referred to as TC8405B.

A. XBT/CTD SURVEYS

The three hydrographic surveys over Southeast Hancock Seamount were conducted July 9-10 (TC8405A), July 26-28 (TC8405B), and January 31- February 1 (TC8501). For both the TC8405A and TC8405B surveys (Figure 4.1), 1000 m CTD casts were made at the corners and midpoints of the perimeter of the 40 km x 40 km sampling grid, as well as duplicate shallower 240 m casts over the seamount summit. A Plessey Instruments CTD was used for all of the casts. Inside the 40 x 40 km^2 area, three XBT transects, crossing over the summit, were made to provide a closely spaced quasi-synoptic picture of the thermal structure of the upper layer around Southeast Hancock. These transect lines were run east-west, NNW-SSE, and NNE-SSW, such that they equally partitioned the area. The XBT station spacing varied from 5 km near the perimeter to 1.25 km near the summit. The two summer surveys used Sippican T-7 XBT probes, which typically provide a temperature profile to a depth of about 750 m. The salinity data from the CTD casts were linearly interpolated spatially to the XBT station positions. Using a rosette sampler, water samples were collected for chlorophyll and salinity analysis in the upper 240 m over the seamount and at the corners of the 40 x 40 km^2 survey area. Twelve samples were collected at depths of 240, 200, 170, 140, 120, 100, 80, 60, 50, 25, 10 m and surface at each of the 12 hydrocast stations. Five hundred milliliters of seawater from each sample were filtered through a 2.4 cm diameter glass microfiber filter at sea, fixed in 90% acetone, sealed in 10 ml Nalgene filmware bags, and frozen for analysis at the laboratory. For calibration purposes, a reversing thermometer was placed on the deepest sample bottle.

The TC8501 survey used a sampling scheme similar to the TC8405 surveys, but XBT transect lines were slightly longer and station spacing was closer. The station spacing near the seamount summit was reduced to a only 0.5 km. The TC8501 survey used only the shallower Sippican T-4 probes, which provide data to a depth of only 450 m. Water samples for chlorophyll analysis, and salinity and temperature calibration were taken as described for the summer surveys.

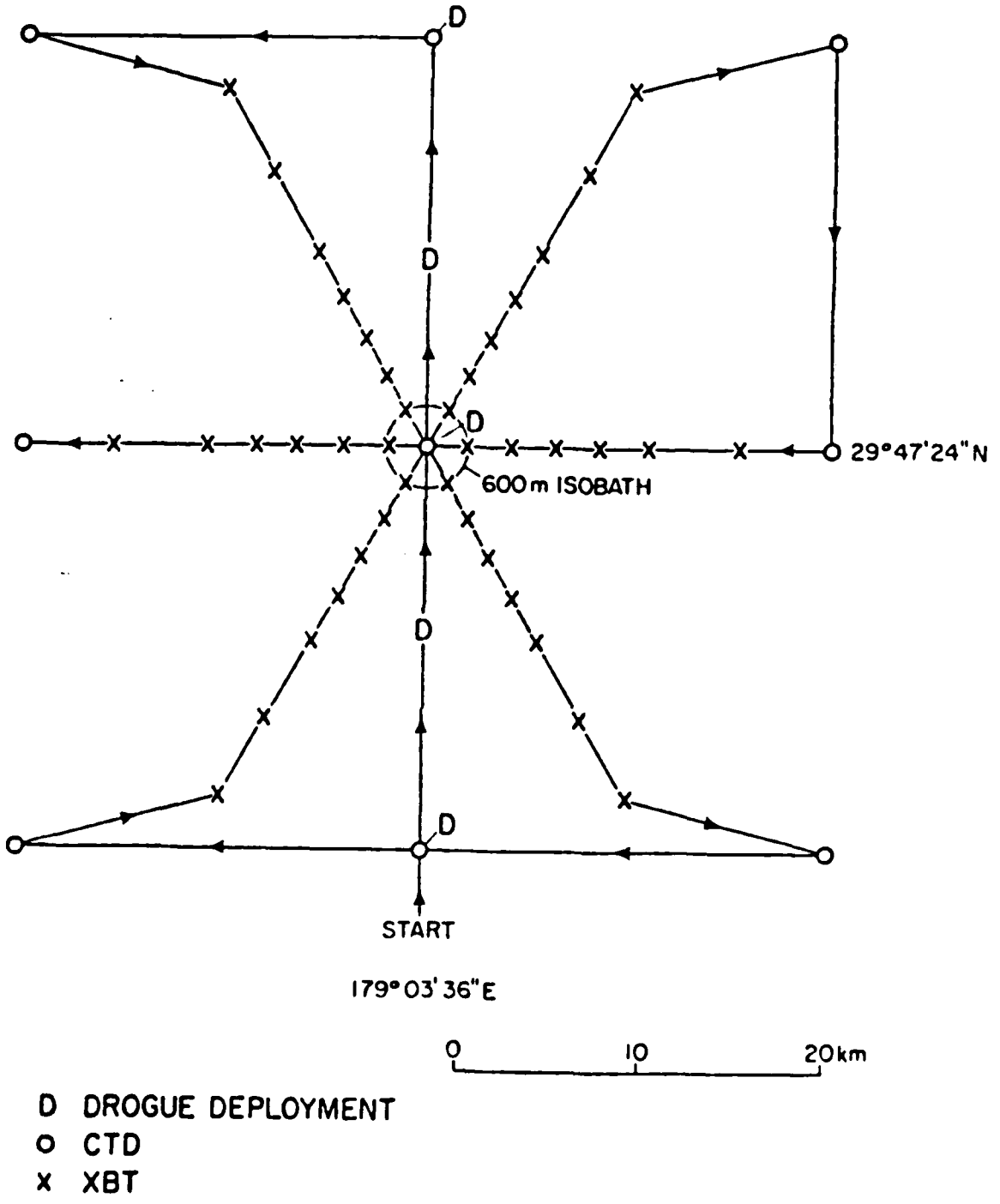

Fig. 4.1. Sampling scheme for the TC8405A and TC8405B summer surveys over Southeast Hancock Seamount.

1. *Limited Navigational Control*

Due to limited navigational aids in the vicinity of Hancock Seamount, accurate and continuous position determination was not possible during any of the three surveys considered here. There were no nearby terrestrial features to enable accurate visual or radar bearings. Additionally, Hancock Seamount is located in a region not covered by any continuous, high-accuracy, radionavigation systems, such as Loran-C. Station positioning for the hydrographic surveys was therefore restricted to satellite, Omega, and celestial navigation. The true worldwide Omega system accuracy, to one standard deviation, is between 1.8 and 3.7 km (Maloney, 1978). Likewise, the accuracy of celestial navigation, which is dependent upon the ability of the observer and weather conditions, is the order of 1-5 km. Clearly, neither of these two means of navigation were adequate for the high-resolution hydrographic surveys undertaken here.

Although the NAVSAT satellite navigation system is accurate to 50-100 m for a moving ship, it does not provide continuous positioning. Reliable satellite position fixes may be obtained only when an orbiting satellite has a maximum altitude, relative to the observer, between 15^{o} and 75^{o} . As a general rule, each satellite will yield four fixes per day, two on successive orbits, and two more on successive orbits twelve hours later. Ideally, a NAVSAT fix could be obtained about every 90 minutes. However, this sequence may be disturbed, as the satellite, while above the ship's horizon, may pass at too great or too small an altitude to permit position determination. The number of usable satellite passes is also a function of the observer's latitude, since the separation distance between successive polar orbits increases toward the equator. During the surveys, there were periods as long as six hours between satellite fixes.

Thus, for the surveys to be analyzed here, navigation and station positioning were primarily by dead reckoning between irregularly spaced satellite fixes. Bathymetric navigation, using the topography of the ocean floor to obtain positioning information, was used to improve the dead reckoning positions. Bottom depths were recorded at each of the XBT/CTD stations. Using available satellite fixes, dead reckoning positions, courses and speeds, station bottom depths, and the available bathymetric charts, hand-contoured bathymetric charts of the survey area with station positions were drawn (Figures 4.2, 4.3, and 4.4). These charts are unverified and are likely erroneous on an absolute scale of 1-3 km. However, the relationship between station positions and depth at the respective positions is quite close. And, since this investigation is

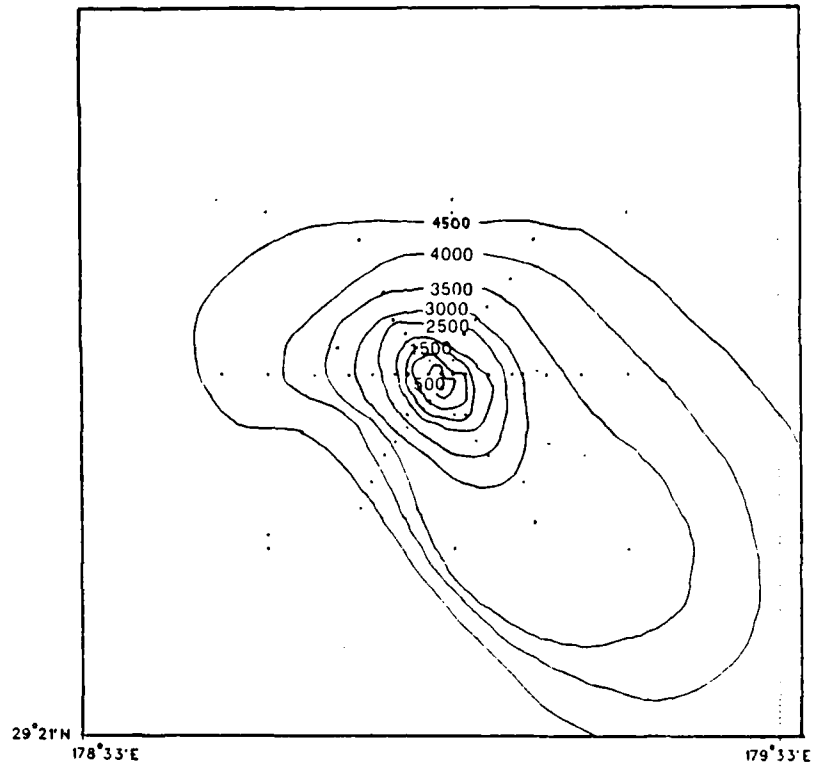

Fig. 4.2. Station positions and hand-contoured bathymetry for the TC8405A survey. Positions and depths are based on all available positioning information, including satellite fixes, dead reckoning, station bottom depths, and the available bathymetric charts.

concerned with flow/topography interactions, absolute positioning, although very desirable, was not as critical as the determination of station positions relative to the bathymetry. Hopefully, these objectively contoured charts of the bathymetry and station positioning will minimize the errors in the analysis.

2. *Data Processing and Analysis*

The CTD data, originally recorded on magnetic discs, were initially processed at the Honolulu Laboratory using CTD processing software developed at NOAA's Pacific Marine Environmental Laboratory (PMEL). The program accepts the original data file with frequency, conductivity, and density data, and, after editing, outputs depth, temperature, salinity, sigma-T, and the Brunt-Vaisala frequency. A depth editing scheme verified that the depth increased, deleting points with decreasing depth. A

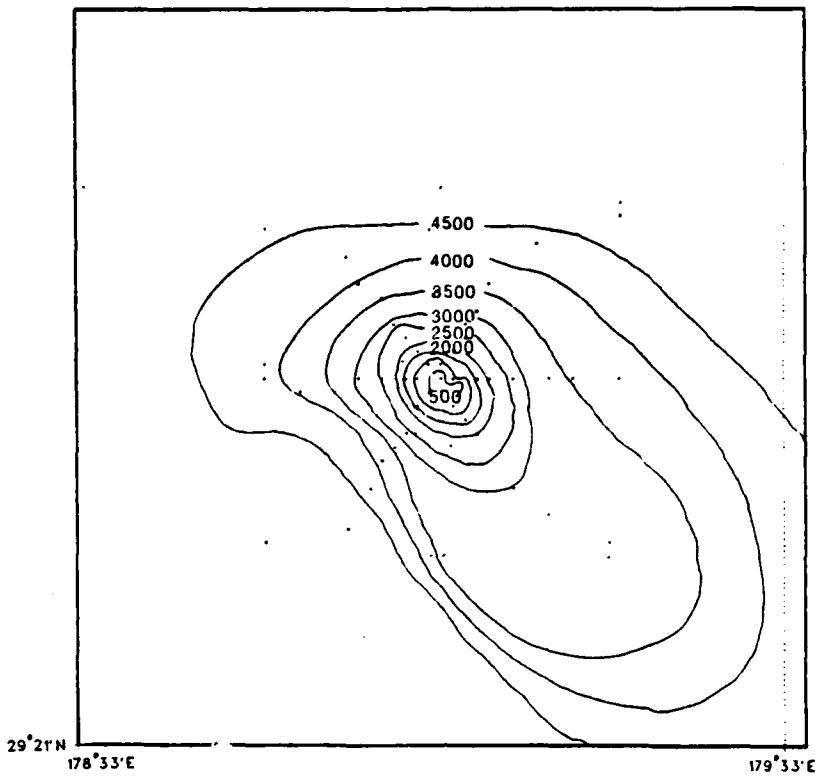

Fig. 4.3. Stations positions and hand-contoured bathymetry for the TC8405B survey.

single point editing routine checked the middle of three data points against the outer two, deleting points not satisfying specified critical limits. The final output data was then copied to magnetic tape for additional processing and analysis on the mainframe at NPS.

The XBT data were recorded on a Sippican analog chart recorder and later hand digitized. Temperature/depth pairs were digitized at 0.5°C intervals. These digitized temperature profiles were then plotted side-by-side and visually checked for errors (Figure 5.1).

B. SURFACE DROGUE DEPLOYMENTS

Drifting buoys with drogues at 10 m were deployed on three occasions to try to determine the absolute velocities of the surface currents in the vicinity of the seamount. According to the cruise report (Uchiyama, 1984), the drogue consisted of a 76-liter

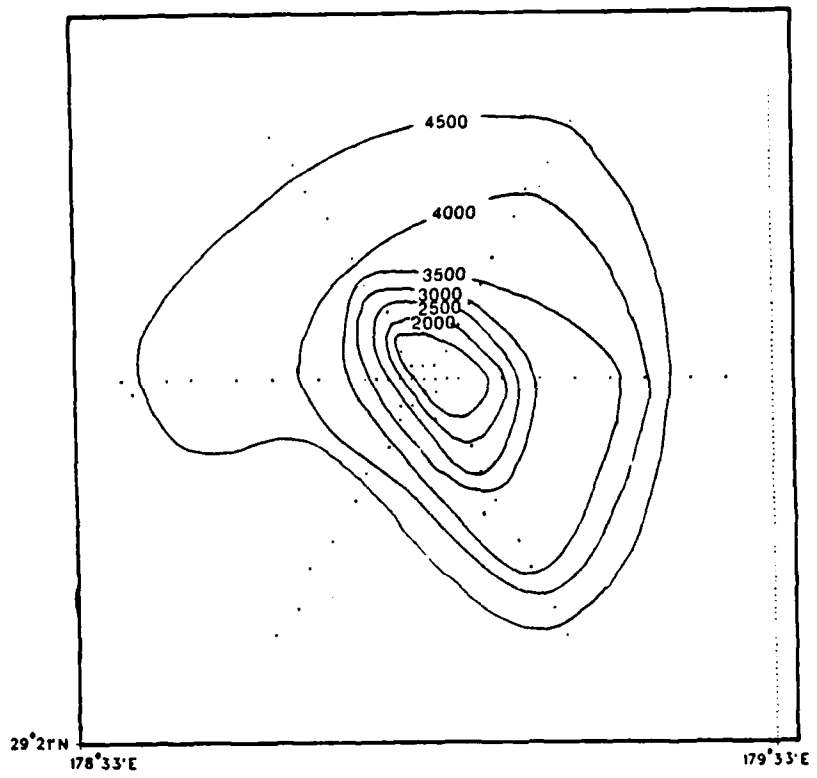

Fig. 4.4. Station positions and hand-contoured bathymetry for the TC8501 survey.

plastic garbage can suspended 10 m below the surface. The surface assemblage consisted of an inflatable float 50 cm in diameter attached to a 4 m long bamboo pole about 1.5 m from the bottom end. A triangular plastic flag with markings was attached to the top of the pole. A strobe light was also attached to the top of the pole to enable tracking at night. A 6-volt battery to power the strobe was attached to the pole near the float. There was a 6 kg weight attached to the bottom of the pole to keep it upright. The garbage can was suspended from the float by a 10 m 3/8-inch polypropylene line with a 3 kg weight on the bottom. Additionally, there was a longline radio beacon with a range of 150 nm attached to the float with a 10 m line.

A marker float was moored over the summit of Southeast Hancock to use as a navigational reference point during the deployments. This marker consisted of a float assembly similar to that used for the drogue surface floats, except it had a pot light

marker with a visual range of about 1 km and a 1 m sack filled with aluminum cans to act as a radar reflector. The marker was anchored on the seamount with a fish trap and 730 m of line, allowing a scope of about 3:1.

On July 7, five drogues were set 10 km apart on a north-south track, with the center drogue over the summit of Southeast Hancock. All drogues moved northward in a C-shaped pattern against the wind. All drogues were retrieved about 12 hours after deployment due to a couple of inoperable strobes. A single drogue was redeployed over the summit on July 8, and tracked for 41 hours. It remained over or very near the summit for about 24 hours before beginning to move southward. On July 13, three drogues were deployed 5 km apart on a north-south track, again with the center drogue over the summit. One of these drogues was tracked for only nine hours, when it was retrieved due to a weak radio transmission. The other two drogues were tracked for about 25 hours. Overall, the southern drogue moved northwest, the summit drogue moved due west, and the northern drogue moved southwest. Although these deployments were generally too short to satisfactorily remove tidal effects, the movements of the three July 13 drogues to the northwest, west, and southwest, respectively, at least qualitatively agree with the ship drift derived climatological surface currents (Figure 3.8), which showed southwest flow in June and northwest flow in July.

The July 7-8 and July 13-14 drogue deployments were made under windy conditions with moderate sea and swell. Although drogue movement did not appear to be significantly affected by the wind, visual tracking was difficult. The final drogue deployment, on July 22-23, was conducted during calm wind and sea conditions resulting from a stationary low pressure region over Hancock Seamount. During this final drogue deployment, five drogues were deployed as follows: over the summit, and 5 km to the north, south east, and west of the summit. With the calm sea condition, it was possible to track all five drogues from above the seamount with the polaris and radar. These drogues all appeared to move north initially as in the July 7-8 observations, but then the north, summit, and west drogues drifted south and westward. The east and south drogues started to the north and then drifted southward away from the seamount. All five drogues were tracked for only 14-15 hours, which is too short to allow tidal constituents to be delineated.

Surface current measurements could not be made during the winter cruise due to high winds and seas.

V. THERMOHALINE STRUCTURE OVER SOUTHEAST HANCOCK SEAMOUNT

A. VERTICAL PROFILES OF TEMPERATURE, SALINITY, AND STABILITY

1. *Temperature and Salinity Profiles*

For both the summer TC8405A and winter TC8501 cruises, temperature and salinity profiles were plotted side-by-side (staggered) to allow a visual inspection of the data (Figure 5.1). Although the profiles shown were obtained from CTD casts, similar staggered plots of temperature were made for the XBT transects. The TC8405A temperature profiles show warm surface temperatures (27°C), strong gradients in the seasonal thermocline, and moderate gradients in the main thermocline. By contrast, the TC8501 temperature profiles show much cooler winter surface temperatures (18°C), much weaker gradients in the seasonal thermocline, and similar moderate gradients in the main thermocline. In the summer, salinity varies significantly in the upper 40-60 m, increases to a maximum between 120 and 200 m, decreases to a minimum between 650 and 750 m, and then gradually increases again to the the bottom of the casts (1000 m). Although no data were acquired below 1000 m, it appears that the salinity increases gradually below the 1000 m level. In the winter, salinity has a maximum at the surface, where the variability is negligible, followed by a weak negative salinity gradient to a minimum between 680 and 750 m, followed by slight increase to the bottom of the casts.

2. *T-S Plots*

T-S plots for the TC8405A and TC8501 surveys (Figure 5.2) display much more spatial variability in the upper ocean for the summer than for the winter. The T-S plot for the TC8405B survey looks virtually identical to that for TC8405A, therefore it is not shown. Below the surface layer, or below the 17°C isotherm, the variability is quite small for all three surveys.

3. *Brunt-Vaisala Frequency*

A large difference in the vertical thermohaline structure between summer and winter surveys is evident in plots of the Brunt-Vaisala frequency (Figure 5.3). The two summer survey plots show a high-stability layer at the seasonal thermocline between 40 and 200 m. By contrast, no such stable layer exists during the winter survey, which shows no indications of a seasonal thermocline. Again, higher spatial variability in summer is evidenced by the standard deviation curves.

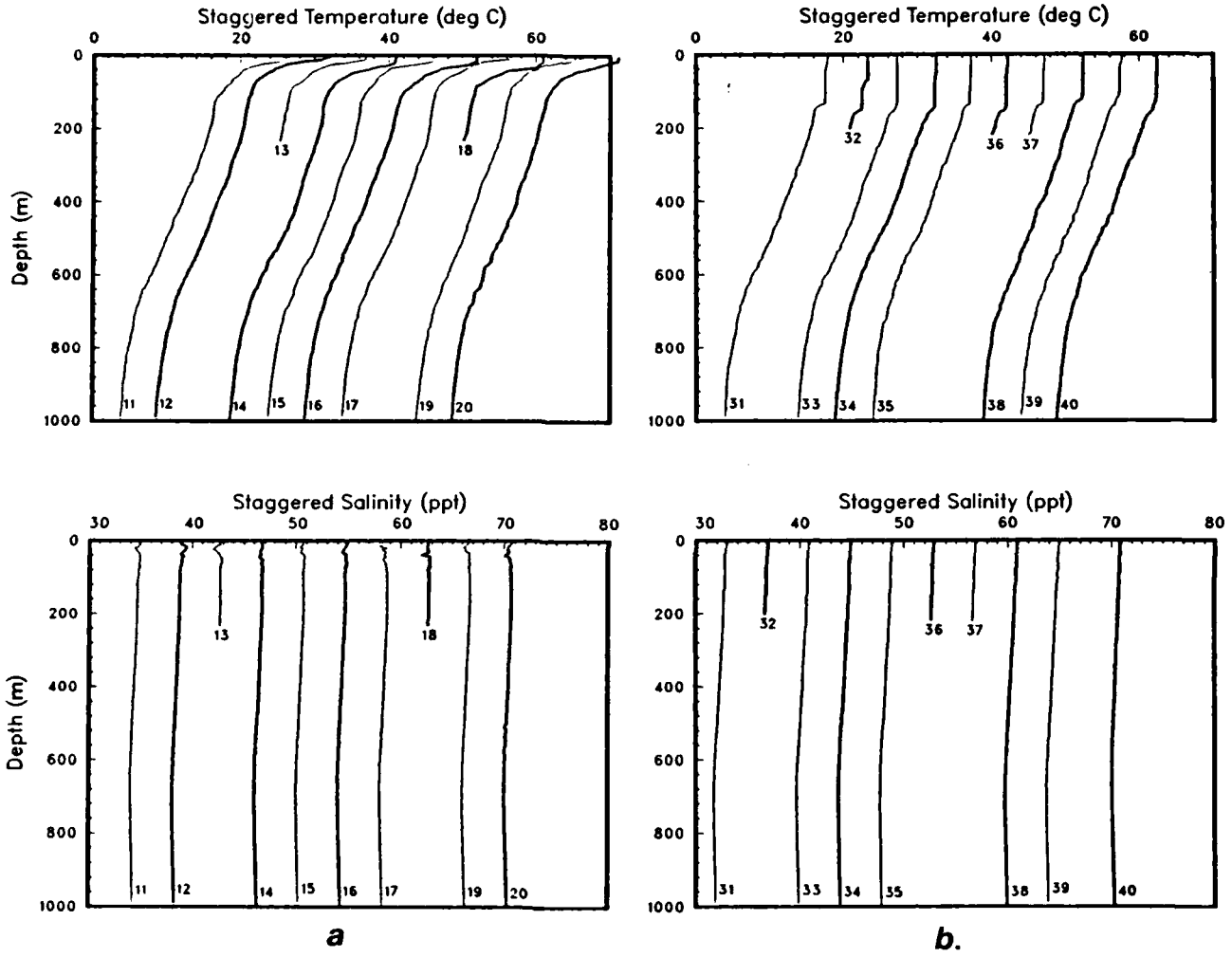

Fig. 5.1. CTD temperature profiles, staggered by multiples of 5°C, and salinity profiles staggered by multiples of 4 ppt for (a) TC8405A, and (b) TC8501.

B. TEMPERATURE TRANSECTS

As discussed in Chapter 2, one of the most readily distinguishable indications of the existence of a Taylor column is the presence of a thermal dome or an uplift of the isotherms over or near the seamount. Such deflections of isotherms over a seamount are likely to be superimposed upon other processes affecting the vertical structure, and might therefore be difficult to detect. Also, sensor variability, particularly for the XBT transects, is likely to cause some small, erroneous isotherm deflections. With this in mind, vertical transects of the temperature field, as produced from the XBT/CTD survey data, were carefully examined. In this section, the surveys, as well as the individual transects, are presented in the chronological order in which they were acquired. Although the actual transects were NNW-SSE, SSW-NNE, and E-W, the vertical section plots are labeled NW-SE, SW-NE, and E-W, respectively. The time required to complete each of the three surveys was 27 hours, 24 hours, and 31 hours for the TC8405A, TC8405B, and TC8501, respectively. Therefore, except where it is noted, the remaining discussion will presume synopticity.

1. *TC8405A*

The thermal structure over Southeast Hancock Seamount for the TC8405A survey is depicted in the three vertical temperature transects shown in Figure 5.4. (Later, the same data are presented in horizontal, rather than vertical sections). The strong seasonal thermocline in the upper 100 m is evident. Hence, the regime may be treated as a two-layered system.

There are also numerous deflections of the isotherms, suggestive of mesoscale variability. The NNW-SSE transect reveals an apparent dip of the isotherms over the flanks of the seamount, with a noticeable uplift directly over the seamount. The horizontal length scale of this apparent thermal doming over the seamount appears to be about 30 km. Using the following equation from Pond and Pickard (1983):

$$\lambda_1 = (g'(h_1 h_2)/(h_1 + h_2))^{1/2}/|f| ,$$

the first baroclinic Rossby radius of deformation for a two-layer fluid was calculated to be 18.1 km, where $g' = (\Delta\rho/\rho)(g)$ is the reduced gravity, $h_1 = 100$ m, and $h_2 = 900$ m. If the horizontal length scale of the thermal doming is indeed O(30 km), then rotational effects are of the same order as the buoyancy effects. The dipping and uplifting do not appear to penetrate beyond the strong pycnocline into the upper layer. Further, the deflections appear to be superimposed upon a general downward slope of

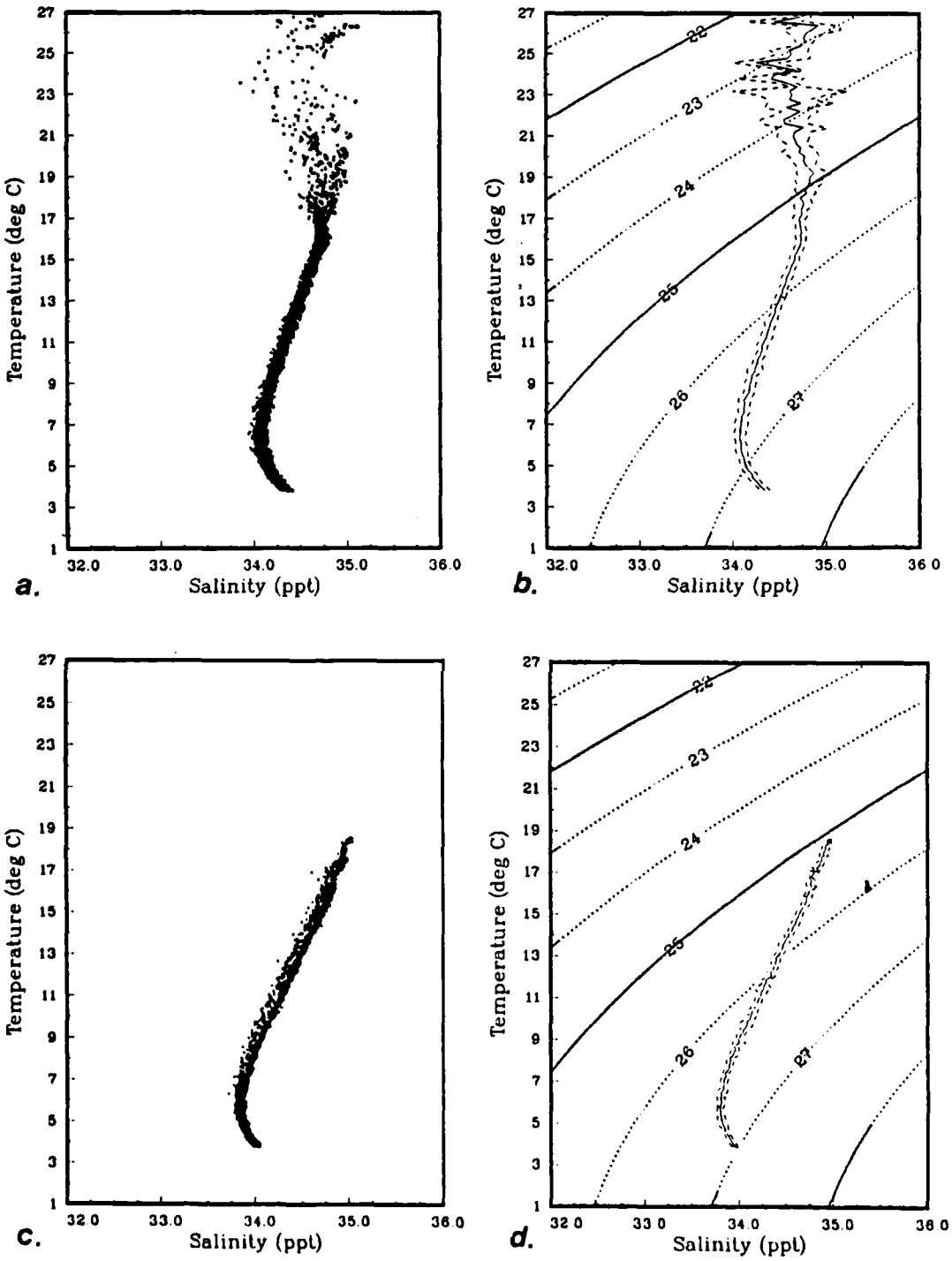

Fig. 5.2. (a) T-S pairs and (b) mean T-S relation, with + and - one standard deviation curves for TC8405A; (c) T-S pairs and (d) mean T-S relation for TC8501.

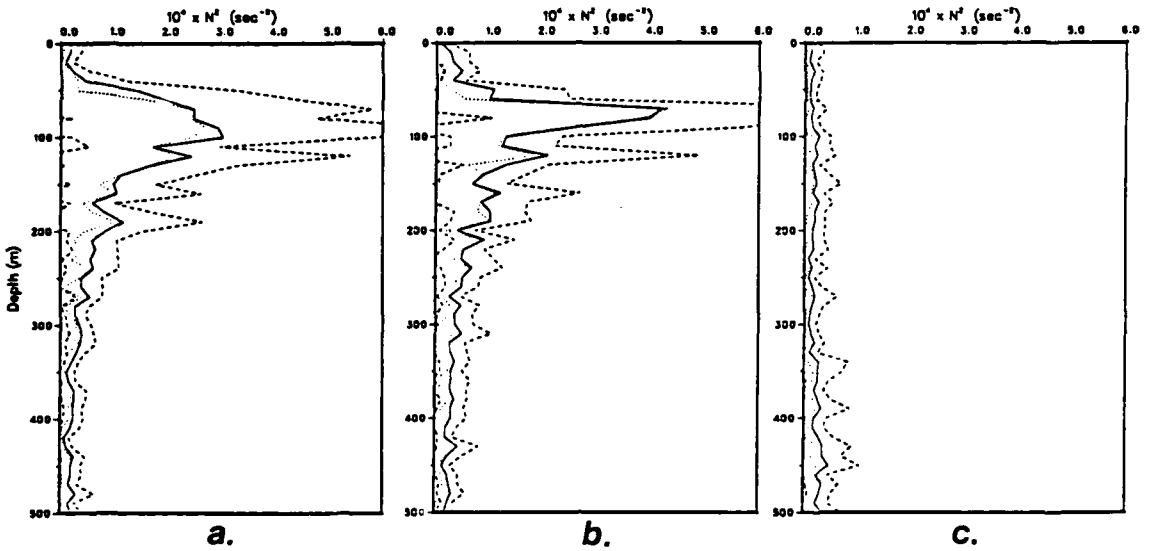

Fig. 5.3. Brunt-Vaisala frequency for (a) TC8405A, (b) TC8405B, and (c) TC8501. Mean N^2 profile (——), with + and - one standard deviation (---). The N^2 profile from T(z) and S(z) is also shown (...).

the isotherms in the upper 200 m from the SSE corner to the NNW corner, suggesting a southwestward component of the surface flow. The small wave-like deflections, as exhibited by the 16°C isotherm for example, may be partially due to XBT probe variability.

Whether or not this type of thermal doming indicates the existence of a Taylor column or related feature remains undetermined. The actual flow over a seamount is likely to be much more complex than steady state theory predicts. Observations represent a superposition of effects from an array of physical processes occurring in the ocean. Therefore, it is unlikely that perfect, symmetric upward deflections of the isotherms over a seamount, as predicted by steady state barotropic Taylor column theory, will ever be observed, at least not without a time series of observations. With this in mind, the upward deflections shown here and in many of the vertical sections which follow may be as good an observation of Taylor column characteristics as can be expected from synoptic or quasi-synoptic data of this nature.

The SSW-NNE transect exhibits a sharp dip of the isotherms followed by a similarly sharp uplift of the isotherms as the seamount is approached from the SSW. Here, the isotherms are shown to deflect downward about 60 m and then upward

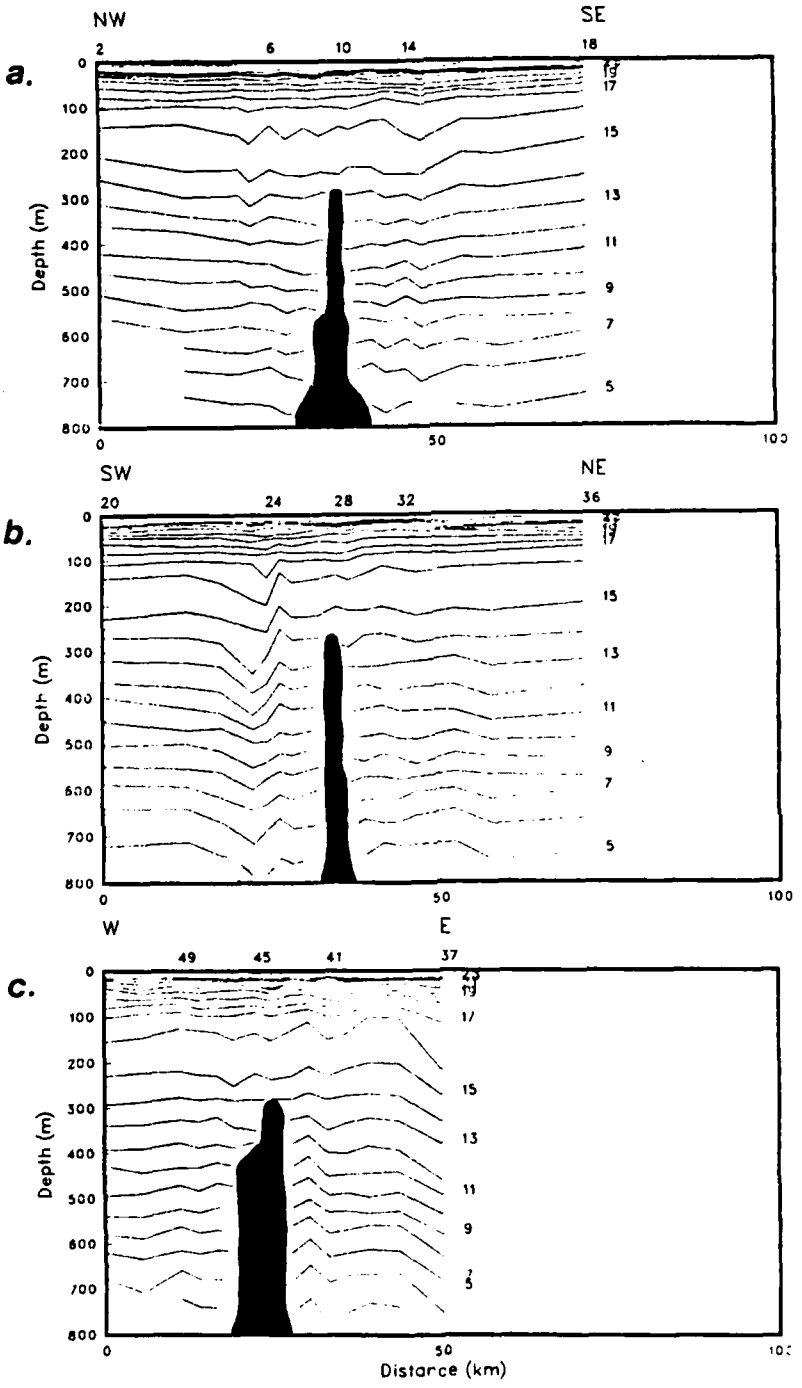

Fig. 5.4. TC8405A vertical temperature transects showing along-track isotherms (^{o}C) for (a) NNW-SSE transect, (b) SSW-NNE transect, and (c) W-E transect. Tick marks along the upper horizontal axis show station positions. Some station numbers are given.

about 75 m. This sharp deflection of the isotherms is reminiscent of deflections associated with mountain lee waves. As discussed in Chapter 2, scale analysis showed the summer surveys to fall into Gill's (1982) quasi-geostrophic flow regime for mountain waves. Thus, this strong deflection of the isotherms may represent an oceanic mountain lee wave. Although this is inconclusive evidence, it certainly supports the speculation that wave-topography interactions might provide an upwelling mechanism by which nutrients could be transported to the euphotic zone. This point will be further discussed as more data are presented.

The SSW-NNE transect also shows an uplift of the isotherms over the seamount, similar to that mentioned for the NNW-SSE transect. The dipping of the isotherms over the NNE flank is less pronounced than observed for the NNW-SSE transect. The horizontal length scale of this thermal uplift appears to be 35-40 km. Again, the effects seem restricted to the lower layer. There is a gentle slope of the isotherms within the upper 200 m of water downward from the NNE corner to the SSW corner, suggesting a possible surface flow to the southeast.

In the E-W section, there are also indications of an uplifting of the isotherms over the seamount. This transect is about 20 km shorter than the first two transects. If the eastern limit of the thermal doming coincides with the eastern limit of the transect, then it looks as though the horizontal scale of the uplifting is 45-50 km. The eastern limit of the transect reveals a sharp downward isotherm deflection of 80-100 m. Without a hydrographic station further to the east, the validity of this strong deflection cannot be confidently ascertained. Although the deflections of the isotherms appear to penetrate further into the upper layer than in the other transects, they nevertheless seem to lose their identity well before the surface is reached.

Summarizing, all three vertical sections of the TC8405A survey showed thermal doming over horizontal length scales of 30-50 km, apparently confined below the pycnocline. Also, intense vertical motions associated with wave-topography interactions are suggested by the strong deflection of the isotherms shown in the SSW-NNE transect.

2. *TC8405B*

The TC8405B survey, conducted 16 days after the TC8405A survey, had both similarities and differences relative to the earlier survey (Figure 5.5). For example, the seasonal thermocline remained in the upper 100 m, as well as deflections of the isotherms over the seamount.

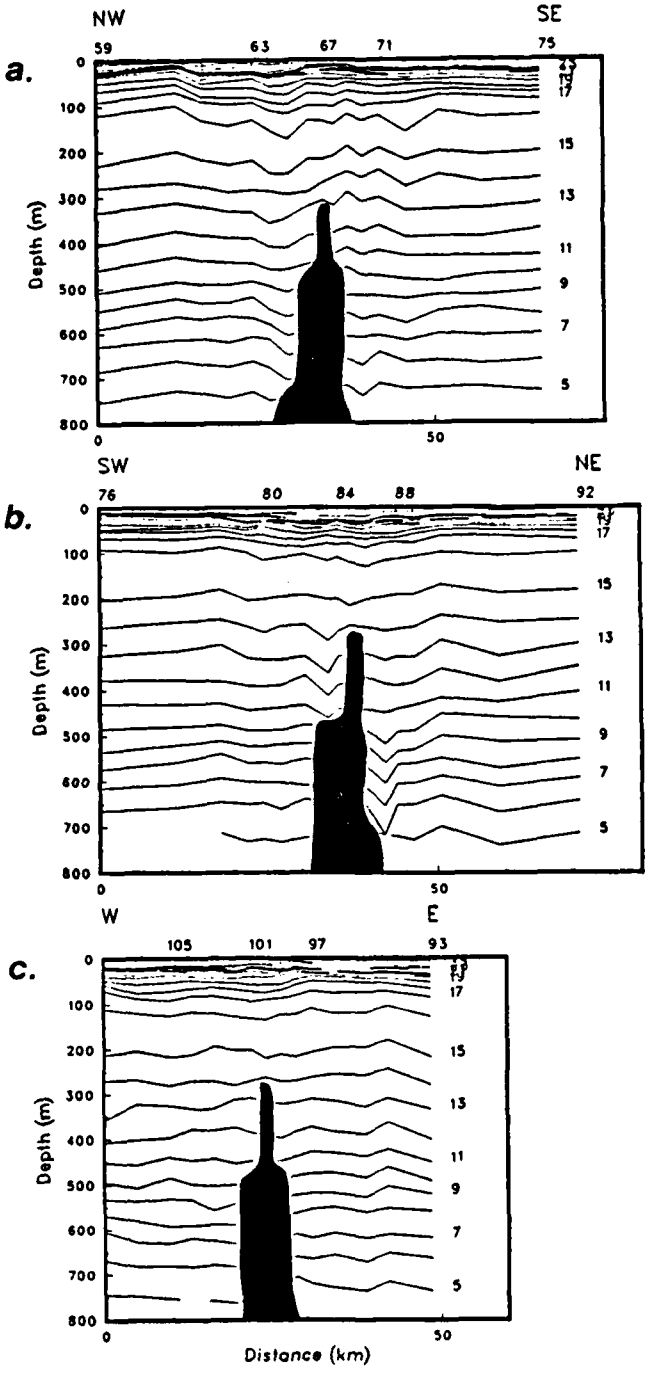

Fig. 5.5. TC8405B vertical temperature transects slowing along-track isotherms (^{o}C) for (a) NNW-SSE transect, (b) SSW-NNE transect, and (c) W-E transect.

Starting with the NNW-SSE transect, there does not appear to be an overall slope of the isotherms across the width of the transect in the upper 200 m, as was observed for the TC8405A NNW-SSE transect. There is a slight depression of the isotherms in the upper 100-150 m across a width of about 35 km, centered over the seamount. Below this, there again appears to be some thermal doming over the summit, perhaps displaced slightly to the SSE and with a smaller horizontal length scale of about 20 km. The extreme NNW station indicates a continued downward slope of the isotherms, suggesting a possible larger scale thermal doming. The doming of the isotherms over the summit has a positive slope from NNW to SSE. This slope is superimposed on a similar larger scale slope of the isotherms across the transect below the 200 m level. This localized sloping of the thermal dome may be associated with the downward deflection of the isotherms just to the NNW of the summit. Downward deflections of isotherms over seamount slopes, such as shown here and in the vertical sections for the TC8405A survey, also appear in many similar sections presented by others (Meincke, 1971; Owens and Hogg, 1980; Roden and Taft, 1985; Genin and Boehlert, 1985). Of these, only Meincke (1971) mentions this depression of the isotherms over seamount slopes. He explains the observed depression as a consequence of a varying vertical range of the tidal mixing regime and the lateral diffusion of momentum related to a "quasi-geostrophic" current.

The SSW-NNE transect appears to have many of the same features, but with smaller magnitudes. Again, there is no overall slope of the isotherms within the upper 200 m. A slight depression of the isotherms, having a horizontal length scale of about 30 km, is again present in the upper layer, but here the depression appears to penetrate down to about 500 m. It also appears to be superimposed on a larger scale doming over the seamount. This apparent doming has a horizontal length scale of 60-70 km. As with the NNW-SSE transect, it would have been desirable for this transect to have been longer, extending well away from the seamount. The thermal doming appears to extend further to the SSW than does the transect, just as the thermal doming for the NNW-SSE transect showed indications that it might extend further to the NNW. There are numerous instances where thermal doming, associated with interactions of the flow with the Emperor Seamounts, extends well over 75-100 km from the summit (Roden and Taft, 1985).

As with the SSW-NNE transect on the TC8405A survey, this transect on the TC8405B survey displays intense vertical deflections of the isotherms, again suggestive

of strong wave-topography interaction and vertical motion. Below the 450 m level, there is an intense 50 m depression of the isotherms over the NNE flank of the seamount. Above the 450 m level there is a strong depression over the SSW flank. Although there is not enough evidence to make any conclusion with certainty, it appears that these two features may be related. This feature and the strong vertical deflection described for the TC8405A survey display similar form and magnitude, but here the depression is shifted about 20 km to the NNE. Thus, we have more suggestive evidence supporting the proposed wave-topography interaction hypothesis.

The E-W transect shows the typical strong stratification of the upper 100 m, but with a gentle wave-like character. Below the pycnocline, there are no sharp deflections of the isotherms, nor is there a well-defined thermal dome. Because the isotherms tend to slope downward at both ends of the transect, the presence of a large scale thermal feature is suggested. To the east of the seamount the isotherms are raised slightly on average compared with those to the west.

3. *TC8501*

Recall, the transects for the winter TC8501 survey were longer and used only the shallower T-4 XBT probes. The longer transects were helpful in identifying larger scale thermal features and their approximate horizontal scales. The shallower probes restrict the study to the upper 400-450 m, thereby limiting the conclusions which can be made about the vertical structure around the seamount. The vertical sections differ markedly from those of the two summer surveys. No longer is there a strong seasonal thermocline in the upper layer, nor the associated two-layer system. With weak stratification, deflections of the isotherms caused by the topography are expected to extend throughout the water column. Thus, if Taylor columns are present, it is expected that they will be of the barotropic type.

Commencing with the E-W transect, the vertical section shows the isotherms to the east of the seamount to be relatively level from the surface to 400 m, except at the eastern extreme where they start to turn downward. To the west of the seamount, the isotherms slope steeply downward to the west, and then fluctuate in a wave-like manner. Overall it appears as though there is a large thermal dome extending from about 20 km west of the summit east to beyond the eastern limit of the transect. This thermal doming extends from the surface to the maximum depth of the casts, 400-450 m. The isotherms deflect upward 60-70 m. This is clearly another case where it would have been desirable to have a longer transect. Assuming the downward trend

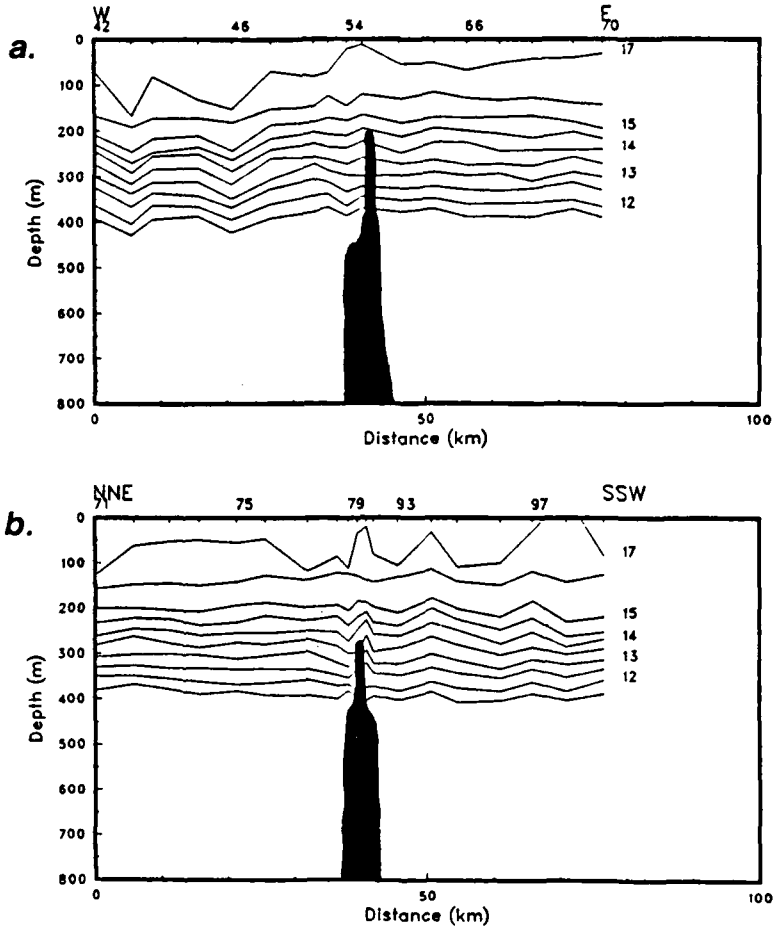

Fig. 5.6. TC8501 vertical temperature transects showing along-track isotherms (^{o}C) for (a) W-E transect and (b) NNE-SSW transect.

of the isotherms at the eastern end of the transect continues in a manner symmetric with the downward slope at the western end, the horizontal length scale of the thermal doming would be 60-65 km, which is larger than all but one of the scales noted for the summer surveys. Recalling that many of the isotherms for the summer surveys are at least slightly bent downwards at both ends of the transects, it is not known whether the length scales are indeed shorter for summer conditions or whether they merely misinterpreted due to the limited transect length. If the horizontal length scales do differ from summer to winter, what is the physical explanation? A time series of the temperature structure along the transects or even a single transect may be necessary to answer this question.

In the NNE-SSW transect, a narrow, prominent thermal dome located directly over the summit is easily recognized. As with the E-W transect, this feature extends from the surface to the maximum depth sampled, 450 m. The isotherms deflect sharply upwards 40-80 m, and then sharply downward on the other side of the summit. As with the summer surveys, there is an apparent dip of the isotherms to the NNE of the summit, next to the thermal dome. On the larger scale, there is an apparent uplifting of isotherms from about 25 km NNE of the summit to about 30 km SSW of the summit. This larger feature is more difficult to recognize and appears to be confined to the depth range between 125 and 325 m. Interestingly, as with the E-W transect, which had relatively level isotherms to the east of the seamount and wave-like isotherms to the west, this transect displays relatively flat isotherms NNE of the seamount and more variable wave-like isotherms to the SSW. Thus, both transects suggest relatively high variability to the west of the summit and relatively low variability to the east. If it is assumed that the incident flow is from the north, as suggested by the climatological mean (Figure 3.8), then this east-west change in variability can be explained by upstream flow-topography interactions. With reference to Figure 3.1, showing the bathymetry of Hancock Seamount, there are no topographic barriers to the north or northeast of Southeast Hancock, but there are several other peaks to the northwest (for example, Northwest Hancock Seamount). Thus, incident flow from the north would be unimpeded to the north and northeast of the Southeast Hancock, but would encounter these other topographic features to the northwest. This could induce the observed spatial variability of the thermal structure.

Drogue measurements could not be made during this survey. It would have been interesting to compare the high variability of the temperature structure observed to the west, and the low variability observed to the east, with the surface currents.

The NNW-SSE transect shows a large scale thermal dome from about 30 km NNW of the summit to 30-40 km SSE of the summit, again suggesting a horizontal length scale of 60-70 km. This feature extends vertically from 450 m to at least 100 m, and perhaps all the way to the surface. There is a narrow uplift directly over the summit superimposed over the larger scale dome. The isotherms deflect upwards about 50 m. There does not appear to be a large-scale slope of the isotherms across the transect. Based on an expanded scale (Figure 5.7), the isotherm deflections over the seamount are more pronounced, with vertical deflections up to 100 m. As discussed for many of the other transects, the isotherms dip over the flanks of the seamount.

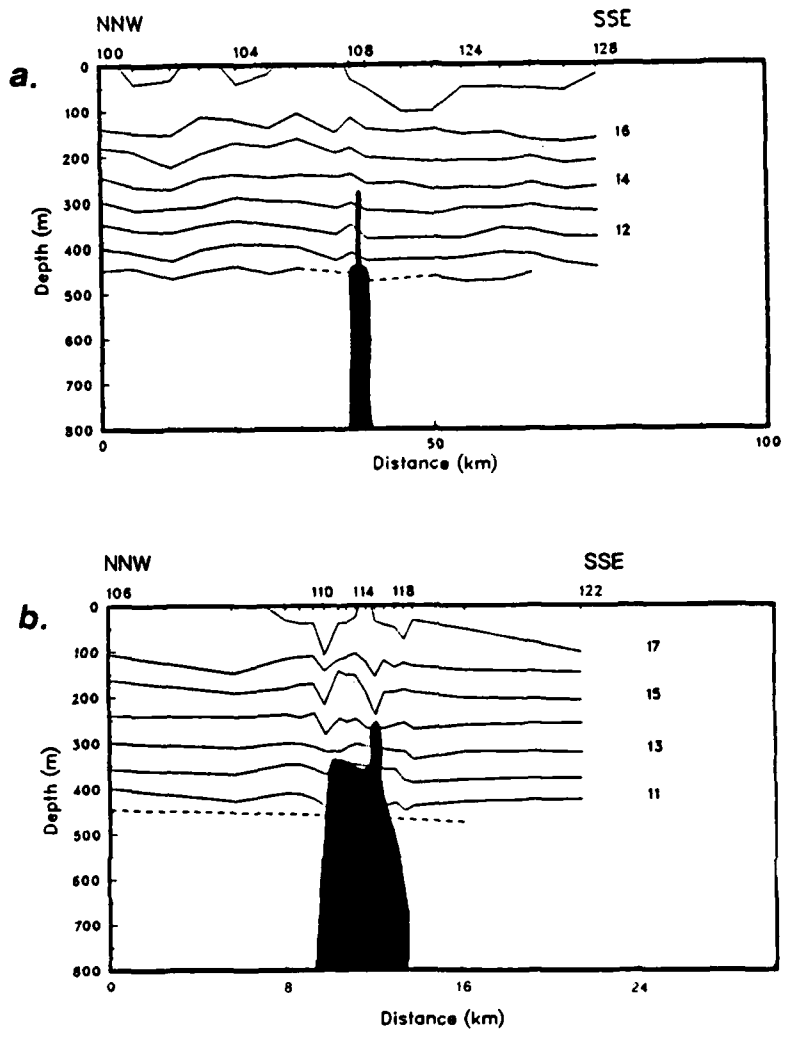

Fig. 5.7. TC8501 vertical temperature transects showing along-track isotherms (^{o}C) for (a) the NNW-SSE transect, and (b) an expanded scale version of (a).

Summarizing the winter survey, the three vertical sections showed relatively large horizontal scale (60-70 km) thermal doming over the seamount. In all cases, the doming appeared to extend throughout the observed upper water column, suggestive of a barotropic Taylor column.

C. HORIZONTAL TEMPERATURE, DYNAMIC HEIGHT, AND VELOCITY FIELDS

Horizontal plots of the temperature field at specified depths, dynamic height, and geostrophic velocity were made using a time-space objective analysis routine. A

correlation analysis of data between different spatial coordinates was performed to allow optimum weighting factors to be specified in the objective analysis program. All available XBT and CTD data for the respective surveys were then input into the objective analysis routine, which plotted contours of the various fields.

1. *Temperature Maps*

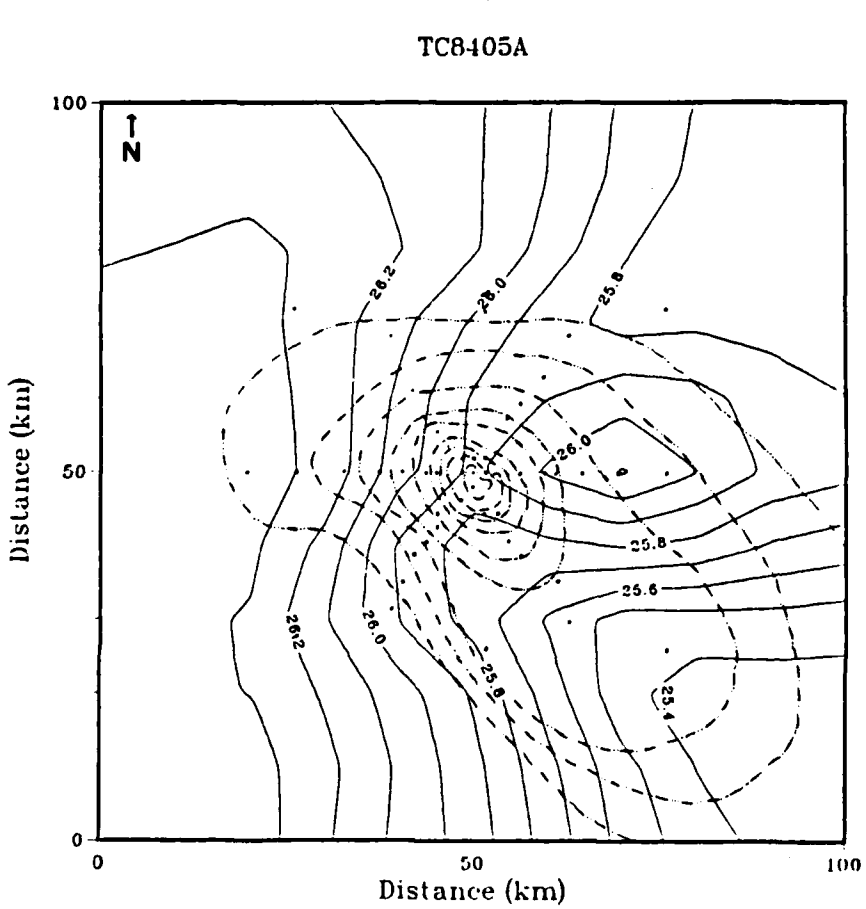

Fig. 5.8. Sea surface temperature (^{o}C) field for TC8405A. Contour interval is 0.1^{o}C. Station positions (black dots) and bathymetry (dashed and dotted lines) are also shown. Isobaths are contoured every 500 m.

Maps of the temperature fields for each of the surveys were made for 50 m depth intervals between the surface and 450 m, with additional maps at 500, 600, and 700 m for the two summer surveys. Although maps at other depths are discussed, only the surface, 200, 400, and 700 m maps are presented. For the most part, features discussed in the maps are consistent at all depths in the particular layer, i.e., surface layer, bottom layer, etc. The temperature contours overlay the hand-contoured

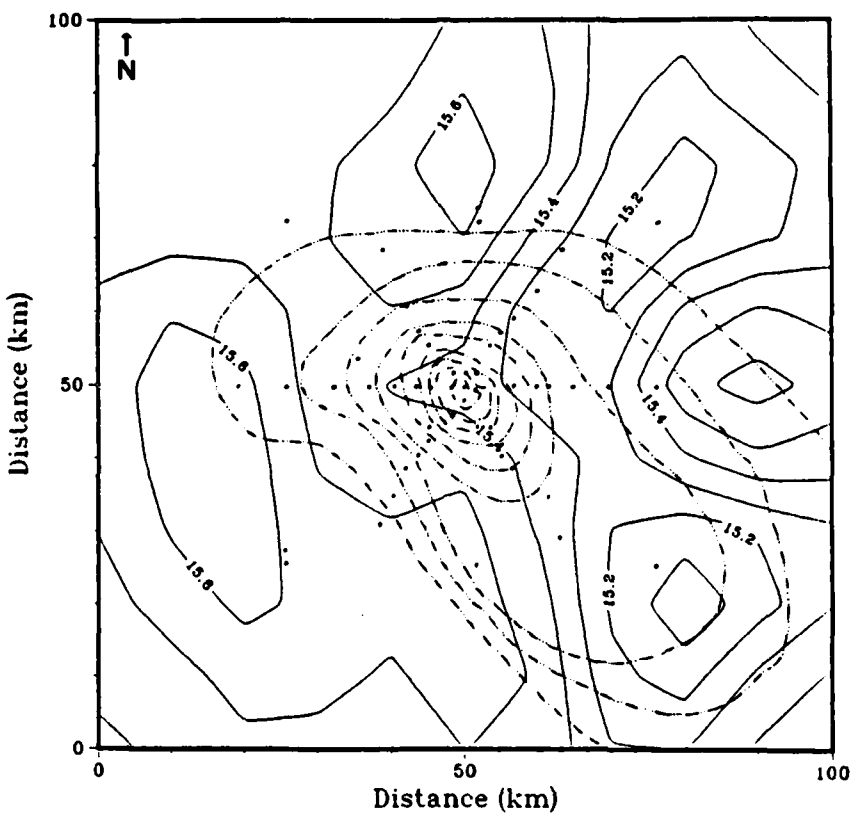

Fig. 5.9. Temperature (°C) field at 200 m for TC8405A. Contour interval is 0.1°C. Station positions (dots) and bathymetry (dashed and dotted lines) are also shown. Isobaths are contoured every 500 m.

bathymetry to emphasize the relationship of the warm and cold features to the bathymetry of the seamount. Station positions are also plotted to show the distribution of data. This is to help the reader visualize the limitations of the objective analysis. Contours drawn near or outside the perimeter of the sampling grid are based on relatively few data and should therefore be regarded as suspect. The discussion regarding these maps is limited to the major warm and/or cool features and their relation to the bathymetry. It is important to keep in mind the hypotheses suggested in the introduction and the theoretical discussion concerning flow over topography. Since Taylor columns are one of the primary mechanisms suggested to explain the productivity over seamounts, much of the analysis will discuss whether the observations support this hypothesis.

TEMP 400 M

TC8405A

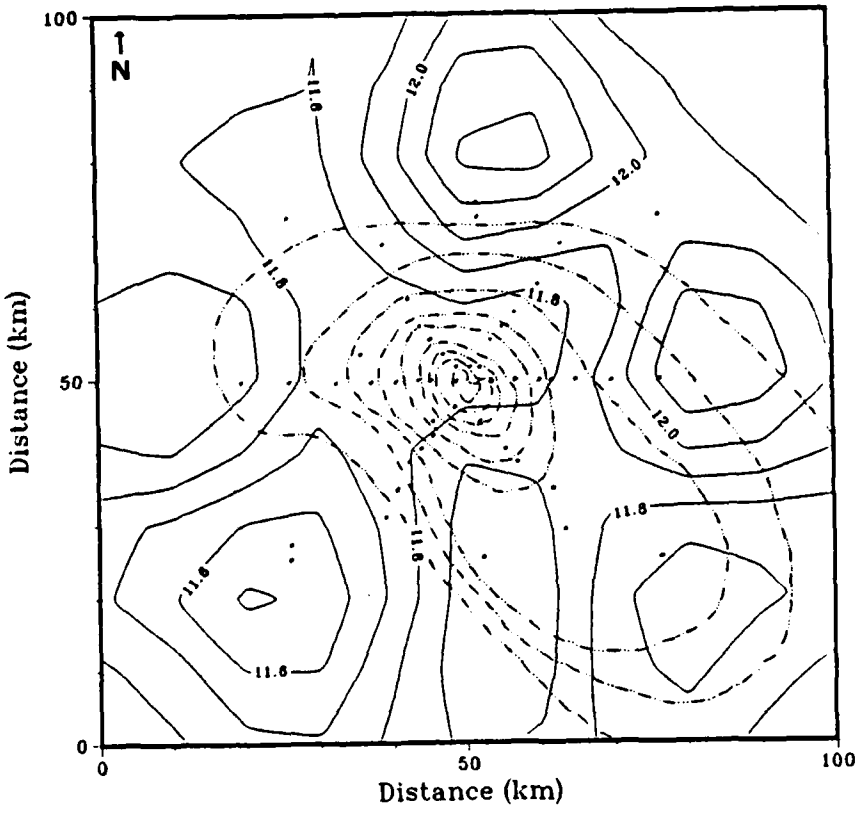

Fig. 5.10. Temperature (^{o}C) field at 400 m for TC8405A. Contour interval is 0.1^{o}C. Station positions (dots) and bathymetry (dashed and dotted lines) are also shown. Isobaths are contoured every 500 m.

Beginning with the SST map for the TC8405A survey (Figure 5.8), there are two primary features of interest. First, the SST decreases from west to east, suggesting a possible mean geostrophic surface flow to the north. Second, a relatively warm feature is observed to the east of the seamount summit. Clear evidence of a cold feature over or near the summit, as would be expected for a barotropic Taylor column, is lacking. This does not imply that a Taylor column is not present over the seamount at the time of the observations. It merely indicates that if a Taylor column is present, it does not extend to the surface.

Proceeding to the horizontal map of temperature at 200 m (Figure 5.9), a strong deflection of the 15.4^{o}C isotherm to the west is observed directly over the seamount. This represents a relatively cold intrusion of water over the seamount at

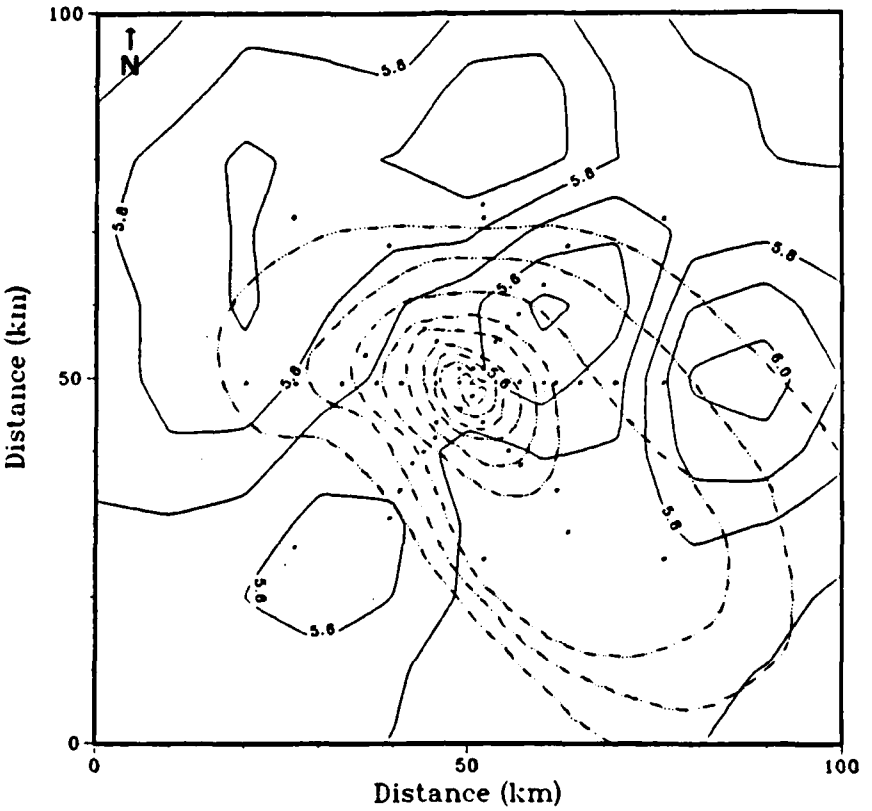

Fig. 5.11. Temperature (^{o}C) field at 700 m for TC8405A. Contour interval is 0.1^{o}C. Station positions (dots) and bathymetry (dashed and dotted lines) are also shown. Isobaths are contoured every 500 m.

200 m. A similar feature is also observed in the 100 and 150 m maps. No similar feature is observed in the 50 m map. Continuing downward to the 400 m map (Figure 5.10), a cool feature still appears to be present over the seamount, but it is expanded in size and of weaker intensity. Although the cool feature is less well defined and appears as a weak deflection of the isotherms to the east, it nevertheless maintains its identity at 400 m. A cool feature is also observed over or near the summit in the 500 and 600 m maps. Likewise, a relatively cool tongue of water extends from SW to NE over the seamount at 700 m (Figure 5.11). Here, the coldest water is displaced slightly NE of the summit. Summarizing, a cool feature occurred over or near the summit at all depths except at the surface and at 50 m. Although inconclusive, this type of behavior conforms reasonably well with what would be expected of a stratified Taylor column.

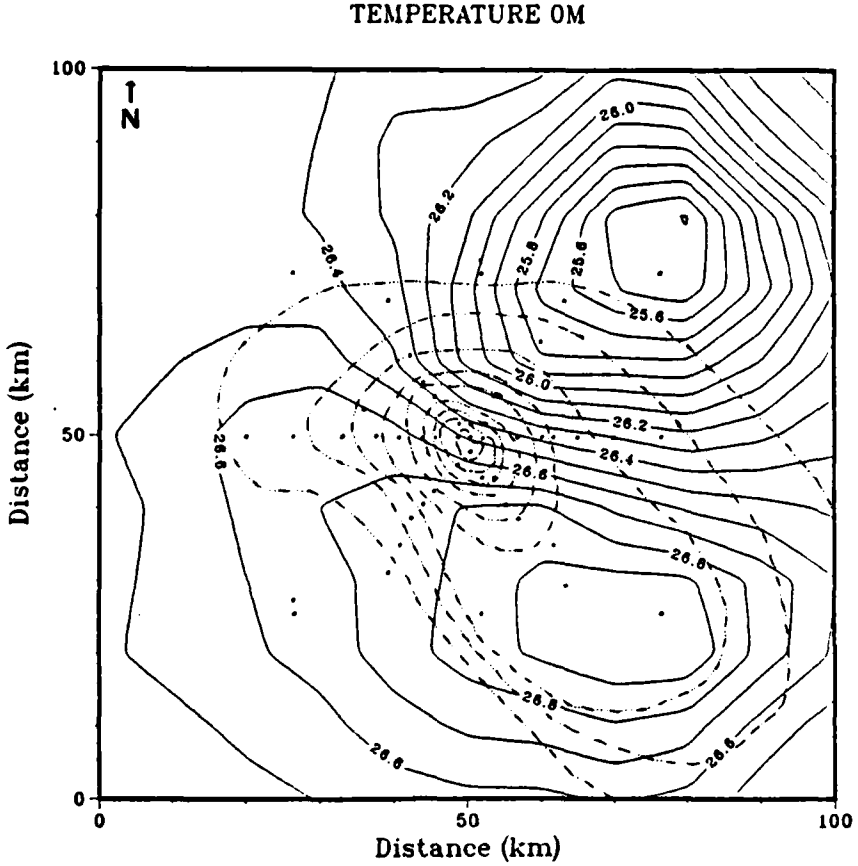

Fig. 5.12. Sea surface temperature (°C) field for TC8405B. Contour interval is 0.1°C. Station positions (dots) and bathymetry (dashed and dotted lines) are also shown. Isobaths are contoured every 500 m.

Presenting similar maps of temperature observed 16 days later, Figures 5.12-5.15, provide an indication of the variability of the thermal structure in the vicinity of the seamount. The SST map, Figure 5.12, shows a significantly different isotherm pattern. Here, the temperature gradient has become much stronger, and the isotherms have realigned from a predominatly NxE-SxW configuration to a predominantly WNW-ESE configuration. Also, the warm feature to the east of the seamount during the TC8405A survey is no longer present. Thus, considerable temporal variability is associated with the seamount. Furthermore, there once again are no indications of a cool feature associated with the seamount at the surface.

The map of the temperature field at 200 m (Figure 5.13) also looks surprisingly different from the same field 16 days prior. Although the overall isotherm

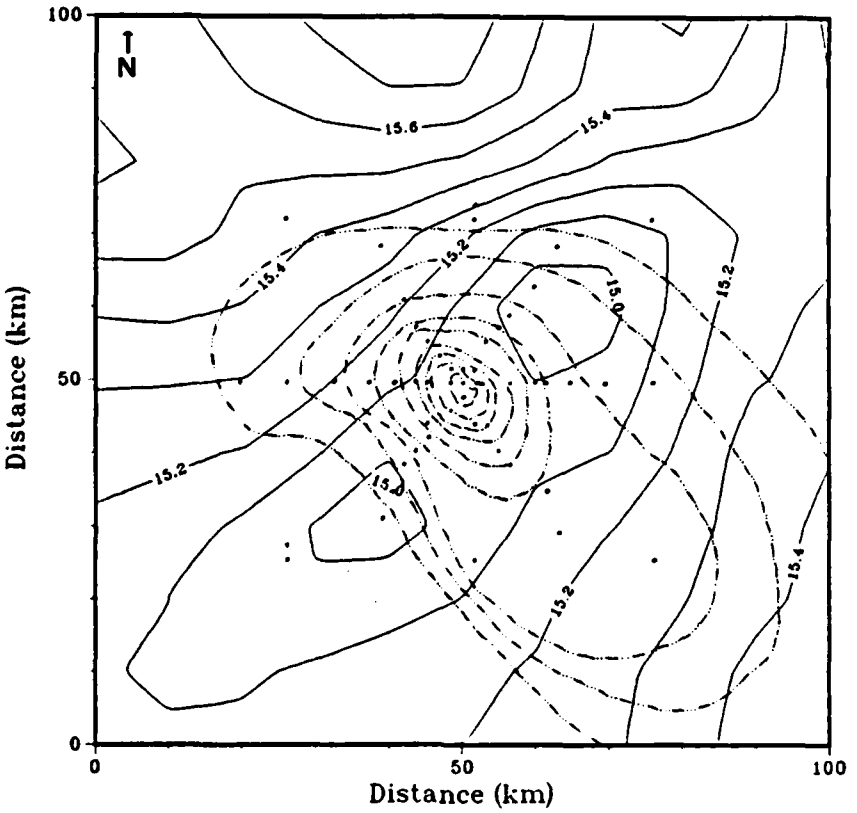

Fig. 5.13. Temperature (^{o}C) field at 200 m for TC8405B. Contour interval is 0.1^{o}C. Station positions (dots) and bathymetry (dashed and dotted lines) are also shown. Isobaths are contoured every 500 m.

pattern is very different, a tongue of relatively cool water lies over the seamount in a SW-NE line, somewhat reminiscent of the cool tongue observed below 500 m in the TC8405A maps. Unlike the earlier survey, this cool feature was not observed at 100 m. The first evidence, although weak, of the cool feature appears in the 150 m map. Temperature plots at 250 and 300 m indicate a cool tongue similar to that observed at 200 m. The cool feature is not as evident in the 400 m map (Figure 5.14). There does appear to be a deflection of the 11.8^{o}C isotherm around the summit and a cool feature centered about 10 km ExS of the summit. This cool feature becomes more defined in successively deeper maps, as shown in the 700 m map (Figure 5.15). As with the TC8405A survey, the cool feature appears to become larger and more defined with increasing depth.

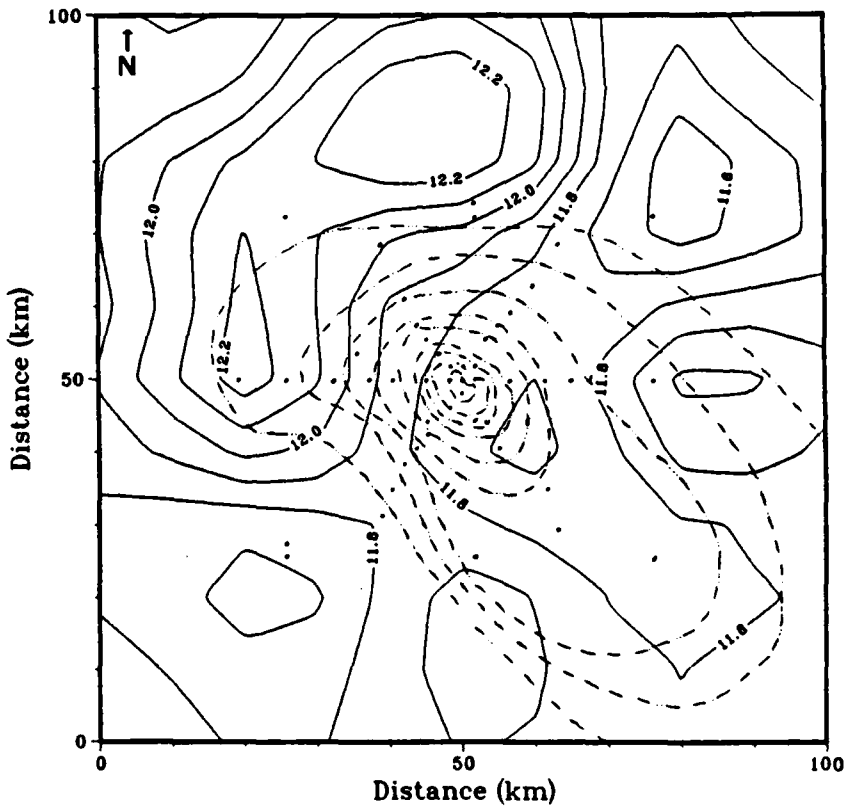

Fig. 5.14. Temperature (^{o}C) field at 400 m for TC8405B. Contour interval is 0.1^{o}C. Station positions (dots) and bathymetry (dashed and dotted lines) are also shown. Isobaths are contoured every 500 m.

To briefly summarize the summer surveys, both indicated the presence a cool feature below the surface layer with no indications of such a cooling above the pycnocline. The TC8405B survey showed the top of the cool feature to be about 50 m deeper than for the TC8405A survey. Thus, both summer surveys showed evidence in agreement with theoretical stratified Taylor column dynamics. This evidence is insufficient, however, to prove existence or non-existence of a Taylor column over Southeast Hancock.

Proceeding to the winter TC8501 survey, Figures 5.16-5.18 are presented to allow an examination of the winter conditions and a comparison with the summer surveys just discussed. As before, the bathymetry and station positions are shown to accommodate interpretation. The spatial variation of the SST (Figure 5.16) shows a

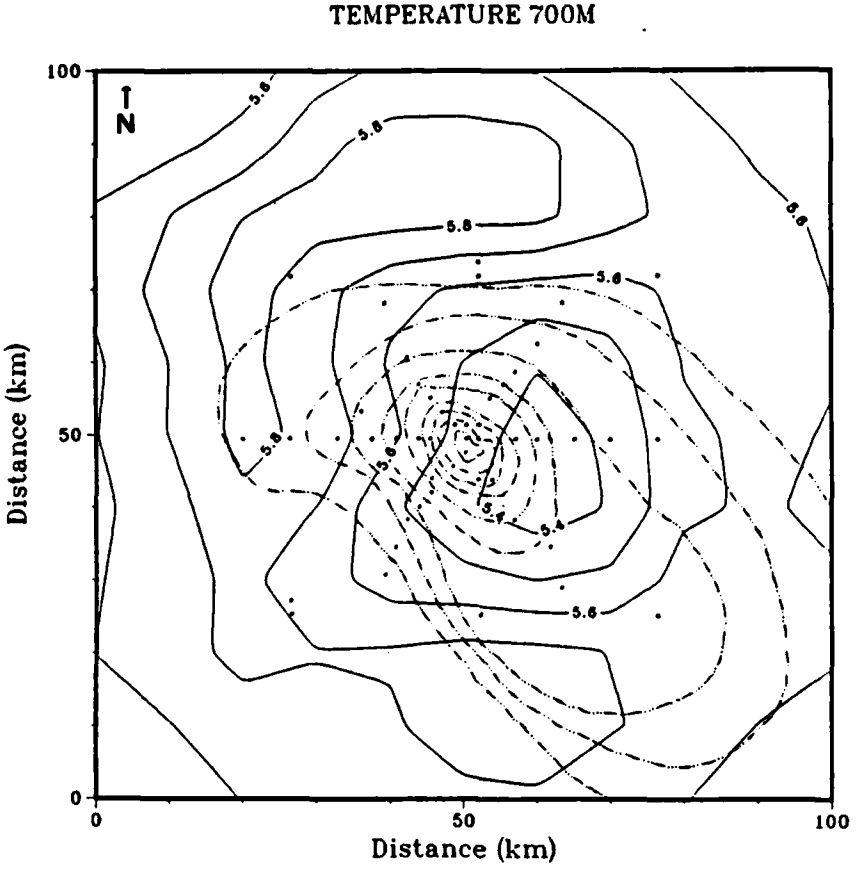

Fig. 5.15. Temperature (^{o}C) field at 700 m for TC8405B. Contour interval is 0.1^{o}C. Station positions (dots) and bathymetry (dashed and dotted lines) are also shown. Isobaths are contoured every 500 m.

deflection of relatively cold isotherms, forming a cool tongue extending from the SSE across the eastern edge of the seamount summit. Thus, unlike the two summer surveys, the winter survey shows a cool feature over the seamount at the surface, as would be expected for a barotropic Taylor column. There also appears to be a region of relatively warm water, with closed isotherms, to the west of the summit. The relative positions of the warm feature to the cool feature are suggestive of the interaction between warm cyclonic features and cool, stationary anticyclonic features described by Huppert and Bryan (1976). In review, their numerical and analytic results showed a cool anticyclonic feature remaining relatively stationary over an obstacle and a warm cyclonic feature which either remains attached to the anticyclonic feature or is shed and advected downstream, depending on the oncoming flow. Maps of temperature at

TC8501

SST

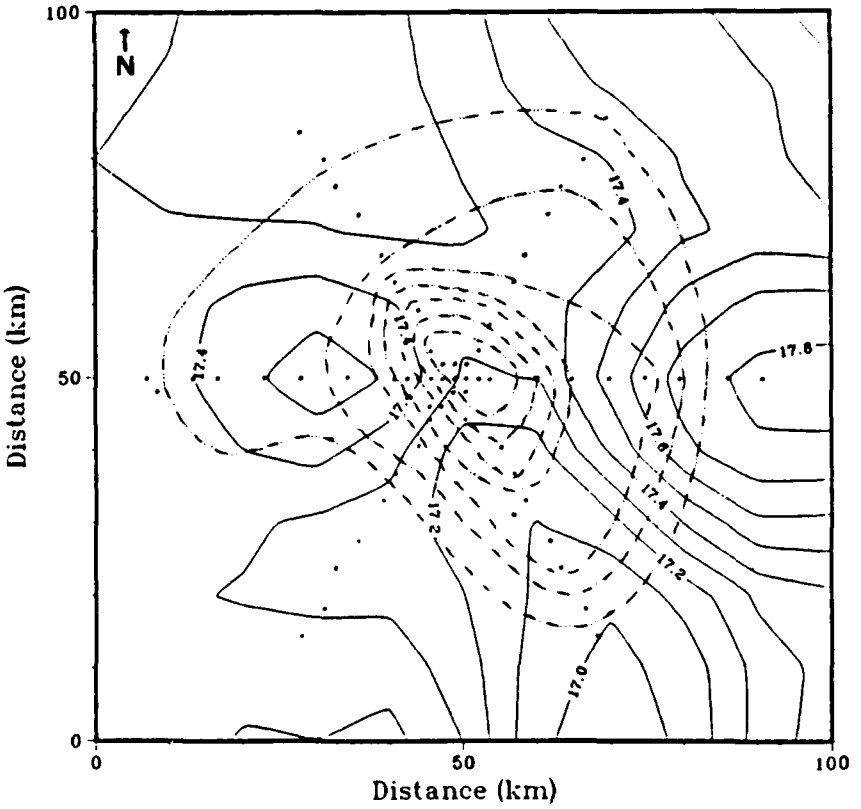

Fig. 5.16. Sea surface temperature (°C) field for TC8501. Contour interval is 0.1°C. Station positions (dots) and bathymetry (dashed and dotted lines) are also shown. Isobaths are contoured every 500 m.

50 and 100 m (not shown) show similar warm and cool features over the seamount, with increasing cyclonic and anticyclonic character with depth, respectively. At 150 m, the centers of these two features separate slightly, but the gradient between them intensifies. The map at 200 m (Figure 5.17) shows a much expanded anticyclonic feature still to the east of the summit, and a greatly weakened cyclonic feature still to the west of the seamount. Proceeding deeper, the distinct character of the two features begins to weaken. Warm and cool regions are still clearly evident in the 400 m map, although it does not have closed isotherms for either feature (Figure 5.18).

Summarizing, maps of temperature in the winter showed a cool feature over the seamount and a warm feature to the west at all depths down to 400 m. The intensity of both features weakened with increasing depth.

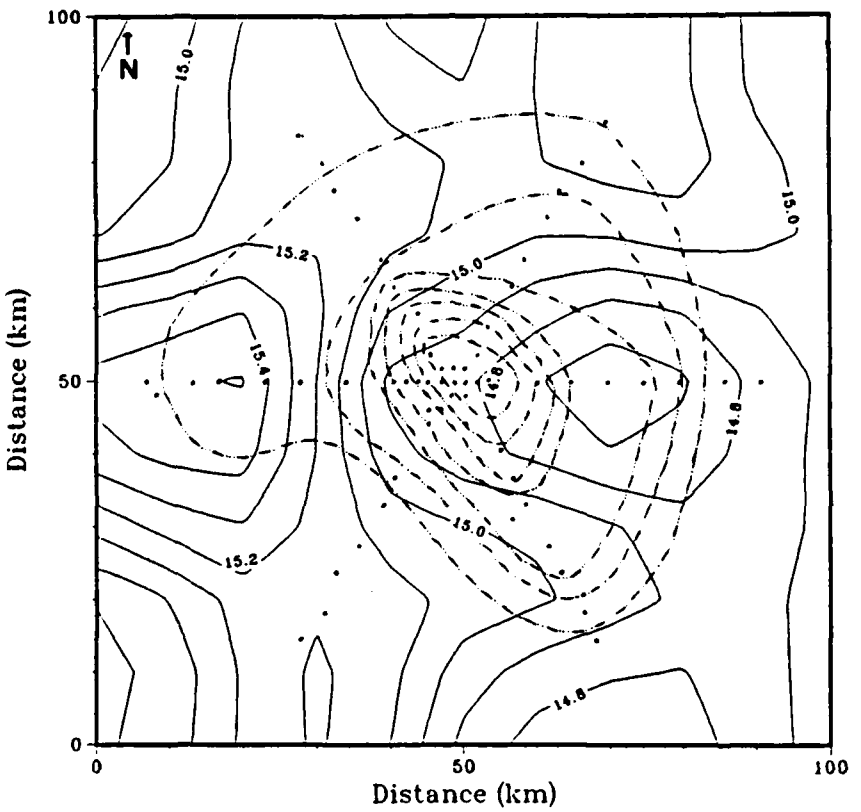

Fig. 5.17. Temperature (°C) field at 200 m for TC8501. Contour interval is 0.1°C. Station positions (dots) and bathymetry (dashed and dotted lines) are also shown. Isobaths are contoured every 500 m.

2. *Maps of Dynamic Height and Geostrophic Velocity*

Vertically integrating the density field, computed from both temperature and salinity fields allows the determination of dynamic height, maps of which allow a qualitative deduction of the geostrophic velocity characteristics. For many applications, the dynamic height of an upper level is computed relative to some deeper assumed level of no motion. For the purposes of this investigation, however, the flow at the bottom around the seamount is equally as interesting as the flow at the surface. In fact, for the case of a stratified Taylor column, the flow is predicted to be bottom-intensified. Therefore, dynamic topography maps are presented for both the surface layer relative to selected deeper reference levels, and for the deep layer relative to shallower reference levels. Geostrophic flows at the selected isobaric surface are

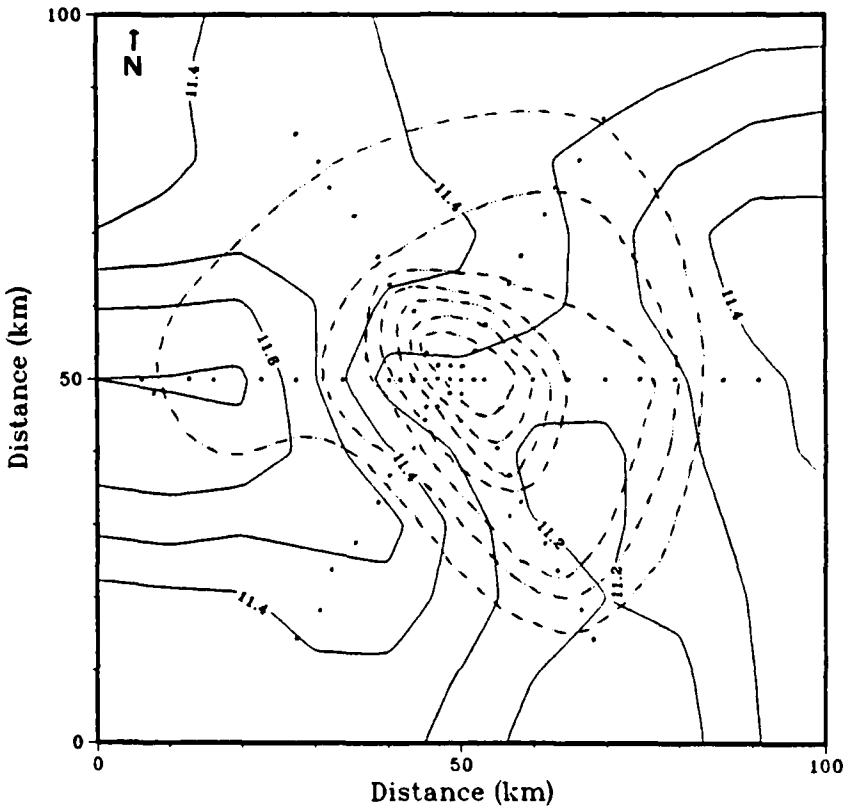

Fig. 5.18. Temperature (^{o}C) field at 400 m for TC8501. Contour interval is 0.1^{o}C. Station positions (dots) and bathymetry (dashed and dotted lines) are also shown. Isobaths are contoured every 500 m.

along the dynamic height contours with the hills to the right of the flow for the case with reference levels below the selected surface, and to the left of the flow for the case with the reference level above the selected surface. The speed of the flow is inversely proportional to the horizontal separation of the contours. Rather than relying solely on visual interpretion of the velocities as described, the geostrophic velocities have been computed numerically and plotted on the dynamic topography maps. The computed velocities are relative to a reference level assumed to have no motion; without actual measurements of the current structure, there is no way to test the validity of this assumption. All of the maps show velocities relative to the actual velocity at the reference level. Thus, depending on the true velocities at the chosen reference levels, the computed velocities could be very much in error. Furthermore,

since the true velocity varies temporally and spatially, the data are not truly synoptic, as assumed in the analysis.

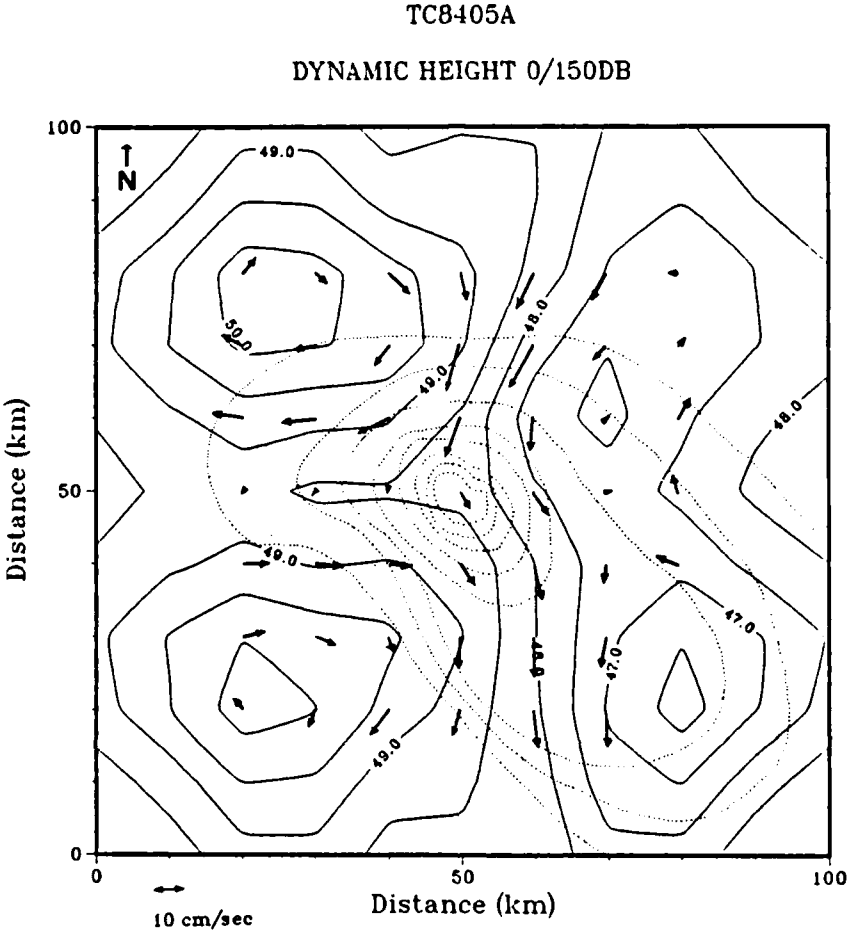

Fig. 5.19. Dynamic topography (solid lines) and geostrophic velocity (arrows), 0/150 db, for the TC8405A survey. Dynamic height contours are in dynamic centimeters. Velocity scale is given in lower left corner. Isobaths (dotted lines) showing bathymetry of Southeast Hancock Seamount are contoured every 500 m.

From the map of the dynamic height and geostrophic velocity at the surface relative to 150 m (Figure 5.19), there is a predominantly N-S stream. The effect of the topography on the flow can be seen by following the 48.5 dynamic centimeter contour from north to south. Proceeding to the SSW, this contour begins to bend to the southwest as it crosses over the 3500 m isobath. When the contour reaches a point almost due west of the summit, it bends sharply to the right and proceeds westward to a point about 25 km west of the summit, where it turns sharply back to the east.

TC8405A

DYNAMIC HEIGHT 0/500DB

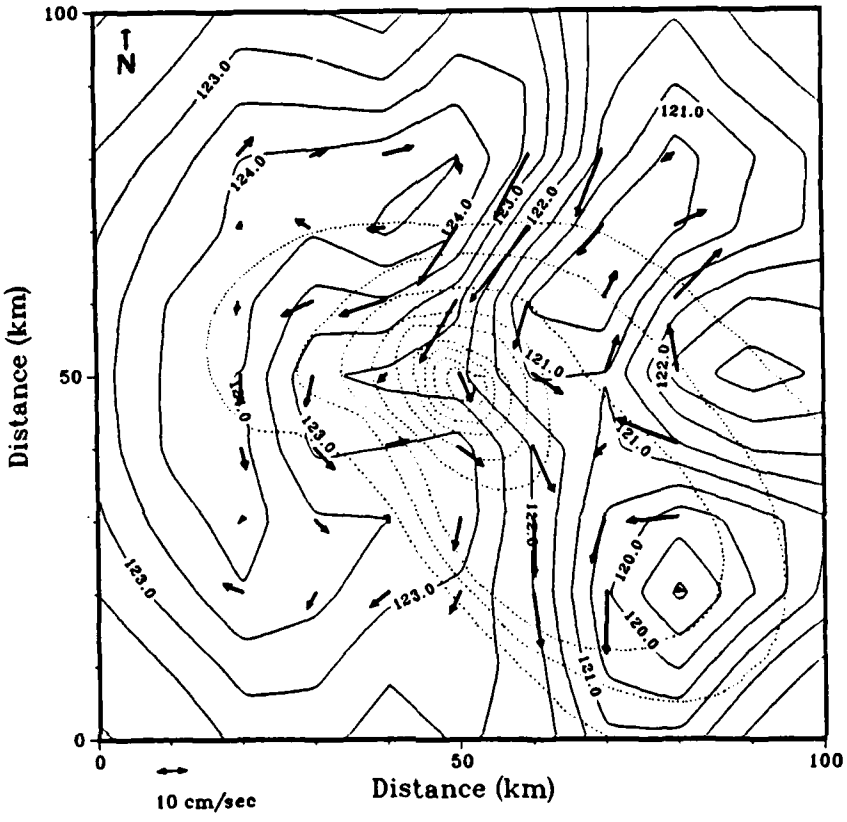

Fig. 5.20. Dynamic topography (solid lines) and geostrophic velocity (arrows), 0/500 db, for the TC8405A survey. Dynamic height contours are in dynamic centimeters. Velocity scale is given in lower left corner. Isobaths (dotted lines) showing bathymetry of Southeast Hancock Seamount are contoured every 500 m.

Approaching the summit from the west, it turns southward and resumes a SSW course. Similarly, the velocity vectors show a weak (10 cms^{-1}) SSW incident flow north of the summit being deflected in a counterclockwise path around the seamount. A region of weak, relatively stagnant flow is observed to the west of the summit, or to the right of the incident flow from the north, as theory predicts. The velocity vectors seem to follow the bathymetric contours reasonably well, as predicted by conservation of potential vorticity. The maximum geostrophic speeds are 10-15 cms^{-1}.

The 0/200 db, 0/300 db, 0/400 db, and 0/500 db maps of dynamic topography and geostrophic velocity are similar to the 0/150 db plot, except the dynamic height

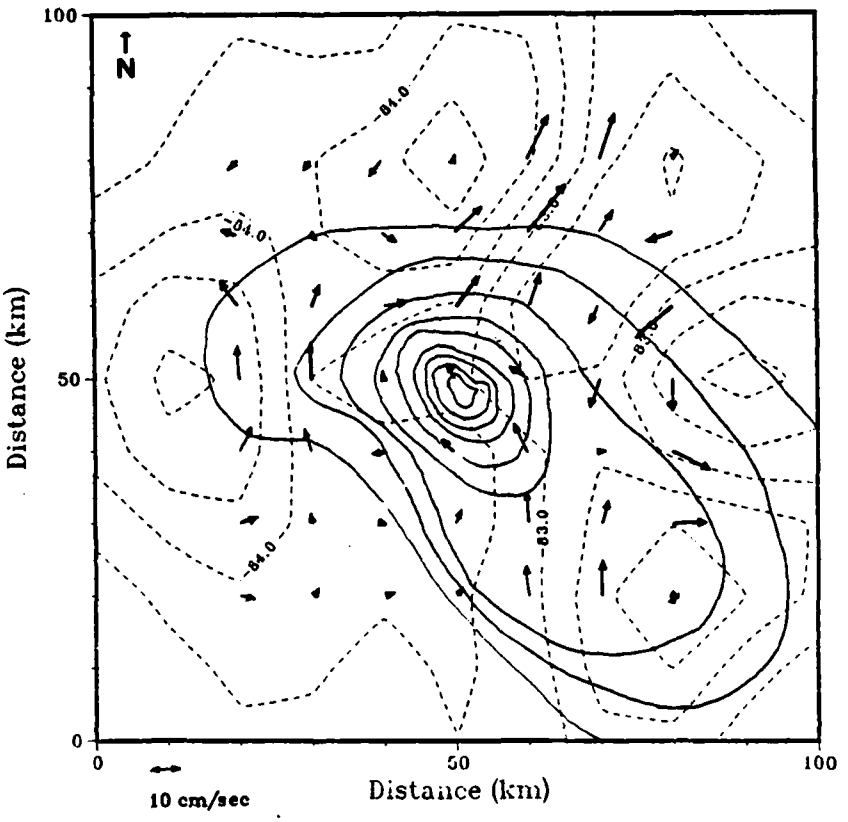

Fig. 5.21. Dynamic topography (dashed lines) and geostrophic velocity (arrows), 450/80 db, for the TC8405A survey. Dynamic height contours are in dynamic centimeters. Velocity scale is given in lower left corner. Isobaths (solid lines) showing bathymetry of Southeast Hancock Seamount are contoured every 500 m.

gradients and the corresponding geostrophic velocities both increase with increasing reference depth, as shown in the 0/500 db map (Figure 5.20). The fact that the effects are additive implies that the thermohaline pattern is consistent with depth below 150 m. Successively deeper reference levels decrease the size and better define the boundaries for the relatively stagnant region to the west of the summit. The velocity vectors shown in Figure 5.20 reveal a strong cyclonic tendency of the flow around the relatively stagnant feature. The maximum surface speeds relative to 500 db are shown to be about 30 cms^{-1}, over twice the speed computed for the surface flow relative to 150 db.

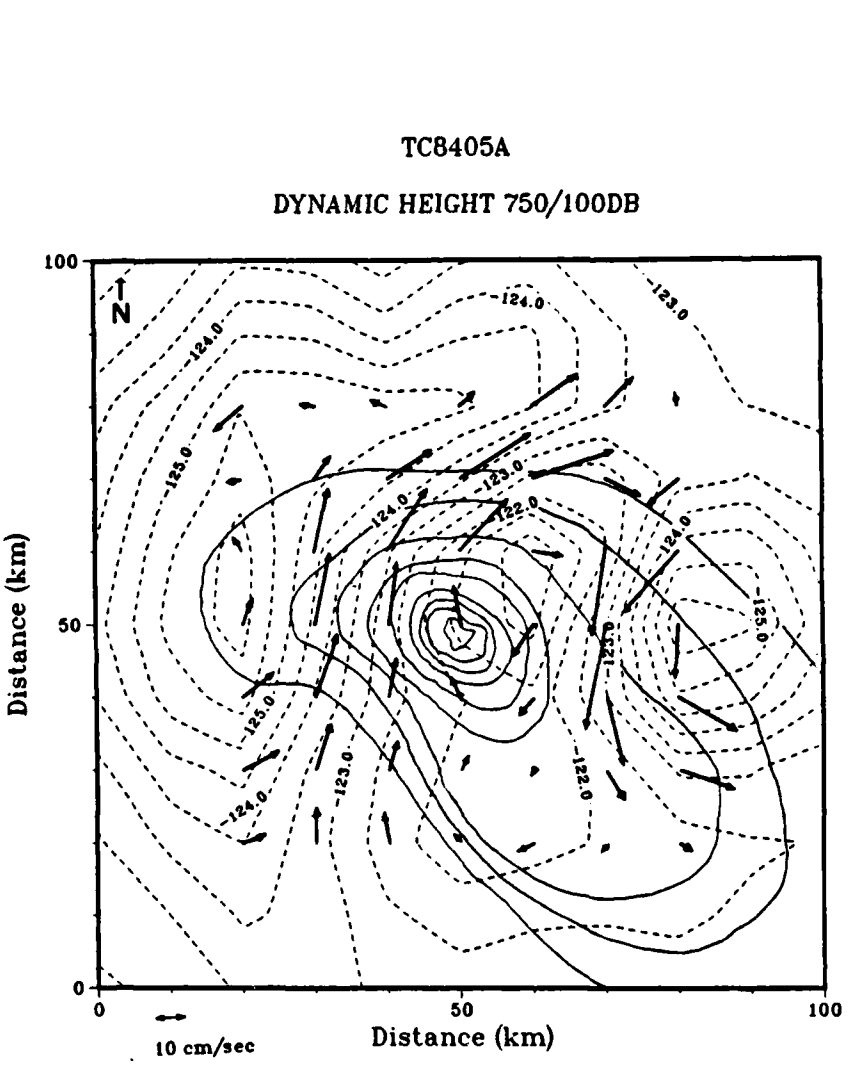

Fig. 5.22. Dynamic topography (dashed lines) and geostrophic velocity (arrows), 750/100 db, for the TC8405A survey. Dynamic height contours are in dynamic centimeters. Velocity scale is given in lower left corner. Isobaths (solid lines) showing bathymetry of Southeast Hancock Seamount are contoured every 500 m.

These computed surface velocities are relative to the 150 and 500 m reference levels, respectively. If the true velocities at these reference depths are different than zero, then the surface velocities described are equally different from the plotted values. In fact, if it is assumed that the surface velocity is zero, then the surface velocities plotted above represent the velocities at 150 and 500 m, respectively, except the directions are reversed. In this case, the flow at 150 and 500 m would be anticyclonic and the velocities would be shown to increase with depth, as predicted by Taylor column dynamics for the stratified case. Although it is unlikely that there is no flow at the surface, it is not unlikely that the flow around the seamount might be anticyclonic

and increase with depth. Ideally, direct measurements of the currents at various depths could be used to determine a suitable reference level. However, since no such measurements are available, other information, such as the vertical and horizontal temperature structure, are incorporated into the analysis. In particular, the vertical structure indicated the possibility that during the summer surveys the water column may be represented by a two-layer system, with the boundary being roughly between 80 and 100 m. Dynamic topography/geostrophic velocity maps of the upper and lower layers, respectively, were used to test the validity of this two-layer assumption. The 0/150 db and 0/500 db maps showed similar features, but with stronger gradients and higher velocities for the 0/500 db map, indicating similar processes above and below 150 m. On the other hand, the 450/80 db map (Figure 5.21), showing the dynamic height and velocity at 450 m relative to 80 m, looks very similar to the 0/400 db and 0/500 db maps, but with reversed signs. This suggests that the upper 80 m may not have much influence either way. Since the vertical sections of the thermal structure indicate a two-layer system, and these dynamic topography plots suggest little influence of the upper 80-100 m, it seems reasonable to map the dynamic height at the deeper levels relative to this boundary between the two layers (the pycnocline).

Figure 5.22 shows the dynamic topography and geostrophic velocity at 750 m relative to 100 m. This plot shows that relative to 100 m, the flow at 750 m has a strong anticyclonic rotation centered about a point located about 10 km northeast of the summit. A weak incident flow (10-15 cms^{-1}) approaches the seamount from the south. Upon encountering the seamount, the flow west of the seamount accelerates to 30-35 cms^{-1} and then turns anticyclonically to the right. Part of the flow then continues to the northeast, while the remainder of the flow rotates as an anticyclonic eddy. Surprisingly, this plot is significantly different from the 450/80 db map, indicating a strong influence of the layer between 450 and 750 m. Although the 450/80 db map also shows an apparent incident flow from the south and anticyclonic flow around the seamount, the velocity is weaker and the center of the stream is 30 km east of the center of the stream at 750 m. The flow does not appear to accelerate as it flows around the seamount, as observed in the 750/100 db map. Thus, the flow appears to accelerate significantly between 450 and 750 m, indicating the presence of bottom-intensified anticyclonic flow in agreement with stratified Taylor column theory. Due to the numerous assumptions required in the analysis, these maps cannot be construed as conclusive evidence for the existence of a Taylor column over Southeast

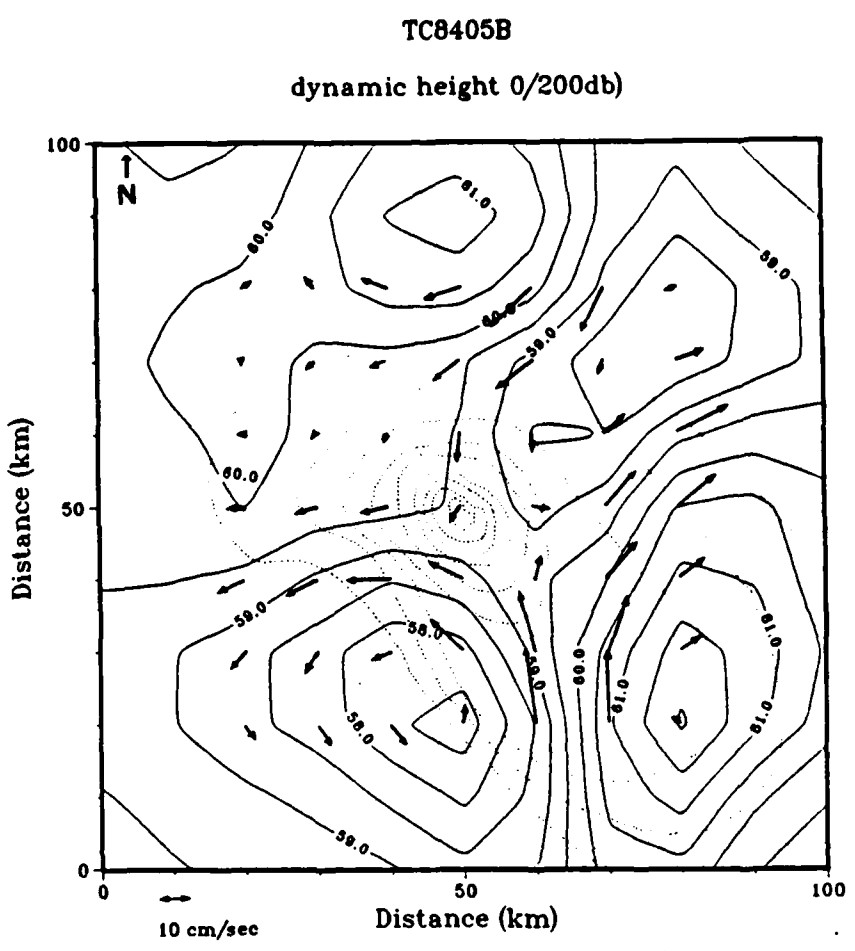

Fig. 5.23. Dynamic topography (solid lines) and geostrophic velocity (arrows), 0/200 db, for the TC8405B survey. Dynamic height contours are in dynamic centimeters. Velocity scale is given in lower left corner. Isobaths (dotted lines) showing bathymetry of Southeast Hancock Seamount are contoured every 500 m.

Hancock Seamount. However, the results are not inconsistent with the Taylor column hypothesis.

The 0/200 db, 0/300 db, 0/400 db, and 0/500 db dynamic topography/geostrophic velocity maps for the TC8405B survey (Figures 5.23-5.26) display features similar to those described for the TC8405A survey. A comparison between the 0/200 db and 0/500 db maps (Figures 5.23 and 5.24) indicates that approximately 40-60 % of the flow can be accounted for by the upper 200 m of the water column. Moreover, the 450/100 db map (Figure 5.25) shows significantly weaker velocities, implying a significant baroclinic component of the geostrophic current in the

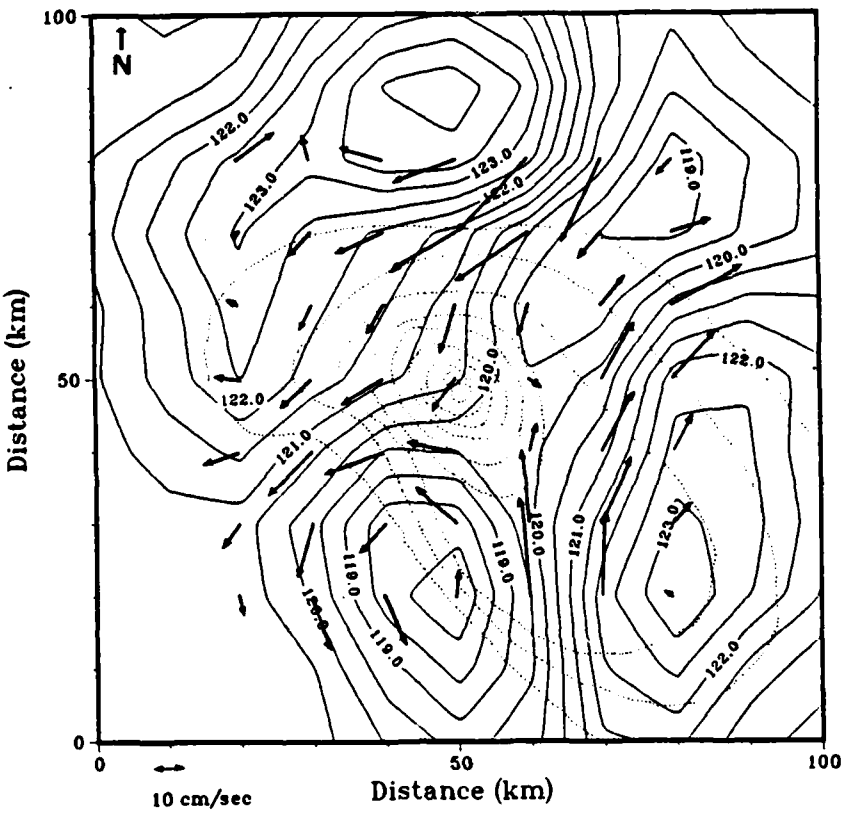

Fig. 5.24. Dynamic topography (solid lines) and geostrophic velocity (arrows), 0/500 db, for the TC8405B survey. Dynamic height contours are in dynamic centimeters. Velocity scale is given in lower left corner. Isobaths (dotted lines) showing the bathymetry of Southesat Hancock Seamount are contoured every 500 m.

upper 100 m. The 0/500 db plot shows two relatively strong streams or jets moving in opposing directions located on opposite sides of the seamount. The 0/200 db, 0/300 db, and 0/400 db plots show the same general features, but with proportionately lesser magnitudes. The first jet meanders in a NE to SW line which crosses over the NW flank of the seamount. The maximum velocity associated with this feature is 30-35 cms^{-1}. The second jet flows north and then diverges as it approaches the SE flank of the seamount. The majority of the flow deflects to the right on a northeastward course. The remainder is deflected left on a westward course where it encounters and joins the first southwestward jet. The divergence, as depicted by the

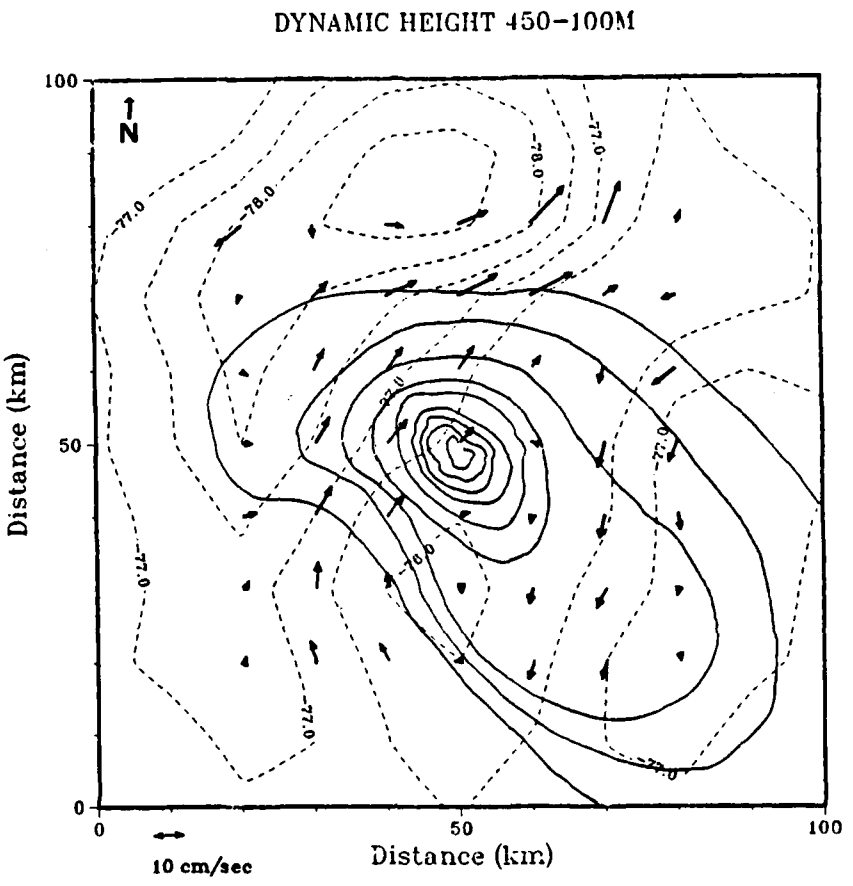

Fig. 5.25. Dynamic topography (dashed lines) and geostrophic velocity (arrows), 450/100 db, for the TC8405B survey. Dynamic height contours are in dynamic centimeters. Velocity scale is given in lower left corner. Isobaths (solid lines) showing the bathymetry of Southeast Hancock Seamount are contoured every 500 m.

119.5 and 120.0 dynamic centimeter contours, seems to be related to the divergence of the isobaths. In the lee of the divergence area, just to the east of the summit, there is a region of weak, relatively stagnant flow. Flow along diverging isobaths can be related to upwelling (Janowitz, 1982). Perhaps the region of weak, relatively stagnant flow between the diverging isobaths represents the upwelling necessary to explain the high productivity observed over Southeast Hancock. In either case, this mechanism for upwelling by divergence of flow along isobaths needs to be further investigated in the context of seamounts.

TC8405B

DYNAMIC HEIGHT 750/100DB

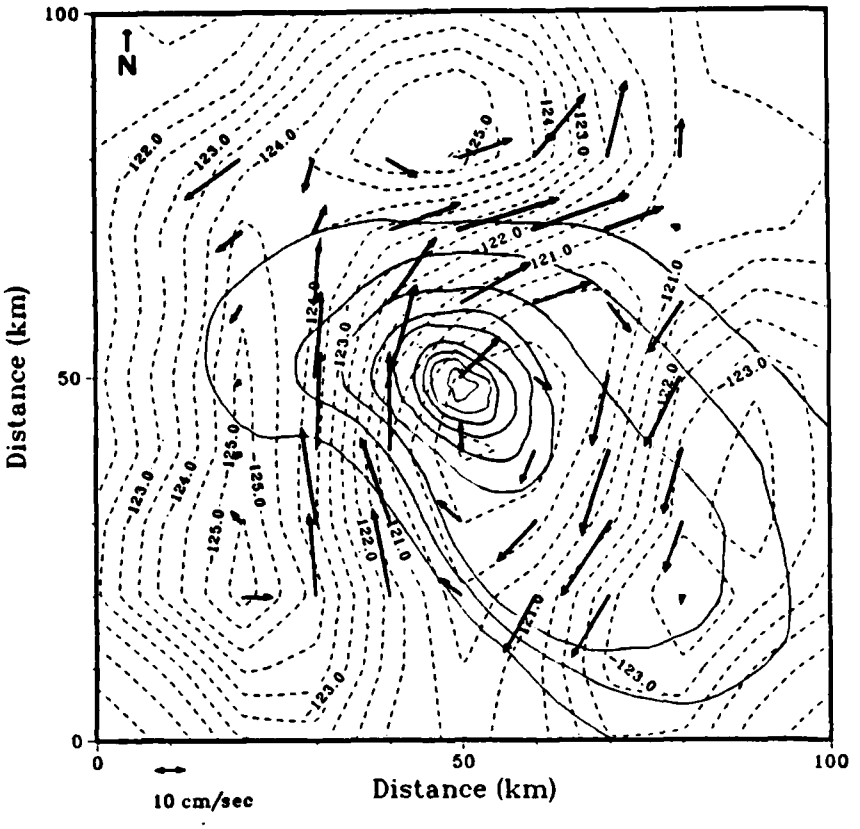

Fig. 5.26. Dynamic topography (dashed lines) and geostrophic velocity (arrows), 750/100 db, for the TC8405B survey. Dynamic height contours are in dynamic centimeters. Velocity scale is given in lower left corner. Isobaths (solid lines) showing the bathymetry of Southeast Hancock Seamount are contoured every 500 m.

As with the TC8405A survey, the lower layer geostrophic flow is examined relative to 100 m, thereby neglecting some of the effects of the moderate upper layer baroclinic flow (Figure 5.26). Similar to the case 16 days earlier, the 750/100 db map shows significant differences from the 450/100 db map, again implying a strong effect between 450 and 750 m. This map clearly displays closed dynamic height contours and a strong anticyclonic flow around the seamount at 750 m. The incident lower layer flow appears to be from the south. There is a 30-35 cms^{-1} northward jet to the west of the summit. This strong jet then turns anticyclonically, roughly following the isobaths. Part of this strong jet then turns left to resume its northward flow, while the remainder

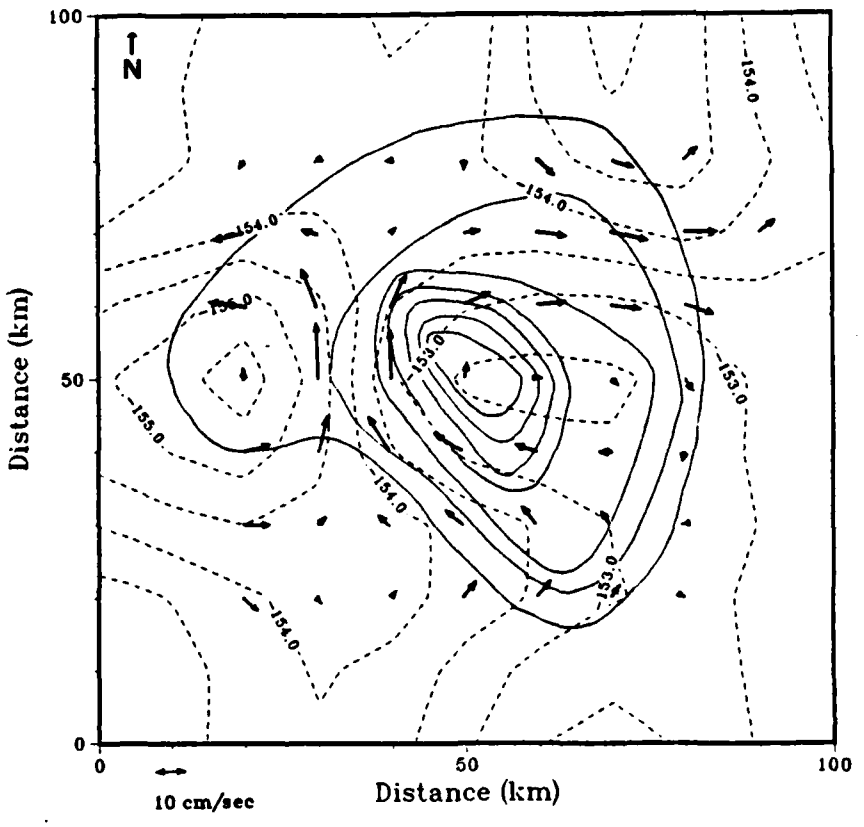

Fig. 5.27. Dynamic topography (dashed lines) and geostrophic velocity (arrows), 400/0 db, for the TC8501 survey. Dynamic height contours are in dynamic centimeters. Velocity scale is given in lower left corner. Isobaths (solid lines) showing the bathymetry of Southeast Hancock Seamount are contoured every 500 m.

continues anticyclonically around the seamount. The southward component of the anticyclone has a speed of 25-30 cms^{-1}. This strong anticyclonic feature appears to be centered 5-10 km east of the summit. The velocity weakens significantly near the center.

Summarizing, the TC8405B survey is characterized by a moderate surface current, which differs from the moderate, bottom-intensified, anticyclonic flow observed at 750 m. These features are all consistent with a Taylor column of the stratified type.

Although the details of the flow were quite different for the two summer surveys, both were characterized by features which could, at least plausibly, be

interpreted by Taylor column dynamics. The dynamic topography and geostrophic velocities for the winter TC8501 survey are presented next. Similarities and differences between winter and summer conditions will be noted where appropriate. Considering the weak stratification and low stability of the water column during the winter, as described by the vertical plots of temperature and buoyancy frequency, features are expected to be somewhat homogeneous throughout the water column. Indeed, the 0/80 db, 0/200 db, 0/300 db, and 0/400 db maps display similar features which become better defined with increasing reference level depth. The intensity of the features remain consistently weak for all of the depth intervals examined. Since we are interested in the flow near the seamount, the 400/0 db plot is presented, remembering that it represents the flow at 400 m relative to an assumed zero flow at the surface (Figure 5.27). This map shows relatively weak anticyclonic flow around the eastern half of the seamount and an apparent cyclonic flow to the west of the seamount. These two oppositely rotating flows are separated by a relatively strong jet (20 cms^{-1}), apparently accelerated due to the superposition of the northward components of the two rotating flows. This relationship of anticyclonic and cyclonic features is again reminiscent of the numerical results of Huppert and Bryan (1976). It is also remarkably similar to the TC8405B summer case (Figures 5.25 and 5.26). The anticyclonic flow follows the isobaths reasonably well. The 0/80 db and 450/100 db maps indicate homogeneity of the flow throughout the upper 400 m of the water column. Unavailability of data below 400 m prevents a full comparison between the winter and summer surveys of the baroclinic component of the flow between 450 and 750 m.

Summarizing the winter survey, the flow appears to have an anticyclonic feature over the seamount which linearly intensifies with depth, and a weak cyclonic feature to the west. Each of these features are characteristics of a barotropic Taylor column.

VI. CONCLUSIONS AND RECOMMENDATIONS

Three mechanisms to explain the abundant fishery once found over the southern Emperor-northern Hawaiian Ridge seamounts are suggested: larval retention by hydrodynamic trapping, nutrient enrichment by seamount-induced upwelling, and attraction of organisms to stationary physical substrates to which they can attach and orient themselves. The first two hydrodynamic mechanisms were examined theoretically and found to be related to Gill's (1982) quasi-geostrophic flow regime for wave-topography interactions. More specifically, Taylor column dynamics were investigated and suggested as a physical mechanism which could explain both larval retention and nutrient enrichment over seamounts.

Data from three hydrographic surveys over Southeast Hancock Seamount conducted during summer 1984 and winter 1985 were examined for evidence supporting these hydrodynamic mechanisms. The two summer surveys, TC8405A and TC8405B, reveal a strong pycnocline at a depth of 80-100 m, suggesting a two-layer system. There was thermal doming over the seamount in the lower layer, below the pycnocline, for both summer surveys. The horizontal length scale of the thermal doming was 30-50 km, roughly twice the first baroclinic Rossby radius, indicating that the rotational effects are of the same order as the buoyancy effects. Both surveys show evidence that the observed thermal doming may be superimposed on a larger scale thermal doming which could not be resolved with the data here due to limited transect lengths. Maps of temperature at fixed depths show a cool feature over or near the seamount summit at all depths down to 750 m, except in the upper 50-100 m. Significant differences in the thermal structure for the two summer surveys, which were separated by just 16 days, suggest strong temporal variability.

The dynamic height/geostrophic velocity maps for the first summer survey (TC8405A) show relatively weak baroclinic flow in the upper 100 m, moderate anticyclonic flow around the seamount at 450 m, and relatively strong anticyclonic flow around the seamount at 750 m, relative to the flow pattern nearer the surface. The flows at 450 and 750 m were determined relative to the pycnocline at 100 m. Thus, the geostrophic calculations are consistent with the presence of bottom-intensified anticyclonic flow over the seamount, in agreement with theoretical stratified Taylor column dynamics.

The dynamic topography/geostrophic velocity maps for the second summer survey (TC8405B) imply a significant baroclinic flow in the upper 100 m. The flow at the surface, relative to 500 m, has two relatively strong jets in opposing directions on opposite sides of the seamount. One of these flows diverges as the seamount is approached, apparently in response to the divergence of the isobaths. A region of weak, relatively stagnant flow in the lee of this divergence is observed. It is postulated that this divergence may cause upwelling, similar to that induced by diverging isobaths described by Janowitz (1982). If the moderate upper layer flow is not considered, the dynamic topography/geostrophic velocity maps at 450 and 750 m, relative to 100 m, again imply a relatively strong, bottom-intensified, anticyclonic flow in the lower layer, in agreement with stratified Taylor column theory.

Additionally, the NNW-SSE transects for both summer surveys showed sharp, localized vertical deflections of the isotherms suggesting wave-topography interaction and possibly strong vertical motions similar to what is observed for atmospheric flow over mountains. These deflections may be transient effects associated with internal tides and waves or wind-induced upwelling. Thus, the observations also appear consistent with the hypothesis that strong wave-topography interactions may upwell nutrients into the euphotic zone over the seamount.

The winter survey (TC8501), characterized by weak stratification, showed thermal doming to extend through the entire observed water column, unlike the summer surveys where the thermal doming was confined below the seasonal pycnocline. The length scale of horizontal thermal variability was 60-65 km, which is larger than that of the summer surveys. The maps of temperature at fixed depths reveal a cool feature (anticyclone) over the seamount and a relatively warm feature (cyclone) to the west of the seamount. Both features appear at all depths from the surface to 400 m. The dynamic topography maps confirm that both the anticyclonic and cyclonic features extend through the upper 400 m. The weak anticyclonic flow around the seamount at all depths agrees with barotropic Taylor column theory. Also, the association with the cyclonic feature to the west resembles the numerical results of Huppert and Bryan (1976) for the weakly stratified case.

The winter data also show evidence that an upstream topographic feature can cause variability in the incident flow. High variability is observed downstream of an upstream seamount, while low variability is observed in the region away from the influence of the upstream seamount. Thus, seamounts having other topographic

features upstream are likely to have more complex, non-steady incident flow. Such unsteadiness may tend to de-stabilize the balance required to maintain a Taylor column. A complex incident flow would make detection of oceanic Taylor columns even more difficult.

Although the available data cannot demonstrate conclusively that the high productivity often observed over seamounts is due to the proposed hydrodynamic mechanisms, none of the indications contradict this hypothesis. Both summer surveys show features consistent with a two-layer system having bottom-intensified anticyclonic flow around the seamount, as would be expected for a stratified Taylor column. Likewise, the winter survey, described by homogeneous anticyclonic flow around the seamount, suggests the existence of a barotropic Taylor column.

The results of this investigation clearly reveal deficiencies in the present state of our understanding of topographic-scale hydrodynamic processes. Certainly, our understanding of the interaction between the ocean currents and topographic features of the sea floor is inadequate to satisfactorily describe or explain the complex physical and biological phenomena observed in the vicinity of seamounts. To better our understanding of these processes, future research efforts need to concentrate on smaller spatial and temporal scales. Only in the past decade or so has there been a noticeable shift in physical oceanographic studies toward mesoscale processes. The importance of these smaller scale processes is not limited to local implications, such as the seamount fishery described here, but extends to the global ocean energy balance.

As spatial scales decrease, there must be a corresponding increase in the required temporal resolution. Although the assumption of synopticity was necessary for the data presented here, the observed temporal variability of the thermal structure over the seamount, as displayed by the changes between the two summer surveys, emphasizes the importance of true synopticity. Under the assumption of synopticity, significant spatial variability was described. As the degree of synopticity decays, however, the division between spatial and temporal variability becomes less distinct. Hence, there is a necessity for future efforts to investigate both small spatial and temporal scales. More specifically, future seamount research should include closely-spaced continuously-recording instrument arrays which can measure the 3-dimensional density structure and or the velocity field over a long enough time period to resolve the temporal scales of variability. It would also be desirable to determine the mean large-scale incident flow.

To further investigate the hypothesized upwelling mechanisms, it would be necessary to examine the frictional effects of the bottom boundary layer, including turbulence, which would require the instrumentation array to extend through this near-bottom layer. A thorough investigation of the bottom boundary layer would also require a high resolution bathymetric survey of the seamount, such as could be obtained using the SEABEAM multi-beam echo-sounding bathymetric surveying system. In addition to an observational research effort, topographic-scale numerical modeling studies should be continued, particularly in an examination of the bottom boundary layer processes and the hypothesized upwelling mechanisms.

LIST OF REFERENCES

Alaka, M.A., ed. 1960: *The airflow over mountains, Tech. Note 34.* World Meteorol. Organ., Geneva.

Bakun, A., In press: Local retention of planktonic early life stages in tropical demersal reef/bank systems: the role of vertically- structured hydrodynamic processes? *IOC Workshop Report #40 (Supplement)*, Intergovernmental Oceanographic Commission, Unesco, Paris.

Bannon, P.R., 1980: Rotating barotropic flow over finite isolated topography. *J. Fluid Mech., 101*, 281-306.

Blackburn, M., 1965: Oceanography and the ecology of tunas. *Oceanogr. Mar. Biol. Ann. Rev.*, H. Barnes, Editor, 3, 299-322.

Boehlert, G.W., 1985: Effects of Southeast Hancock Seamount on the pelagic ecosystem. *Eos, 66*, 1336.

Borets, L.A., 1979: The population structure of the boarfish, (*Pentaceros richardsoni*), from the Emperor Seamounts and the Hawaiian Ridge. *J. Ichthyol., 19*, 15-20.

Buzzi, A., and S. Tibaldi, 1977: Inertial and frictional effects on rotating flow over topography. *Quart. J. Roy. Met. Soc., 103*, 135-150.

Davies, P.A., 1972: Experiments on Taylor columns in rotating stratified fluids. *J. Fluid Mech., 54*, 691-717.

Defant, A., 1961: *Physical oceanography, Vol 1.* Pergamon Press, 729 pp.

Dooley, H.D., 1984: Aspects of oceanographic variability on Scottish fishing grounds. Ph.D. Thesis, University of Aberdeen, 154 pp.

Fukasawa, M., and Y. Nagata, 1978: Detailed oceanic structure in the vicinity of the shoal Kokusho-sone. *J. Oceanogr. Soc. Japan, 34*, 41-49.

Genin, A., and G.W. Boehlert, 1985: Dynamics of temperature and chlorophyll structures above a seamount: an oceanic experiment. *J. Mar. Res., 43*, 907-924.

Gill, A.E., 1982: *Atmosphere-ocean dynamics.* Academic Press, 662 pp.

Greenspan, H.P., 1968: *The theory of rotating fluids.* Cambridge Univ. Press, 327 pp.

Gould, W.J., R. Hendry, and H.E. Huppert, 1981: An abyssal topographic experiment. *Deep-Sea Res., 28*, 409-440.

Herlinveaux, R.H., 1971: Oceanographic features of biological observations at Bowie Seamount, 14-15 August, 1969. *Fish. Res. Board Can., Tech. Rep., 273.*

Hide, R., 1961: Origin of Jupiter's great red spot. *Nature, 190*, 895-896.

Hide, R., and A.Ibbetson, 1966: An experimental study of "Taylor columns". *Icarus, 5*, 279-290.

Hide, R., 1971: On geostrophic motion of a non-homogeneous fluid. *J. Fluid Mech., 49*, 745-751.

Hirota, J., and G.W. Boehlert, 1985: Feeding of *Maurolicus muelleri* at Southeast Hancock Seamount and its effects on the zooplankton community. *Eos, 66*, 1336.

Hogg, N.G., 1973: On the stratified Taylor column. *J. Fluid Mech., 58*, 517-537.

Hogg, N.G., 1980: Effects of bottom topography on ocean currents. In: *Orographic Effects in Planetary Flows*, editors R. Hide and P.W. White, *GARP Pub. Ser., 23*, World Meteorol. Organ., Geneva, 169-207.

Hubbs, C.L., 1959: Initial discoveries on fish faunas on seamounts and offshore banks in the eastern Pacific. *Pac. Sci., 13*, 311-316.

Hughes, S.E., 1981: Initial U.S. exploration of nine Gulf of Alaska seamounts and their associated fish and shellfish resources. *Mar. Fish. Rev., 43*, 26-33.

Huppert, H.E., 1975: Some remarks on the initiation of inertial Taylor columns. *J. Fluid Mech., 67*, 397-412.

Huppert, H.E., and K. Bryan, 1976: Topographically generated eddies. *Deep-Sea Res., 23*, 655-679.

Ingersoll, A.P., 1969: Inertial Taylor columns and Jupiter's great red spot. *J. Atm. Sci., 26*, 744-752.

Jacobs, S.J., 1964: The Taylor column problem. *J. Fluid Mech., 20*, 581-591.

Janowitz, G.S., and L.J. Pietrafesa, 1982: The effects of alongshore variation in bottom topography on a boundary current, or, topographically induced upwelling. *Continental Shelf Res., 1*, 123-141.

Johnson, E.R., 1978: Trapped vortices in rotating flow. J. Fluid Mech., 86, 209-224.

Maloney, E.S., 1978: *Dutton's navigation and piloting, 13th Ed.*. Naval Institute Press, 910pp.

McCartney, M.S., 1972: Taylor columns and Rossby wakes generated by isolated topographic features on a beta-plane. *Notes on the 1972 summer study program in geophysical fluid dynamics at the Woods Hole Oceanographic Institution, WHOI Ref. 72-79*, 60-81.

McCartney, M.S., 1975: Inertial Taylor columns on a beta plane. *J. Fluid Mech., 68*, 71-95.

McConnaughy, B.H., 1978: *Introduction to marine biology, 3rd Ed.* C.V. Mosby, 624 pp.

Meincke, J., 1971: Observation of an anticyclonic vortex trapped above a seamount. *J. Geophys. Res., 76,* 7432-7440.

Merkine, L.O., and E.K. Rivas, 1976: Rotating stratified flow over finite isolated topography. *J. Atm. Sci., 33,* 908-922.

Nicholls, J.M., ed., 1973: *The airflow over mountains: research 1958-76, Tech. Note 127.* World Meteorol. Organ., Geneva.

Owens, W.B., and N.G. Hogg, 1980: Oceanic observations of stratified Taylor columns near a bump. *Deep-Sea Res., 27,* 1029-1045.

Pond, S., and G.L. Pickard, 1983: *Introductory dynamical oceanography, 2nd Ed.* Pergamon Press, 327 pp.

Proudman, J., 1916: On the motion of solids in a liquid possessing vorticity. *Proc. Roy. Soc., A 92,* 408-424.

Queney, P., 1973: Transfer and dissipation of energy by mountain waves. In: *Dynamical meteorology,* P. Mord, ed., Reidel Publ., 97-351.

Roberts, D.G., N.G. Hogg, D.G. Bishop, and C.G. Flewellen, 1974: *Deep-Sea Res., 21,* 175-184.

Roden, G.I., and B.A. Taft, 1985: Effect of the Emperor Seamounts on the mesoscale thermohaline structure during the summer of 1982. *J. Geophys. Res., 90,* 839-855.

Samuels, B.H., 1986: personal communication.

Schmitz, W.J.Jr., 1975: Observations of low-frequency current fluctuations on the continental slope near site D. *J. Mar. Res., 32(2),* 233-251.

Schmitz, W.J.Jr., 1980: Observed and numerically simulated kinetic energies for MODE eddies. *J. Phys. Oceanog., 9(6),* 1294-1297.

Shomura, R.S., and R. A. Barkley, 1980: Ecosystem dynamics of seamounts--a working hypothesis. *Proceedings ofthe Fourth CSK Symposium,* Tokyo, 1979, 789.

Smith, R.B., 1979: The influence of mountains on the atmosphere. *Adv. Geophys., 21,* 87-230.

Stone, P.H., and D.J. Baker, 1968: Concerning the existence of Taylor columns in atmospheres. *Quart. J. Roy. Met. Soc., 94,* 576-580.

Sund, P.N., M. Blackburn, and F. Williams, 1981: Tunas and their environment in the Pacific Ocean: a review. *Oceanogr. Mar. Biol. Ann. Rev., 19, 443-512.*

Sundby, S., 1984: Influence of bottom topography on the circulation at the continental shelf off northern Norway. *FiskDir. Skr. Ser.HavUnders.*, *17*, 501-519.

Takahashi, Y., and T. Sasaki, 1977: from Hohuyo soko-uo gyogyo--Shryo(3) (Northern waters groundfish fishery--Data(3)). *Far Seas Fish. Res. Lab.*, 45 pp.

Taylor, G.I., 1917: Motion of solids in fluids when the flow is not irrotational. *Proc. Roy. Soc.*, *A93*, 99-113.

Taylor, G.I., 1923: Experiments on the motion of solid bodies in rotating fluids. *Proc. Roy. Soc. A 104*, 213-218.

Terada, K., and M. Hanzawa, 1984: Climate of the North Pacific Ocean. In: *World Survey od Climatology, Vol. 15: Climates of the Oceans.* ed. H. Van Loon, 431-503.

Uchida, R.N., and D.T. Tagami, 1984: Groundfish fisheries and research in the vicinity of seamounts in the North Pacific Ocean. *Mar. Fish. Rev.*, *46(2)*, *1-17.*

Uchiyama, James H., 1984: TOWNSEND CROMWELL, cruise 84-05 (TC-110). U.S. Dept of Commerce, National Oceanic and Atmospheric Admin., National Marine Fisheries Service, Southwest Fisheries Center, Honolulu Laboratory, Sept. 25, 1-17.

Uda, M., and M. Ishino, 1958: Enrichment pattern resulting from eddy systems in relation to fishing grounds. *J. Tokyo Univ. Fish.*, *44*, 105-119.

Vastano, A.C., and B.A. Warren, 1976: Perturbations to the Gulf Stream by Atlantis II Seamount. *Deep-Sea Res.*, *23*, 681-694.

Vaziri, A., and D.L. Boyer, 1971: Rotating flow over shallow topographies. *J. Fluid Mech.*, *50*, 79-95.

INITIAL DISTRIBUTION LIST

		No. Copies
1.	Defense Technical Information Center Cameron Station Alexandria, Virginina 22304-6145	2
2.	Library,Code 0142 Naval Postgraduate School Monterey, California 93943-5002	2
3.	Chairman, Department of Oceanography Code 68Mr Naval Postgraduate School Monterey, CA 93942-5000	1
4.	NOAA Liason Officer Post Office Box 8688 Monterey, CA 93943-0688	1
5.	Professor Roland W. Garwood, Jr. Code 68Gd Naval Postgraduate School Monterey, CA 93943-5000	2
6.	Mr. Andrew Bakun Chief, Pacific Fisheries Environmental Group, F/SWC4 P.O. Box 831 Monterey, CA 93942	4
7.	Office of the Director Naval Oceanography Division (OP-952) Department of the Navy Washington, D.C. 20350	1
8.	Commander Naval Oceanography Command NSTL, MS 39529	1
9.	Commanding Officer Naval Oceanographic Office Bay St. Louis NSTL, MS 39522	1
10.	Commanding Officer Naval Ocean Research and Development Activity Bay St. Louis NSTL, MS 39522	1
11.	Chief of Naval Research 800 N. Quincy Street Arlington, VA 22217	1
12.	Chairman, Oceanography Department United States Naval Academy Annapolis, MD 21402	1
13.	Director, Southwest Fisheries Center, F/SWC National Marine Fisheries Service, NOAA P.O. Box 271 La Jolla, CA 92038	1

14.	Assistant Administrator for Fisheries National Marine Fisheries Service 3300 Whitehaven Street, N.W. Washington, D.C. 20235	1
15.	Director, Honolulu Laboratory National Marine Fisheries Service, NOAA P.O. Box 3830 Honolulu, HI 96812	1
16.	Dr. George Boehlert National Marine Fisheries Service, NOAA P.O. Box 3830 Honolulu, HI 96812	5
17.	RADM Kelly E. Taggart Director, NOAA Corps National Oceanic and Atmospheric Administration Rockville, MD 20852	1
18.	Program, Planning, Liason, and Training Division NC2, Room 105, Rockwall Building National Oceanic and Atmospheric Administration Rockville, MD 20852	1
19.	Assistant Administrator for Oceanic and Atmospheric Research, R National Oceanic and Atmospheric Administration Rockville, MD 20852	1
20.	Director, Environmental Research Laboratories National Oceanic and Atmospheric Administration Boulder, CO 80303	1
21.	Director, Pacific Marine Environmental Laboratory National Oceanic and Atmospheric Administration Bin C 15700 7600 Sand Point Way NE Seattle, WA 98115-0070	1
22.	Director, Pacific Marine Center N/MOP National Ocean Service, NOAA 1801 Fairview Avenue, East Seattle, WA 98102	1
23.	Director, Atlantic Marine Center N/MOA National Ocean Service, NOAA 439 West York Street Norfolk, VA 23510	1
24.	LTJG Russell E. Brainard, NOAA Pacific Fisheries Environmental Group, F/SWC4 P.O. Box 831 Monterey, CA 93942	5
25.	Mr. Patrick Gallacher Code 68Ga Naval Postgraduate School Monterey, CA 93943-5000	1
26.	Asst. Prof. David C. Smith IV Code 68Si Naval Postgraduate School Monterey, CA 93943-5000	1

27.	Asst. Prof. Philip A. Durkee Code 63De Naval Postgraduate School Monterey, CA 93943-5000	1
28.	Capt. Glen R. Schaefer, NOAA Code 68Sc Naval Postgraduate School Monterey, CA 93943-5000	1
29.	Mr. Paul A. Wittmann Fleet Numerical Oceanography Center Monterey, CA 93943-5001	1
30.	Dr. Michele M. Reinecker Code 68Rr Naval Postgraduate School Monterey, CA 93943-5000	1